Interactive comment on "Determining the infrared radiative effects of Saharan dust: a radiative transfer modelling study based on vertically resolved measurements at Lampedusa" by Daniela Meloni et al.

Anonymous Referee #1

Received and published: 21 September 2017

General comments: This paper lies in the framework of the ChArMEx/ADRIMED experiment, that took place in the Mediterranean in summer 2013. Three vertical profiles of atmospheric and aerosol properties, made at Lampedusa in conjunction with surface, airborne and satellite IR broadband and narrowband radiation as well as radiosonde are analyzed in order to 1) identify the sensitivity of the different radiative measurements to mineral dust microphysical properties (size distribution and refractive index) and 2) analyze their impact in term of radiative forcing. The main result of this study is that if LW irradiance is poorly sensitive to aerosol microphysical properties compared to brightness temperature, the IR dust radiative forcing is non-negligible, and strongly depends on size distribution (SD) and refractive index (RI). This study highlights the importance of a precise knowledge of the dust microphysics to infer correctly their radiative effect. The paper is an interesting sensitivity study of the radiative variables to the aerosol microphysics, leading, in particular, to the conclusion that spectrally resolved measurements of brightness temperature is more fitted to infer dust properties than broadband LW irradiances. However, the part that concludes on the most appropriate refractive indices is less convincing. Such a study would require a more detailed analysis of the differences between refractive indices (at minimum a figure displaying their values in the spectral domain concerned), as well as a more exhaustive variability in the choice of the indices. Here among the three indices used, two indices are quite similar and only one coming from recent measurement campaign of DiBiagio et al., 2017 is really different. Moreover, the study, based principally on RT simulations, lacks of discussions on the uncertainties due to the RT model itself, as well as to the different hypothesis used. In particular, which is the impact of an error in surface temperature or surface emissivity? An error on the water vapor profile? No reference error is calculated under clear sky condition for example, to distinguish error directly due to the model from errors due to the impact of aerosols properties. The resulting biases obtained with the different aerosol properties configurations cannot therefore be really discussed. For example, large biases between simulated and calculated irradiances are not explained (and apparently not due to wrong aerosol properties), implying that something is missing in the RT model, but not enough discussed. The section on IASI data is not enough developed. All the spectra within a box of about 100 kmx100 km are averaged before analysis, causing a standard deviation in the averaged spectrum larger than the effect of the aerosols properties analyzed! Here again, since no reference errors are given, biases obtained from the different aerosol configurations are finally equivalent and it's not possible to state on the best configuration. This part doesn't really bring new information compared to the previous sections or previous studies, or required a more precise development. Finally, some details on the inputs used are missing. A few details are provided on the size parameters used (the reader has to refer to the paper of Denjean et al. 2016 to have the precisions) and the exact refractive index from DiBiagio et al., 2017 use in this study is not given: 3 different indices are coming from Â´nÂ˘athe source regions (Tunisia, Algeria, Morocco) in DiBiagio et al., 2017 whereas only one is used here without any precision!

We agree with the reviewer that a comprehensive analysis including the impact of the uncertainty on the input parameters on the model simulations (of either irradiances and brightness temperature profiles and of radiances at the top of the atmosphere) is useful to better constrain the results. Following the reviewer's suggestion, a sensitivity study addressing the uncertainties of the modelled radiation quantities due to the uncertainty on the input parameters has been carried out, either in aerosol-free conditions or including the aerosol particles. The main model input parameters

affecting infrared radiation in aerosol-free conditions that have been considered are: integrated water vapour, temperature profile, sea surface temperature, surface emissivity. Each quantity has been perturbed one at a time by the amount of its uncertainty, than all the resulting model uncertainties has been combined to provide the overall uncertainty. Similarly, the sensitivity with respect to AOD and dust complex refractive index has been quantified.
The results have been added to the manuscript under the new Section 3.3.
The model LW irradiance uncertainty decreases with increasing altitude for both the downward and upward components. The estimated model uncertainty on the downward and upward LW irradiances at the surface is 2.2 and 2.0 W m^{-2} for simulations without and with aerosols, respectively. At the Falcon 20 altitude (about 10 km) the uncertainties are 0.6 and 1.5 W m^{-2} for the downward and upward component, respectively, for both simulations with and without aerosol. The upward LW irradiance uncertainty is 1.4 W m^{-2} at TOA, for simulations with and without aerosol..
The estimated uncertainty on ARF is obtained by the combination of the above values, and is 4.2 W m^{-2} at the surface and 2.0 W m^{-2} at the TOA. The uncertainty on AHR is largest at about 4.5 km altitude (0.030 K day^{-1} with aerosol and 0.026 K day^{-1} without aerosol), and close to the surface (0.050 K day^{-1} with and without aerosol).
The uncertainty on the downward WINDOW irradiance is 0.9 and 0.6 W m^{-2}, with and without aerosol, respectively. The estimated uncertainty on the modelled zenith BT is 0.7 and 0.3 K, with and without aerosol, respectively.
The aerosol-free CLIMAT BT is much sensitive to SST and surface emission, with slightly larger values at 600 m (0.3 K) than at 5670 m (0.28 K). The overall uncertainty for the case with aerosol is 0.31 K at 600 m and 0.37 K at 5670 m.
The uncertainty on the spectral BT at TOA in the atmospheric window varies between 0.25 and 0.29 K in aerosol-free conditions, and between 0.32 and 0.50 K with aerosol.

The model-measurement differences have been discussed in the text taking into account the uncertainties on the model estimates.

A figure displaying the spectral complex refractive indices used in this study has been added as Supplement Material (Figure S1). With this regard, a summary of the most common complex refractive indices of desert dust is provided in Di Biagio, C., Boucher, H., Caquineau, S., Chevaillier, S., Cuesta, J., and Formenti, P.: Variability of the infrared complex refractive index of African mineral dust: experimental estimation and implications for radiative transfer and satellite remote sensing, Atmos. Chem. Phys., 14, 11093-11116, doi:10.5194/acp-14-11093-2014, 2014.
Moreover, the spectral (0-40 μm) normalized extinction coefficients, single scattering albedoes, and asymmetry factors computed using the combination of SDs and RIs described in the text for each layer of the three profiles have been shown in Figure S2, S3, and S4 of the Supplement Material.

The dust refractive indices that we use in the 0-40 μm range have been chosen because they are specific for the source regions found during the ChArMEx campaign (like those from Tunisia, Algeria, Morocco by Di Biagio et al., 2017), or because they are widely used in the retrieval of satellite products or in climate models (like the ones from OPAC by Hess et al., 1998, and by Volz, 1973).
OPAC and Volz (1973) have very similar real and imaginary parts, except for the 9.5-14 μm spectral interval, where we explore the dust impact on the surface irradiance (in the 8-14 μm window) and brightness temperature (9.6-11.5 μm) and in the CLIMAT and IASI brightness temperatures (BTs). The results in Table 3 of the manuscript confirm that the model-measurement differences in the 9.6-11.5 μm BT can be significant (0.7 K) when the OPAC size distribution is used, while are modest (0.4 K) with the *in situ* size distribution.
Other dust refractive indices found in literature were taken into account, although the results are not reported in the manuscript: for example, the Volz (1972) one, which is equivalent to the one

published in Shettle and Fenn (1979). The imaginary part is much lower than that of OPAC and Volz (1973), so lower surface LW and WINDOW irradiances and infrared BT are expected, with consequently modest radiative effect.
The aerosol optical properties obtained with the Longtin et al. (1988) dust refractive index were already examined in a previous paper (Meloni et al., Altitude-resolved shortwave and longwave radiative effects of desert dust in the Mediterranean during the GAMARF campaign: Indications of a net daily cooling in the dust layer, J. Geophys. Res. Atmos., 120, 3386–3407, 2015).

All the three refractive indices by Di Biagio et al., 2017 (Algeria, Tunisia, Morocco) have been used in the study, since the analysis by Denjean et al. (2016) based on back-trajectories and MSG-SEVIRI satellite products shows that dust collected during F35, F38, and F4 flights have different source regions (details are given in Table 1 of Denjean et al., 2016). More specifically, for flight F35 the dust layer above-3.5 km originated from southern Algeria, while the dust layer between 1.5 and 0.5 km was transported from southern Morocco. On 28 June (F38) dust was lifted from Tunisia. Finally, on 3 July (F42) dust originated from Tunisia (above 3 km) and from southern Morocco (below 3 km).
A better description of the choice of the appropriate refractive index on the base of the dust source region was added in Section 3.1.1 (page 9, lines 1-19). We have used different refractive indices from Di Biagio et al. (2017) for each flight and each dust layer based on the source regions found in Denjean et al. (2016). For F35 we used the refractive index for Algerian dust in layer 3 (see Figure 3), that for Moroccan dust in layer 2, and the OPAC water soluble refractive index for layer 1, i.e. below the dust layer. Similarly, the Tunisian dust refractive index is used for F38 flight in layer 2 and the OPAC water soluble one in layer 1. For F42 the Tunisian and the Moroccan dust refractive index are used in layer 2 and 1, respectively.
We clarified the choice of the dust refractive index in Section 3.1.1 and prepared a new Table 2 which includes three tables, one for each day. The tables present the combination of SD and RI used in each layer identified by the lidar and ATR-42 measurements, and the AOD value at 8.6 µm.

Specific comments:
- p2line 21Â˘ a: Â´nÂ˘aMost of these studies have been carried out close to the dust source regions and did not take into account the possible modifications in dust optical properties during long range transport. “: You can also find some studies dealing with the variation of the aerosol properties with transport (e.g. Maring 2003; Ryder et al., 2013; Weinzierl et al., 2017 and so on). Moreover, I don’t see the link with the subject of this paper since there is no discussion on the possible change of dust properties with transport. Maring, H.: Vertical distributions of dust and sea-salt aerosols over Puerto Rico during PRIDE measured from a light aircraft, J. Geophys. Res., 108(D19), 1–11, doi:10.1029/2002JD002544, 2003. Ryder, C. L., Highwood, E. J., Lai, T. M., Sodemann, H. and Marsham, J. H.: Impact of atmospheric transport on the evolution of microphysical and optical properties of Saharan dust, Geophys. Res. Lett., 40(10), 2433–2438, doi:10.1002/grl.50482, 2013. Weinzierl, B., ProsPero, J., Chouza, F., FomBa, W., Freudenthaler, V., GasteiGer, J. and Toledano, C.: THE SAHARAN AEROSOL LONG-RANGE TRANSPORT AND AEROSOL–CLOUDINTERACTION EXPERIMENT Overview and Selected Highlights, [online] Available from: http://journals.ametsoc.org/doi/pdf/10.1175/BAMS-D-15-00142.1
We thank the reviewer for suggesting the papers that have been integrated in the Introduction, citing them as example of studies carried out by means of aircraft measurements dealing with the temporal evolution of dust properties occurring during long-range transport.
Our study focuses on the optical properties of transported dust and on its infrared radiative effect in the Mediterranean. The present paper does not aim at assessing how dust optical properties change during transport (Denjean et al., 2016 show indeed that the coarse mode of dust did not change after 5 days of transport possibly due to strong vertical turbulence within the dust layer, preventing the deposition of large particles), but highlights the importance of knowing the dust microphysical and

optical properties to reasonably estimate the IR dust radiative forcing and heating rate at the surface, in the atmosphere, and at the top of the atmosphere.

- P2line 29:
the paper Sellitto et al., 2016 deals with aerosols in the ULTS and not with dust. This reference is not really appropriate here.
The reference has been removed.

- p4line21: why describing AERONET AOD and associated uncertainties if not used? Even not compared in the following to the MFRSR?
We agree with the reviewer. The AERONET AOD is not used because of some missing data, so the sentence in lines 22-23 about AOD uncertainty has been removed.

- P5: For the surface observations, several instruments measuring irradiance are described, but it's not clear if they are all used in this study. Why describing every instrument available if they are not used? Which ones are really used? This section would gain in clarity if simplified.
In Section 2.1 all the ground-based instruments are presented. For sake of clarity, we removed all instruments (like the shortwave radiometers and the pyrheliometer) whose measurements are not used in the analysis.

- P6line13: maybe a summary of the description of the meteorological and dust conditions given in Denjean et al., 2016 would help? It's easier for a reader to get all the relevant information in one paper.
A short description of the synoptic conditions causing dust transport from the Sahara desert to Lampedusa during the campaign has been added in the text.

- P7line15: unity switched from µm to cm-1. Maybe it would be clearer for the reader to stay in µm?
IASI spectral characteristics, like spectral interval, sampling and resolution, are provided in units of cm^{-1}. We have used both µm and cm^{-1} in the text and in figures and table whenever possible to help the reader.

- P8line 18-19: How the AOP (i.e. spectral extinction, single scattering albedo, and phase function at each layer) can be derived from AERONET observation and from Deanjean et al., 2016, in particular for longwave? Observations made by AERONET or Denjean et al. are made in visible wavelength, not in the infrared part of the spectrum. Optical properties cannot be derived in the longwave by these measurements. This sentence is in contradiction with the procedure described later where the size distribution from AERONET and the ATR-42 are used with independent refractive indices to derived these optical properties.
We agree with the reviewer that the sentence in lines 18-19 is misleading. The IR AOPs are not derived from AERONET or airborne observations alone.
The aerosol optical properties in the infrared spectral range are calculated applying the Mie theory using the AERONET and the *in situ* size distributions and the complex refractive indices in the 3-40 µm (OPAC) and in the 2-16 µm (Di Biagio et al., 2017) intervals.
The sentence has been rephrased.

- P9line 14-15: which is the RI used from OPAC? MITR? Must be cleared. Similarly, which RI from DB2017 is used? In Table 2 "Algeria-Tunisia-Morocco dust" is mentioned, but it corresponds to 3 different indices, which one is used?

We used the mineral dust refractive index from OPAC, which is the same for the four dust types (accumulation, coarse, nucleation, transported) of the model. This has been clarified in the text. As for the answer to the reviewer's general comments, we have used different refractive indices from Di Biagio et al. 2017 for each flight and each dust layer based on the source regions found in Denjean et al. 2016. More details are now given in section 3.1.1 and Table 2.

- P9line 19: the sentence "the AOPs are calculated using the AERONET and the in situ SD and the OPAC water soluble RI" have to be rewritten by something like "the AOPs are calculated using either the AERONET or the in situ SD and the OPAC water soluble RI.
We rephrased the sentence according to the reviewer's suggestions.

- P9 line 4: A table given the main parametrization of the SD (radius and width of the distribution size) used would avoid to refer systematically to the paper of Deanjean et al., 2016.
We have produced Table S1 with the median radius, standard deviation, and normalized number concentration for each mode of either the AERONET and the *in situ* log-normal size distributions for the three cases as Supplement material.

- P10 Eq 2: What does the symbol Delta stand for?
The Delta symbol in the heating rate equation represents the variation of net flux and pressure between two contiguous layers.

- P10-11
and Table 3: the uncertainty for the WINDOW irradiance have been changed from 2 to 6 W.m2 from the previous version of the paper. In any cases in the text I read an uncertainty of 3W.m2 (p5, line 19). Which is the good one? In addition, the observed values for the downward irradiance and BT correspond to the average over a 10 minutes interval, what is the standard deviation of the measurement compared to the uncertainty? If the standard deviation is of the order of uncertainty, it means that the signal present small variation within the 10 minutes and maybe it would be better to compare simulations with observation, for every observation within the 10 minutes and average after instead of comparing with the average observation? If the standard deviation is larger, it means that using constant aerosol distribution is not valid.
The measurement uncertainty reported in Table 3 is the expanded (2-sigma) uncertainty, but this was not specified in the table caption, so it seems to disagree with what explained in the text (page 5, lines 19-20), referring to ±3 Wm^{-2} as one sigma uncertainty. This has been better specified in the revised paper.
However, the CGR3 participating to the ChArMEx campaign has been recently tested by PMOD/WRC to assess the possible effect due to the leakage of solar radiation on the WINDOW irradiance. The tests have shown that the effect is negligible, and so the WINDOW irradiance data used in the present analysis have to be reconsidered because they were corrected by subtracting a shortwave stray-light correction of about 4 Wm^{-2} per 1000 Wm^{-2} solar irradiance. So in the revised paper the CGR3 expanded uncertainty returns to be ±2 Wm^{-2} and the WINDOW irradiance data have been corrected, either in Table 3 and in Figure 2.
The standard deviations of the LW and WINDOW irradiance, and of the zenith BT over the 10 minute interval are much lower than the measurement uncertainty. For example on 22 June the standard deviation values are 0.2 Wm^{-2} for the LW irradiance, 0.3 Wm^{-2} for the WINDOW irradiance, and 0.1 K for the BT. We assume that no significant variations occur within the 10 minute interval and that differences can be calculated between the average value and the model simulation. A sentence has been added in the text to state the very low variability within the 10 minute time interval.

- All the section 4.1 need

to be slightly reorganized. In particular, the sentence line 23-24 page 10 is very general for the three days and the three variables, and therefore need to be at the beginning of the paragraph, as well as the sentence line 18-21, which is the associated explanation or put at the end of the section as conclusion. Furthermore, the paragraph need an overall analysis of the results obtained at the end: For LW irradiance and WINDOW irradiance, the impact of the refractive index is below the uncertainty of observation, the impact of the RI for a given SD is close to the uncertainty. For WINDOW, simulations always overestimate the observation, implying that the RT model or the calibration is not correct for this simulation and therefore it is not clear to understand what bring this variable in the study: : : On the contrary, for IR BT, the impact of the SD as well as the RI is significant compared to the uncertainty, this variable seems to be more appropriate to analyze AOP.
We agree with the reviewer. Section 4.1 has been revised, the results commented taking into account the model uncertainties, and a concluding sentence has been added at the end of the section. Although the WINDOW irradiance is overestimated by the model, its simulations with different AOPs have been included in the analysis to show that, even when reducing the spectral interval compared to the broadband, the irradiance is not sensitive to varying AOPs.

- P11 line 27: "The average AOD during the descent is assumed as model input.": Which AOD is used? The average column integrated value measured by the MFRSR?
Yes, the AOD measured by the MFRSR during the flight and reported in the IR as explained in section3.1.1 has been averaged and used as model input.

- P11line30-33: there is no reason for which the NOAER simulation agree well for all the profile except close to the surface given the aerosol distribution of Figure 3. Something may be missing in the simulation to reproduce the observed downward irradiance in the lower part of the atmosphere that is not due to aerosols.
Figure 6 shows that model without dust (NOAER) underestimates measurements by an amount that is negligible at higher altitudes and increases close to the surface. This effect is due to emission of infrared radiation by the dust above each altitude layer which induces an increase of the downward LW irradiance, and which depends on the dust optical depth and optical properties.

- P12line 1-3: "This confirms the results found for the surface irradiance, i.e. that the broadband irradiance alone cannot help discriminating which SD and RI provide the best representation of the dust optical properties". This conclusion is not clearly stated in the previous part (see my comment on the section 4.1).
A concluding sentence has been added in Section 4.1 to summarize the results.

- P12line 12-13: "However, while the model-measurement agreement is very good at 600 and 3300 m, where the aerosol impact is small, a systematic overestimation is obtained at 5670 m.": from Figure 7, there is no evidence of a "systematic overestimation […] at 5670 m". COL1 and INSU3 seems to fit well observations at 12_m, whereas an overestimation is obtained at 8.7µm. At 10.6µm COL1 induces an overestimation, but INSU3 an underestimation of the observation. I don't see therefore "a systematic overestimation".
The sentence was present in a previous version of the manuscript and was erroneously maintained in the submitted version. It has been removed. As the reviewer points out, the overestimate of the model depends on spectral band and on aerosol optical properties.

- P12 line 15-16: "These results show that exploring the BT in the thermal infrared is a useful tool to infer dust optical properties if the SD is provided.": this sentence should be slightly attenuated: These results show the better sensitivity of BT to dust optical properties than broadband irradiance but for the two other days, where aerosols are lower or with a smaller AOD, the differences between simulations with different AOP are of the order of the observed uncertainty.

The sentence has been modified according to the reviewer's suggestion in "These results show the better sensitivity of BT to dust optical properties than broadband irradiance", since the paragraph refers to flight F35 only.

- P13line 26: "while no BT increase is detected at 1700 m": I don't understand this sentence, on Figure 9, there is an increase of BT at 1700m.
The reviewer's comment is right. At 1700 m, as well as at 900 m, either the pyrgeometer and the CLIMAT capture the infrared increase due to the island emission. The sentence has been changed in "The spikes at 900 m and around 1700 m indicate that also CLIMAT captures the island emission.".

- As for the section 4.1, this section lacks of a conclusion that summarizes the different simulations. Basically, the LW irradiance is not really sensitive to AOP (impact under the uncertainties). In addition, something appears to be missing in the simulations, because simulated upward irradiances are systematically overestimated by simulation in some part of the profile (for the three cases, even it is less important in the first one). An explanation, or at least some hypothesis, of this overestimation is missing in the paper.
A concluding sentence has been added at the end of the section, explaining that irradiance is not sensitive to the AOPs, while the aerosol perturbation to the upward infrared BT can be appreciated only at altitudes above the bulk aerosol emission, like for the flight F35.
Differences between the measured and the model upward LW irradiance profiles for 28 June and 3 July cannot be explained by a wrong representation of the temperature and humidity profiles in the model, that would have affected the CLIMAT profiles also, as described in the text. What is observed is that the CLIMAT BT profiles are well reproduced at different altitudes, also close to the surface for flight F38, suggesting a proper choice of atmospheric profiles and of sea surface temperature and emission.
We formulated an hypothesis of some negative bias affecting the pyrgeometers' measurements due to the fact that the instrument needs some time (the typical response time is 6 s but for airborne measurements the required time may be significantly longer, as shown for example by Albrecht et al., Pyrgeometer measurements from aircraft, Rev. Sci. Instrum., 45, 33–38, 1974) to establish equilibrium with the air temperature. So we expect that when the aircraft is descending rapidly pyrgeometer measurements may be affected. We verified that during flights F38 (from 3500 to 2000 m) and F42 (from 4800 to 1600 m), where model values are larger than measurements, the vertical velocities were -5.5 and -5.3 m/s, respectively. On the contrary, from 5400 to 4000 m during flight F38, where non-significant biases between model and measurements are observed, the vertical velocity is sensibly lower, about 2.6 m/s. Similarly, during flight F35, when model-measurement differences are small, the vertical velocity is 2.8 m/s.
Opposite to CGR4, the CLIMAT measurements are not affected by the ATR-42 descent speed because the instrumental response time is much shorter (160 ms).

- P14 line 14-15 "The resulting standard deviation on the TOA spectral radiance is around 1% for 22 and 28 June and 0.5% for 3 July": this value requires to be in K, in order to be compared with the radiometric noise and more over to be compared with the impact of the different AOP. Given that 1% corresponds to a variation of about 2.9K (_1% of the surface temperature), this standard deviation is larger than the impact of the aerosol properties themselves. It should be better to apply the simulations to each spectrum and then average the differences.
The IASI spectra have been expressed as BTs, and averaged within the chosen area: the standard deviation (in the 8-14 μm interval) is about 0.6 K for 22 and 28 June, and about 0.3 K on 3 July. These values, although larger than the IASI radiometric noise, express the variability of the TOA BT in the domain. The aim of the simulation of the IASI spectra is to show that including the aerosol the TOA-leaving radiance decreases by an amount which is larger than the model uncertainty and the IASI radiometric noise. Moreover, we want to investigate the sensitivity of the

modelled TOA-leaving radiance to different AOPs. The results in Table 7 show that an appreciable aerosol effect is detected on 22 June and on 3 July, leading to an improvement in the model simulations compared to the aerosol-free case.

- Table 7: In the caption is written "Differences (K) between modelled and measured IASI BT spectra" at the beginning and "Differences are expressed as percent RMSD and standard deviation" at the end. The differences are in K or in %? The sentence "In bold the significant differences with respect to the NOAER simulations." Is not clear. What means "significant differences with respect to the NOAER simulations"? What is the criterion to put in bold the difference?
The differences between model and measurements are calculated in the two spectral intervals 780-980 cm^{-1} and 1070-1200 cm^{-1}. Then for each interval the RMSD and the standard deviation are calculated, with the various AOP and also in the aerosol-free case, and expressed in K. The values that have been highlighted in bold are those for which the TOA BT with aerosol and that without aerosol are different taking into account the respective mean and standard deviation (significant difference). The caption of the table has been corrected.

- P14line23 to p15line 6: this paragraph need to be reorganized by day instead of analysing figure 12, and then Table 7 since the conclusions are the same and it would avoid redundant sentences.
The paragraph has been reorganized in order to present the results more concisely and clearly.

- P15 line 4-5: this sentence repeat statement already given in the previous paragraph or has to be rewritten.
The sentence has been removed.

- P15 line 7-24: the paragraph
describing the analysis of Liuzzi et al. (2017) is very long to finally conclude that the impact of INSU3 is of the same order. Either better details of what this study bring compared to the previous one, or why this study use a simplify RT models compared to the previous one is given, or this paragraph has to be shortened. But for now, it's difficult to see where the author is going.
Liuzzi et al. (2017) use an ad-hoc model to reproduce the IASI TOA spectra with the native spectrometer resolution, with the *in situ* size distribution and Di Biagio et al. (2017) refractive indices, tuning some parameters like SST to achieve a good agreement with the measured spectra. We use a model with lower spectral resolution and all the atmospheric and surface parameters derived from observations.
Achieving similar results of those of Liuzzi et al. (2017) at TOA and reproducing also surface and atmospheric irradiances and BT is not obvious and represents an important result of the closure study.
The description of the analysis carried out by Liuzzi et al. has been shortened and the aim of the simulations of the IASI spectra has been better explained.

- P15 line 10: correct "or" by "for" in "The real part is also generally lower or Shettle and Fen "
Done.

- Section 4.4: it would be interesting to see also the results for the two other days and the AOP INSU1 in order to have an idea of the variations of the radiative forcing from very different cases.
The aerosol radiative forcing and heating rate obtained with the INSU1 AOPs have been added and discussed. The ARF and AHR for the other cases have not been presented because the paper is already long. Below we report the tables with the ARF and ARFE for 28 June and 3 July. The values of the ARF is low on both days, either at the surface and at TOA. When taking into account the uncertainties on the modelled ARF, the ARF is different from zero using INSU1 on 28 June and

with INSU1 and INSU3 (only at the surface) on 3 July. It is worth noticing that the ARFE values are similar in the two days.
The ARF values with INSU3 AOPs are much lower on 28 June and 3 July than on 22 June and we expect an analogous behaviour for the aerosol heating rates.

Table 1. LW ARF and ARFE at the surface, TOA, and in the atmosphere (in W m^{-2}) on 28 June calculated with all the AOPs.

	ARF				ARFE			
AOP	COL1	COL3	INSU1	INSU3	COL1	COL3	INSU1	INSU3
Surface	3.0	1.4	5.7	3.6	14.3	6.7	27.1	17.1
TOA	1.3	0.6	2.5	1.8	6.2	2.9	11.9	8.6
Atmosphere	-1.7	-0.8	-3.2	-1.8	-8.1	-3.8	-15.2	-8.5

Table 2. LW ARF and ARFE at the surface, TOA, and in the atmosphere (in W m^{-2}) on 3 July calculated with all the AOPs.

	ARF				ARFE			
AOP	COL1	COL3	INSU1	INSU3	COL1	COL3	INSU1	INSU3
Surface	3.8	2.1	7.1	4.4	14.7	8.1	27.4	17.0
TOA	1.5	0.8	2.6	1.6	5.8	3.1	10.0	6.2
Atmosphere	-2.3	-1.3	-4.5	-2.8	-8.9	-5.0	-17.4	-10.8

Interactive comment on "Determining the infrared radiative effects of Saharan dust: a radiative transfer modelling study based on vertically resolved measurements at Lampedusa" by Daniela Meloni et al.

Anonymous Referee #2

Received and published: 28 October 2017

Review of paper: acp-2017-591 "Determining the infrared radiative effects of Saharan dust: a radiative transfer modelling study based on vertically resolved measurements at Lampedusa" by D. Meloni et al.

General comments

In this paper radiation closure experiments are made in order to determine the infrared radiative effects of dust and to assess the role of dust size distribution (SD) and refractive index (RI). To this aim, in situ data from aircraft (ATR-42 and Falcon), surface (AERONET, radiometer, pyranometers, pyrgeometers and pyrometer) radiosonde and satellite (IASI) measurements are utilized for the closure. The measurements come from the ADRIMED/ChArMEx campaign in 2013. The vertically resolved simulations are performed with the MODTRAN radiative transfer model (RTM) initialized by insitu vertical and remotely sensed columnar SD and RI along with data for a series of surface and atmospheric parameters relevant to LW radiation transfer, coming from radiosoundings, spectrophotometer measurements, ECMWF reanalysis and MODIS satellite products. The assessment lies in comparing simulated and measured LW irradiances and brightness temperatures (BTs), while the dust LW radiative forcing (ARF) and atmospheric heating/cooling rates (AHR) is estimated with the RTM. Three cases (summer days) during a period of dust intrusions (late June and early July) are examined, and the study is performed for Lampedusa in central Meditteranean, in proximity to northern Africa and Sahara.

The study is detailed and makes synergistic use of a variety of data. Some interesting findings are reported, from which some are not always new, e.g. that the dust LW radiative effects are non negligible or that the heating rate profile of dust depends on its vertical distribution as well as on SD and RI. Yet, some others provide new information and give insight regarding the role of dust SD and RI for their LW radiative and thermal effects and for BT, e.g. that using dust RI from local dust sources (Algeria and Morrocco, DB2017) produces best agreement with observations or that the use of inaccurate, although optically equivalent SD and RI has a large impact on the dust ARF. The paper is well organized and nicely written although it sometimes lacks clarity in the discussion of its results.

The main issue is that the paper seems to fail to convince about the best performance and appropriateness, and to provide a clear message on what is the optimal combination of dust properties for achieving the radiation closure. The relevant messages drawn from the simulations-measurements comparisons of LW and WINDOW fluxes, and of BTs, are not consistent and appear to be somewhat contradictory, as it is for ex- ample the case in Table 3. Even the authors state (page 15, lines 20-21) that "the MODTRAN spectral resolution impacts the standard deviation of the model-measurements differences, making the results obtained with different AOPs equivalent". More specifically:

Main Comments

1) In general, quite small differences between the 7 examined configurations, consisting in different model setups (Table 2), are found between results obtained without aerosols and with aerosols, as well as between the 6 configurations with aerosols (3 columnar and 3 in-situ). This does not help to draw a clear conclusion on which one configuration and aerosol properties combination is the best, although this is expected to be the main finding of such a radiation closure study.

The study is aimed at investigating how dust particles affect various radiation quantities (irradiance and BT at the surface and in the atmosphere, BT at the top of the atmosphere) compared to the aerosol-free case and how the magnitude of the dust radiative effect depends on different aerosol optical properties.
This study has been carried out with information on the atmospheric vertical structure and surface characteristics, as well as on the aerosol burden and physical properties, derived from observations. Specific values of the dust complex refractive index, including some recently determined region-dependent values, have been used. The model outputs are then compared with measurements from various instruments installed on different platforms (from the surface radiometers and pyrometer to the airborne radiometers, to the satellite IASI interferometer).
The aim is not the determination of the best combination of aerosol size distribution and refractive index. In fact, we have used the vertically resolved in situ measured size distribution as a reference, since it is directly measured and, in our opinion, best represents the occurring aerosol properties. Under this assumption, we show that the more recent determination of regionally dependent refractive indices perform better than the frequently used literature values.
The use of vertically averaged SDs derived from AERONET with the most commonly used values of RIs (as it is quite frequently done in similar studies) is finalized at assessing the influence they have on the radiation field.
It must be pointed out that the closure is done on a quite large number of radiation measurements, made at the surface, airborne (and at different altitudes), and on satellite. In our opinion this is a quite unique analysis, and the comparison with different types of radiation measurements gives strong constraints and robustness on the results.
It must be also said that unfortunately the atmospheric conditions occurring during the ChArMEx/ADRIMED campaign did not bring large AOD and this aspect, combined with the model and measurements uncertainties, causes the modelled LW irradiances to be equivalent. Nonetheless, we show that this is not true for the WINDOW and the IR zenith BT, for which significant differences are obtained for the *in situ* SD when using OPAC and DB2017 RIs.
For the day with the largest AOD, i.e. 22 June, we also assessed which combination of SD and RI gives the best model-measurement match for the overall set of LW irradiances (downward at the surface, upward and downward components on the ATR-42 and Falcon 20) by calculating the RMSD of all model-measurement absolute differences, and selecting only those AOPs for which the RMSD is below the ±5 W m^{-2} threshold value. For the AERONET SD all the three RIs meet the requirement (RMSD between 3.2 and 3.3 W m^{-2}), while for the *in situ* SD only the DB2017 (RMSD 4.7 W m^{-2}). This conclusion has been added at the end of Section 4.2. If we assume that the vertically-resolved *in situ* SD is the best representation of the effective SD, the DB2017 RIs provide the best AOPs.

2) The ascertained/computed differences of each one of 7 configurations with respect to measurements (LW, WINDOW, BTs) mostly fall within the range of uncertainty of measurements, making difficult to decide on which one is really the best configuration.
This is true for the LW and WINDOW irradiances, but not for the zenith BT. We added a sentence at the end of Section 4.1 summarizing the best combination of SD and RI that provide the best model-measurement match: “The final results of the analysis of the surface measurements show that irradiances, either broadband and in the 8-14 µm spectral interval, are not useful to reduce the uncertainty on the dust RI, since the impact of different RIs is below the measurement and model uncertainty. On the contrary, narrowband zenith BT seems to be suitable to constrain the dust RI which better represents the dust optical properties either in moderate and in low dust loading conditions. Under the assumption that the in situ SD is the most representative of the real aerosol dimensions, the DB2017 RI provides the best agreement between model and measurements, either LW and WINDOW irradiances, and sky BT in the two cases where the atmospheric meteorological profiles and the in situ SD are measured down to surface level (22 and 28 June).”

3) A main conclusion drawn from the analysis is that there is a systematic model overestimation of upward LW fluxes within the peak of dust layers, in all 3 days. In other words, there seems to be an inherent problem with the modelling tool, which needs to be assessed.
We believe that a modeling problem is difficult to expect, either because the CLIMAT BT, obtained with the same input parameters as the irradiance components, are very well reproduced, and because for the 22 June case the model succeeds in resolving both irradiances and BTs. We have further investigated this aspect and have tentatively attributed the observed bias to the CGR4 slow time response; in fact, significant model-measurements differences are found when the aircraft velocities during the descents are too high. See details of the answer to point 26 of the specific comments.

4) The estimated small differences between the no-aerosol and aerosol configurations, indicate that the RTM LW computations are relatively insensitive to dust.
That is true but depends mainly on the AOD value. For the 22 June case, (AOD at 500 nm of 0.36) the increase in LW irradiance at the surface due to dust compared to aerosol-free conditions (NOAER) is +4.8, 4.7, 3.3, 10.9, 10.6, and 8.1 Wm^{-2} with COL1, COL2, COL3, INSU1, INSU2, and INSU3, respectively. With the *in situ* SD the dust effect is larger than the uncertainty of LW irradiance measurement (5 Wm^{-2}) and of the model (4.2 Wm^{-2}).
The values decrease with AOD: indeed, the values for the 28 June case (AOD at 500 nm of 0.21) are +3.2, 1.7, 6.3, 5.1 Wm^{-2} with COL1, COL3, INSU1, and INSU3. This explains why the simulations in aerosol-free conditions agree with measurements within their uncertainties.
For larger AOD, like the case presented in the paper by Meloni et al., 2015, Altitude-resolved shortwave and longwave radiative effects of desert dust in the Mediterranean during the GAMARF campaign: Indications of a net daily cooling in the dust layer, J. Geophys. Res. Atmos., 120, 3386–3407, the perturbation induced by the dust with AOD at 500 nm of 0.59 was 16.2 and 16.1 Wm^{-2} with AOPs analogous to COL1 and INSU1, respectively. In that case the modelled LW irradiance in aerosol-free conditions is outside the expanded uncertainty of the measurements.

5) The reported conclusions are sometimes contradictory. For example in page 17, lines 14-15 it is stated that dust RI from DB2017 produces the best agreement with observations, but this is not supported by and it is not in line with the results of Table 3 where NOAER and COL1 also provide good results, even better than INSU3, if all three parameters, i.e. LW, WINDOW, BT, and three days are considered.
The sentence refers to the results obtained with the *in situ* size distribution. One point that has been clarified in Sections 4.1 and 4.2 is that we can assume that the *in situ* SD is more realistic than the AERONET one, since the first is derived from vertically resolved optical counter measurements covering the diameter range 0.032-32 μm, while the second is derived from surface visible and near-infrared radiance measurements and is representative of the whole atmospheric column. Under this assumption the best model-measurement agreement is obtained with INSU3 AOPs, as stated in page 15, line 32.

6) It is not clear why BTs were computed and are reported only at 3 levels, which sometimes are not collocated with the peaks of dust layers; why similar BT computations were not made at more levels.
The selected altitudes correspond to those witha horizontal flying attitude of the ATR-42. Moreover, while all the other simulated profiles (upward and downward LW irradiances) where obtained with a single model run, the CLIMAT BTs require a run for each altitude. The vertical profiles of the modelled irradiances show a smooth change with altitude, so we believe that BT at few altitudes are sufficient to describe the vertical variations and adding simulations at other altitudes would not provide additional information.

7) The conclusions drawn from the BT analysis are different from those obtained from the analysis of LW fluxes. This is for example the case of the results of profile 42, in Figures 10 and 11. May this point to a possible modelling problem/inconsistency?
The model has proven to perform well either for the LW fluxes and for the CLIMAT BTs on 22 June, so we cannot justify the results for flight F42 with model inconsistency. We also exclude as a cause an incorrect choice of the model input parameters, like the sea surface temperature, emissivity, and/or the atmospheric temperature/humidity profiles, because the CLIMAT BTs are well reproduced at all altitudes. Following a further check on the data, We found that the bias in the LW irradiances occurs where the ATR-42 descent velocity is high. We believe that the associated fast change of ambient air temperature, associated with the relatively long response time of the CGR4 pyrgeometer, may produce the bias. See details of the answer to point 26 of the specific comments.

8) The role of clouds is not reported. Were all the tree days/cases cloud-free? If so, how is this confirmed/ensured? A relevant discussion should be made since the effect of clouds on LW is significant and interplay or even dominate the effect of dust (e.g. possible implications for Fig. 2).
The three flights were carried out under cloud-free conditions.
The sky conditions at Lampedusa were monitored by the TSI-440 sky imager, collecting hemispheric pictures every minute. The absence of clouds during the flights is also confirmed by the time series of downward SW, LW and WINDOW irradiances, and by the information provided by the zenith-looking pyrometer and lidar at the surface. The profiles of downward LW irradiance from airborne radiometers also show that clouds were not detected: indeed the signal due to cloud emission would have been evident in the measurements with positive spikes, like those in Figure 2.
A sentence has been added to the description of Figure 2, to highlight the large increase in irradiance/BT due to cloud presence.

Specific Comments
1. Page 1, line 28: define IASI acronym.
The acronym has been defined.

2. Page 4, Figure 1: the AERONET AOD may also be overplotted.
We received a comment from Reviewer #1 saying that we presented many instruments but some of them were not used in the analysis, and he/she suggested to describe only instruments and measurements that were actually used. We used MFRSR AOD measurements because of their higher temporal resolution (about 1 minute) compared to that of the Cimel sunphotometer (about 15 minutes). Moreover, some Cimel data are missing because of some malfunctioning of the instrument.
However, di Sarra et al., Empirical correction of MFRSR aerosol optical depths for the aerosol forward scattering and development of a long-term integrated MFRSR-Cimel dataset at Lampedusa, Appl. Optics, 54, 2725-2737, 2015, compare MFRSR and AERONET AOD measurements, deriving a mean bias in AOD not larger than 0.004 and a root mean square difference $\leq$0.031 at all wavelengths. Plotting the available AERONET AOD with the MFRSR AOD would require some discussion. Since the paper is already long we prefer not to add the AERONET AOD measurements.

3. Page 4, line 18: the reported angstrom exponent is high, it is about the maximum one; give a more realistic value (range).
During the first days of the campaign (17-20 June) the Ångström exponent is between 0.3 and 1.75.
The text has been modified accordingly.

4. Page 5, lines 32-35: why? Please explain.
Figure 1 of the paper by Gröbner, J., Wacker, S., Vuilleumier, L., and Kämpfer, N.: Effective atmospheric boundary layer temperature from longwave radiation measurements, J. Geophys. Res., 114, D19116, doi:10.1029/2009JD012274, 2009 is very explicative. 99% of the downward LW irradiance comes from the lowest atmospheric layers, those where most of the water vapour is concentrated. The atmosphere is nearly transparent in the 8-14 μm spectral range, and the radiation in the interval is emitted from the upper layers.

5. Page 5, lines 35-37, "The pyrometer . . . for the IRP BT": this sentence is oversimplified. A quick look at the 3 figures reveals significant differences between BT and irradiances. For example, what happens in June 24 and 25 (when LW-WINDOW curves do not have peaks, opposite to IRP BT)? What about the role of temperature and clouds?
The pyrometer has a narrow field of view (2.6°), the broadband CGR4 has 180° and the CGR3 has 150° FOV. So the pyrometer is able to detect each single cloud entering its FOV, while the same single cloud can have a minor impact on the LW-WINDOW irradiance measured by radiometers with broad FOVs if the rest of the sky is cloud-free. That is the reason why the IRP BT time series has more peaks than irradiances time series.

6. Page 7, line 7: define FWHM acronym.
The acronym has been defined in the revised text.

7. Page 7, line 30: up to which altitudes? How much the use of standard profiles can affect the radiative fluxes? Was any sensitivity study performed to assess this? Especially the LW fluxes should be sensitive.
The standard mid-latitude profiles have been used above the maximum altitude of the radiosounding on 28 June and 3 July, i.e. above 32 km and 26 km, respectively. The surface, as well as the profiles, irradiances and BT are not sensitive to variations of upper level atmospheric profiles.
In the revised manuscript a sensitivity study of the modelled quantities has been performed with respect to the main parameters affecting infrared radiation, either in aerosol-free conditions (i.e. IWV, temperature profile, SST, and surface emission) and with aerosol (we have tested the sensitivity to AOD and to the imaginary part of the dust refractive index).
An increase of 0.3 K in the temperature profile causes a 2.2 Wm^{-2} increase in downward LW irradiance at the surface, decreasing for increasing altitudes (becoming 1.3 Wm^{-2} at the ATR-42 top altitude of 5.7 km, and 0.6 Wm^{-2} at the Falcon 20 altitude of 10 km). The upward LW irradiance increases by 1.8 Wm^{-2} at 5.7 km, by 1.5 Wm^{-2} at 10 km, and by 1.4 Wm^{-2} at the TOA.

8. Page 7, line 33, regarding the absorbing gases: similarly, it would be worth to discuss/assess the sensitivity of fluxes to these parameters, especially given the scaling applied to their vertically distributed values.
The sensitivity of the irradiance to changes in the integrated water vapour has been tested by increasing the average measured value by its uncertainty (+0.2 mm), which is of the same order of magnitude of the IWV standard deviation within the considered time interval.
The downward LW irradiance increases by 0.4 Wm^{-2} at the surface, by 0.1 Wm^{-2} at 5.7 km, and by 0.06 Wm^{-2} at 10 km, while the upward LW irradiance at the TOA decreases by 0.1 Wm^{-2}.
The sensitivity to other absorbing aerosols has not been tested.

9. Page 8, about ECMWF: The use of reanalysis data is inevitable in this case. However, an assessment of the induced uncertainties associated with their coarser resolution could be made by comparing similar ECMWF data with available measurements for the other two days. This could provide an estimation of induced uncertainties in June 22.

As suggested by the reviewer, the ECMWF profiles at 12:00 have been compared with the temperature and relative humidity profiles measured by the radiosonde and by the airborne meteorological instruments. The T profile is well reproduced on both days, although the ECMWF profiles does not capture the fine vertical structures due its vertical resolution. An exception is the atmosphere below 4 km on 28 June, where the profile sounded by the ATR-42 presents lower temperatures compared to that of the ECMWF profile. The RH profile of the ECMWF operational model generally follows the measurements, but differences can be large at certain levels, like around 3 km on 3 July.

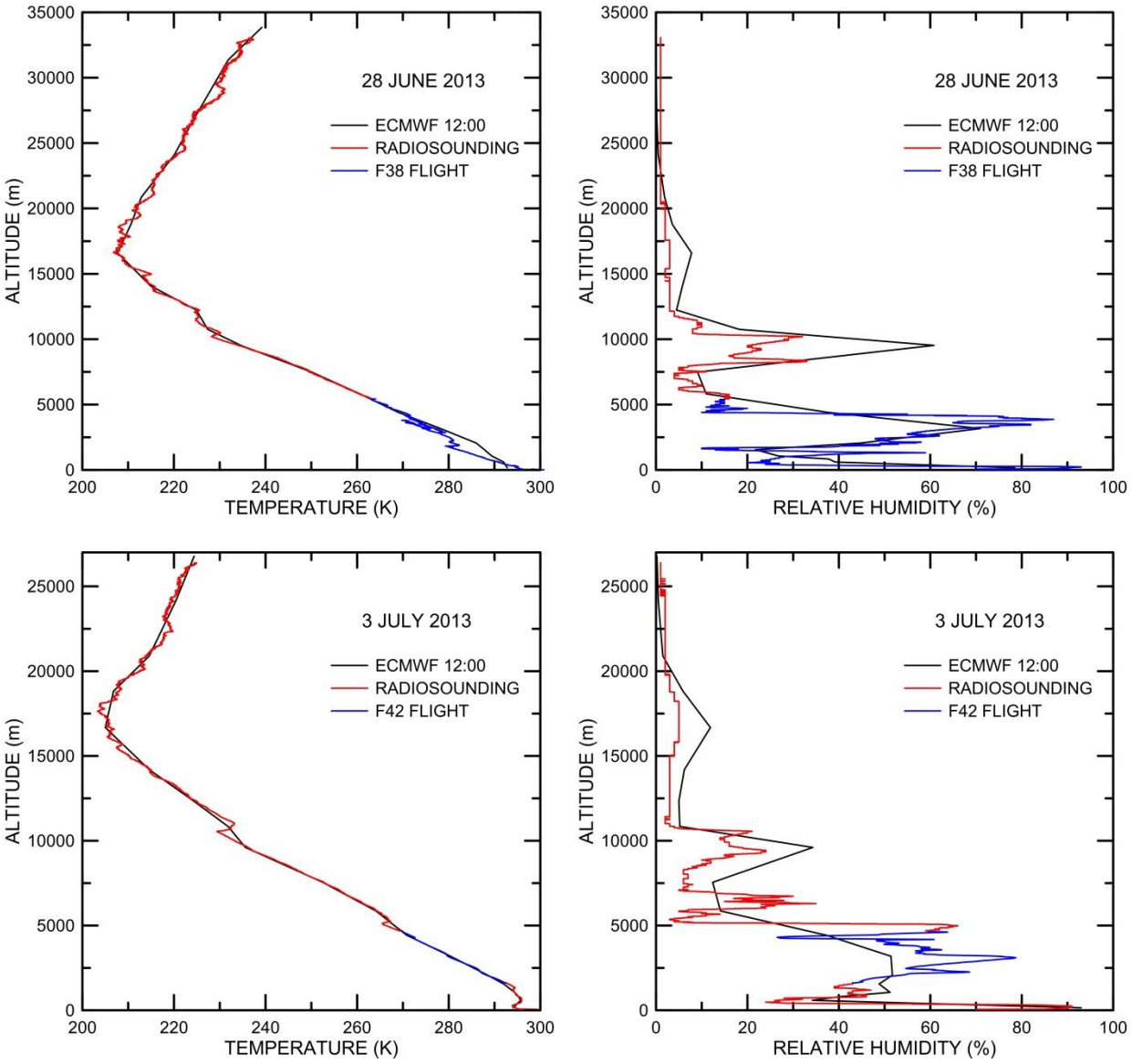

10. Page 8, line 10: a few words about the measured aerosol properties and the identified aerosol layers can be added. For example, apart from the layers and their extension neither information is given nor reference is made to the type of aerosols in each layer, with reference to corresponding measurements that cloud provide this kind of information.

A short discussion on the aerosol stratification identified by the airborne measurements and by the airmass back trajectory analyses has been included in Sections 3.1 and 3.1.1. A detailed analysis is presented in the paper by Denjean et al. (2016).

11. Page 8, line 14: so, what values of emissivity were assumed in the study? Do they differ and how much from day to day.
The values are the same for all the three cases because surface wind speeds are similar. A sentence has been added in the text to better explain, and some spectral values are included.

12. Page 8, Figure 4: the quality should be improved, e.g. by thicknenning the curves, so that the coloured curves can be more easily discerned.
The quality of the figure has been improved.

13. Page 8, line 29: As mentioned, different factors influence and differentiate the AERONET and in-situ SDs, one important being their different value, .e. columnar versus vertically resolved. The value of detailed measurements is that they provide vertically resolved SDs. Therefore, emphasis should be given to them. Discuss a bit more how the measured SDs differ to AERONET ones, referring to their agreement and disagreement. For example, larger differences appear in June 22 than in July 03. Refer to this difference referring to the nature of vertical profiles of Fig. 3 and the type of aerosols that are present in the different layers of every daily profile.
Table S1 has been produced as Supplement Material with the median radius, standard deviation, and normalized number concentration for each mode of either the AERONET and the *in situ* log-normal size distributions for the layers identified in the three cases. The differences in SD among the various layers have been discussed further, as suggested by the reviewer, and related to the transport pathways and to the mixing of dust with pollution particles.

14. Page 9, line 19: explain why this choice of water soluble RI was made and not any other.
Polluted maritime aerosol is the most probable aerosol type characterizing the lowest atmospheric layers over Lampedusa. This is supported by the analysis of the airmass back trajectories in the boundary layer, showing airmasses originating from Europe or recirculating within the Mediterranean basis, and from the chemical analyses carried out on the aerosol samples (Denjean et al., 2016). Water soluble is one of the components of the maritime aerosol, either clean and polluted, according to the OPAC definitions (see Hess et al., 1998). The other components are sea-salt and soot (on for the polluted maritime). Among the components, water soluble and sea salt have similar values of the imaginary part of the RIs below 8 µm and above 11 µm, while the water soluble is more absorbing than sea salt in the 8-11 µm interval. The RI of soot is too absorbing to be representative of the average aerosol. For these reasons the water soluble RI has been chosen.

15. Page 9, lines 20-26: Table 2 is not discussed enough. It should be said more clearly what exactly has been done and how the Mie-based computations of AOD compare to AERONET ones, whenever applicable, i.e. in visible wavelengths.
The combination of the SDs and RIs for the three flights has been better clarified in a new version of Table 2, which includes three tables (one for each flight), describing the SD and RI used in each aerosol layer identified by the ATR-42 and lidar vertical profiles. Moreover, the choice of the different RIs has been better explained in Section 3.1.1.
The spectral AOPs (extinction coefficient, absorption coefficient) accepted by MODTRAN are all referred to the extinction coefficient at 550 nm, for which the vertical distribution, $ext_{550}(z)$, is derived from the lidar backscatter profile and AOD measurements.
So the AOD at 550 nm is fixed, and corresponds to the value obtained from the MFRSR measurements at 500 and 868 nm using the Ångström law. AOPs are allowed to differ in no more than four aerosol layers in the troposphere.
We compute the spectral AOPs from Mie theory for a single particle in a wavelength grid from 2 to 100 µm and including 550 nm, and then divide them by the calculated extinction coefficient at 550 nm. So we have:

$$ext_\lambda(z) = \frac{ext_\lambda(z)}{ext_{550}(z)}$$
$$abs_\lambda(z) = \frac{abs_\lambda(z)}{ext_{550}(z)}$$

This ensures that the values of the AOD at 550 nm remain constant, whatever the AOPs.

16. Page 10, lines 16-17: does this refer to July 03? In Table 3 no results for INSU2 are displayed.
The sentence originally referred to 22 June. Section 4.1 has been modified in order to be clearer for the reader.

17. Page 10, lines 19-20: why the stronger infrared emission? Is it a matter of larger mass? Please explain.
For a particle with diameter D the absorption (and emission according to Kirchhoff law) and scattering properties are calculated with the Mie theory if D is of the same order of magnitude of the wavelength, as is the case for dust particles in the infrared spectral region. According to Mie theory, the absorption and scattering efficiency ($Q_{abs,ext}$) depend on the complex refractive index and on D and the absorption and scattering coefficient ($\sigma_{abs,ext}$) are proportional to Q and to the particle's cross section πD^2. Thus increasing the particles' dimension increases the absorption and emission coefficient.

18. Page 10, line 24: clarify that "all cases" refer to LW, WINDOW and IR BT.
"all cases" refers to the three days.

19. Page 10, line 34: here it should be clarified what is exactly the spectral interval/coverage of the measurements (IRP). This not clear based on what is said in page 7, line 6, about the IRP centered at 3 wavelengths etc. It is essential to clarify what is exactly the spectral coverage of measurements since they are used as the reference to which the simulations are compared, and given the significant sensitivity of theoretical computations to the spectral interval. Also explain why the reduction in WINDOW irradiances has different magnitude despite the same spectral reduction (0.4 microns) in different spectral parts.
The infrared pyrometer (IRP) measures the zenith BT in the 9.6-11.5 µm interval, while the CLIMAT measures the nadir BT in three infrared channels centred at 8.7, 10.6, and 12 µm with about 1 µm full width at half maximum. The sentence on page 10, line 34, refers to the WINDOW irradiance, measured by the PMOD/WRC CGR3 modified pyrgeometer, which is sensitive to the radiation in the 8-14 µm spectral interval.
The sensitivity analysis carried out on the WINDOW irradiance shows that reducing the spectral interval by a small amount (0.4 µm) significantly reduces the downward irradiance, and the reduction depends on where in the spectrum the reduction is operated: this is caused by the asymmetry of the irradiance spectrum with respect to the centre of the interval.

20. Section 4.1: what is missing is a critical approach providing insight into possible physical reasons for better agreement between the 7 examined cases. A quite exhaustive and very detailed description of results is made, referring to various numbers (Table 3). This is not enough while it turns to be confusing to the reader. What is more important is to determine which set of AOPs is more efficient and compared better to the measurements for the 3 cases. The discussion should conclude on this, stating at least if there is a "best" choice or if there is not and why. Moreover, in both cases, the discussion should provide a physical basis for the outcome of the analysis and the closure of Table 3. For example, a summary of the results of Table 3 should point to NOAER being the most efficient simulation, providing better results than the other 6 sets of AOPs in 4 cases (out of totally 9, i.e. 3 days by 3 parameters). NOAER is followed by COL1 (3 cases with best performance) and INSU3 (2 cases). So, questions may arise, like why simulations without aerosols

should be more appropriate/realistic, or why INSU3, which may be expected to be the most realistic, is finally not.
Section 4.1 has been modified to better present the results and the conclusions. We state that for the conditions met during the campaign, with moderate and not really large AOD, the surface irradiances are not useful to reduce the uncertainty on the dust RI, since the impact of different RIs is below the measurement and model uncertainty. This also explains why NOAER simulations agree with measurements within their respective uncertainties. On the contrary, narrowband zenith BT seems to be suitable to constrain the dust RI which better represents the dust optical properties either in moderate and in low dust loading conditions, assuming that the *in situ* airborne measurements better describes the local aerosol distribution. Indeed, in the two cases where the atmospheric meteorological profiles and the *in situ* SD are measured down to surface level (22 and 28 June) the zenith BT is well reproduced with the DB2017 RIs.

21. Page 12, line 3: as to upward LW, authors may want to comment on why the smallest differences are for COL1 in Table 5, while the smallest RMSDs in Table 4 are for INSU1.
Tables 4 and 5 show that the upward LW irradiance at Falcon 20 and ATR-42 altitudes is reproduced within model and measurement uncertainties with all AOPs, including the NOAER case. The fact that COL1 AOPs give the best match with Falcon 20 measurements while INSU1 AOPs provide the best agreement with the ATR-42 ones may be attributed to different reasons: among them, the Falcon 20 passage is not exactly simultaneous with the ATR-42; the Falcon 20 simulations may be affected by the ECMWF temperature/humidity profile above 6 km, while the ATR-42 upward irradiance rely on the *in situ* measurements of the meteorological vertical profiles.

22. Figure 7: why only points for NOAER, COL1 and INSU3 are given and not for the other cases? All these appear in Table 6.
Overlapping the points corresponding to all AOPs would have made the Figure 7 very difficult to read. After the reviewer's suggestion, we have considered that presenting the results of COL3, instead of COL1, may be better to show the dust perturbation compared to NOAER and the effect of changing the SD, but not the RI, compared to INSU3. The estimated uncertainties on the calculated BTs are also shown.

23. Page 12, lines 15-16: add "in-situ" before SD. This sentence needs to be re-written, since it is introduced all suddenly without being given evidence and discussed based on the results of Fig. 7.
The sentence has been modified as follows: "These results show the better sensitivity of BT to dust optical properties than broadband irradiance. When considering that *in situ* SD better represents the local aerosol distribution, the DB2017 RI from Algeria and Morocco provide the best model-measurement agreement".

24. Page 12, lines 17-19: while discussion is made no results are shown/given.
This comment is not clear. Figure 6 for the upward LW irradiance and Figure 7 for the CLIMAT BTs show that model simulations with and without aerosols are overlapped below 4 km, and differ at higher altitudes, where the aerosol effect is discernible. Moreover, the differences in BT due to dust compared to the aerosol-free simulations are provided on page 12, lines 19-20.

25. Section 4.2.1: A quite exhaustive discussion is made making frequent reference to numbers that differ a while between the 6 examined cases. Also the question arises why NOAER sometimes performs equally or better than dust-including cases. It could point to potential artifacts due to counteracting effects of other parameters than aerosol, which affect the LW radiation transfer and BT.

The limited aerosol effect is due to the moderate AOD measured during the flights and not to modelling problems, and this is the reason why in some cases (more often for the irradiance but not for the BT) the NOAER simulations agree with measurements. This aspect has been remarked in the revised manuscript (Sections 4.1, 4.2.1, and in the conclusions).

26. Page 12, lines 35-36, "These differences . . . airborne instrumentations": so is there an inherent problem with the model?
We cannot state that there is problem with the model, because the same input parameters allow to fairly reproduce the CLIMAT BTs. Moreover, the LW irradiance is well reproduced below 2000 m and above 4000 m and at the Falcon20 altitude. As discussed, a possible bias in the CGR4 measurements may be found when the air temperature is fastly changing, due to inhomogeneities in the instrument temperature. For example the ATR-42 path (Figure 4b) shows a steep aircraft fall from 3.5 km to 1.2 km. A rapid decrease in altitude, with a consequent increase in temperature, may be not registered by the pyrgeometer, which has 6 seconds response time (1/e), but needs a longer time to establish equilibrium with the ambient air temperature (as also found by Albrecht et al., Pyrgeometer measurements from aircraft, Rev. Sci. Instrum., 45, 33–38, 1974). The same problem may have affected the irradiance measurements on 3 July. This may also explain the slight overestimation of the downward LW irradiance by the model in the same altitude ranges where the upward component is overestimated. The CLIMAT BT measurements is not expected to suffer from the same problem because the response time of the instrument is much faster (about 160 ms).

27. Page 14, line 20" add "was" before "evaluated".
Done.

28. Page 14, line 21, "resampled": how it was done?
IASI spectra have been averaged in 15 cm^{-1} intervals. The first interval is centred at 652.5 cm^{-1} and includes the BT values between 645.0 and 660.0, the second interval is centred at 667.5 cm^{-1}, and so on.

29. Page 14, lines 32-37: why there is difference on what provides the best match with reference to best match with the measured spectra and BTs?
The IASI spectra used in the comparison with the model are averaged over a region, instead of instantaneous measurements like those from CLIMAT. Moreover, IASI and CLIMAT measurements are not simultaneous. Finally, measurements are made over different spectral intervals, and the AOPs producing the best agreement with the mode result may somewhat differ. This has been stated in the text.

30. Page 15, lines 2-3: this is not applicable to 780-980/cm for June 22 and 28.
The sentence states that when the AOD is sufficiently large the aerosol perturbation to the BT simulated in aerosol-free conditions is significant, so this does not apply for the 28 June case. About 22 June, this applies clearly to the 1070-1200 cm^{-1} interval for different AOPs, and only for the COL1 combination in the 780-980 cm^{-1} interval.

31. Page 15, lines 20-22, "In our case, . . . AOPs equivalent.": what exactly is it meant by this? By which means. Please explain. Is it implied that this (having very high resolution) is preferable? If so, why? If valid, it would mean that AOPs are not important for accurately computing LW radiation and dust LW radiative effects. Is this the meaning?
The sentence refers to the fact that MODTRAN resolution (0.1 cm^{-1}) is lower than that of the IASI measurements and of the σ-IASI-as radiative transfer model (0.01 cm^{-1}), so we do not expect model-measurements differences as low as those found by Liuzzi et al. (2017). The sentence has been eliminated and text has been modified, also to answer to Reviewer #1, as follows: "The

limitation in the MODTRAN5 resolution does not allow to reproduce the high resolution IASI spectra: however, the scope of simulating the IASI measurements is to show that TOA BTs are sensitive to the dust presence and to the various AOPs, and that they can be reproduced with the same input parameters that allow to simulate irradiance and BT at the surface and in the atmosphere.".

32. Page 15, line 28, "The combination . . . downward": this is not clearly evidenced in the discussion of sections 4.1 and 4.2.
The sentence has been moved at the end of Section 4.2.

33. Page 26, Table 2: the Table needs further/better explanation, it is not very easy for the reader to understand what exactly is the information given in this Table.
We agree with the reviewer. A new Table 2 has been prepared, which includes three tables, one for each day. The tables present the combination of SD and RI used in each layer identified by the lidar and ATR-42 measurements, and the AOD value at 8.6 μm.

34. Page 37, Figure 5: what have been the criteria for the design of flight paths.? Nothing is said about this and deserves to be mentioned in the text.
This aspect has been treated in Section 2.1(Aircraft strategy) of the paper by Denjean et al. (2016). In particular the following text explains the flight strategy: "The general flight strategy consisted of two main parts. First, profiles from 300m up to 6 km above sea level (a.s.l.) were conducted by performing a spiral trajectory 10–20 km wide to sound the vertical structure of the atmosphere and identify interesting dust layers. Afterwards, the identified dust layers were probed by straight levelled runs (SLRs), where the aircraft flew at fixed altitudes, to provide information on dust spatial variability and properties. Horizontal flight legs in the dust layers lasted 20–40 min to allow aerosol collection on filters for chemical analyses in the laboratory".
The sentence "The ATR-42 sounded the atmosphere during profile descents and ascents to infer the vertical structure and composition and identify layers with different properties" in Section 2.2 clarifies the criteria beyond the flight paths.

35. Page 44, Figure 12: wavelengths could be added, e.g. on the top x-axis.
The top x-axis has been expressed in wavelength units, as suggest by the reviewer.

Determining the infrared radiative effects of Saharan dust: a radiative transfer modelling study based on vertically resolved measurements at Lampedusa

Daniela Meloni[1], Alcide di Sarra[1], Gérard Brogniez[2], Cyrielle Denjean[3,4], Lorenzo De Silvestri[1], Tatiana Di Iorio[1], Paola Formenti[3], José L. Gómez-Amo[5], Julian Gröbner[6], Natalia Kouremeti[6], Giuliano Liuzzi[7], Marc Mallet[8], Giandomenico Pace[1], Damiano M. Sferlazzo[9]

Correspondence to: Daniela Meloni (daniela.meloni@enea.it)

[1]Laboratory for Observations and Analyses of Earth and Climate, ENEA, Rome, Via Anguillarese 301, 00123, Italy
[2]Laboratoire d'Optique Atmosphérique, University of Lille 1, France
[3]Laboratoire Interuniversitaire des Systèmes Atmosphériques, UMR-CNRS 7583, Université Paris-Est-Créteil et Université Paris Diderot, Institut Pierre Simon Laplace, France
[4]now at Centre National de Recherches Météorologiques, UMR 3589, CNRS, Météo-France, Toulouse, France
[5]Departament de Física de la Terra y Termodinàmica, Universitat de València, Spain
[6]Physikalisch-Meteorologisches Observatorium Davos/World Radiation Center, Davos Dorf, Dorfstrasse 33, 7260, Switzerland
[7]School of Engineering, University of Basilicata, Potenza, Via dell'Ateneo Lucano 10, Italy
[8]CNRM UMR 3589, Météo-France/CNRS, Toulouse, France
[9]Laboratory for Observations and Analyses of Earth and Climate, ENEA, Lampedusa, Contrada Capo Grecale, 92010, Italy

Abstract. Detailed atmospheric and aerosol properties, and radiation measurements were carried out in summer 2013 during the Aerosol Direct Radiative Impact on the regional climate in the MEDiterranean region (ADRIMED) campaign in the framework of the Chemistry-Aerosol Mediterranean Experiment (ChArMEx) experiment. This study focusses on the characterization of infrared (IR) optical properties and direct radiative effects of mineral dust, based on three vertical profiles of atmospheric and aerosol properties and IR broadband and narrowband radiation from airborne measurements, made in conjunction with radiosonde and ground-based observations at Lampedusa, in the central Mediterranean. Satellite IR spectra from the Infrared Atmospheric Sounder Interferometer (IASI) are also included in the analysis. The atmospheric and aerosol properties are used as input to a radiative transfer model, and various IR radiation parameters (upward and downward irradiance, nadir and zenith brightness temperature at different altitudes) are calculated and compared with observations. The model calculations are made for different sets of dust size distribution (SD) and refractive index (RI)~~ices~~, derived from observations and from the literature. The main results of the analysis are that the IR dust radiative forcing is non negligible, and strongly depends on ~~size distribution (SD)~~SD and ~~refractive index (RI)~~RI. When calculations are made using the *in situ* measured size distribution, it is possible to identify the refractive index that produces the best match with observed IR irradiances and brightness temperatures (BTs). The most appropriate refractive indices correspond to those determined from independent measurements of mineral dust aerosols from the source regions (Tunisia, Algeria, Morocco) of dust transported over Lampedusa, suggesting that differences in the source properties should be taken into account. With the *in situ* size distribution and the most appropriate refractive index the estimated dust IR radiative forcing efficiency is +23.7 W m^{-2} at the surface, -7.9 W m^{-2} within the atmosphere, and +15.8 W m^{-2} at the top of the atmosphere. The use of column integrated dust SD from AERONET may also produce a good agreement with measured irradiances and BTs, but

with significantly different values of the RI. This implies large differences, up to a factor of 2.5 at surface, in the estimated dust radiative forcing, and in the IR heating rate. This study shows that spectrally resolved measurements of ~~brightness temperatures~~BTs are important to better constrain the dust IR optical properties, and to obtain a reliable estimate of its radiative effects. Efforts should be directed at obtaining an improved description of the dust size distribution, its vertical distribution, and at including regionally-resolved optical properties.

1 Introduction

Aerosol radiative effects in the infrared or longwave (LW) spectral range have been recognized to be non-negligible compared to that in the solar region for large particles like marine aerosols (e.g. Markowicz et al., 2003) and desert dust (e.g. Vogelmann et al., 2003; Otto et al., 2007; Osborne et al., 2011; di Sarra et al., 2011; Sicard et al., 2014; Meloni et al., 2015 and references therein). The major uncertainty affecting the LW aerosol direct radiative effect (ARF) is due to the poor knowledge of the ~~infrared~~ IR aerosol optical properties, i.e. the aerosol optical depth, single scattering albedo and phase function.

Desert dust has the largest capability to perturb the IR radiative field, due to the particles' large size and the abundance at the global level, which peaks in the arid regions and their surroundings (Prospero et al., 2002; Ginoux et al., 2012).

Several field campaigns worldwide have been devoted to study the dust microphysical, chemical, and optical properties, with a focus in the infrared radiative effects: Saharan Dust Experiment, SHADE (Highwood et al., 2003), Radiative Atmospheric Divergence using Atmospheric Radiation Measurement (ARM) Mobile Facility, Geostationary Earth Radiation Budget (GERB) data, and African Monsoon Multidisciplinary Analysis (AMMA) stations, RADAGAST (Slingo et al., 2008), Saharan Mineral Dust Experiment, SAMUM (Ansmann et al., 2011), Geostationary Earth Radiation Budget Intercomparison of Longwave and Shortwave radiation, GERBILS (Haywood et al., 2011), NASA AMMA, NAMMA (Hansell et al., 2010), carried out in Africa, Asian Pacific Regional Aerosol Characterization Experiment, ACE-Asia (Seinfeld et al., 2004), and the Asian Monsoon Years field experiment (Hansell et al., 2012) in Asia. Most of these studies have been carried out close to the dust source regions and did not take into account the possible modifications in dust optical properties during long range transport. Other papers (e.g. Maring et al., 2003; Ryder et al., 2013; Weinzierl et al., 2017) examine the microphysical and/or chemical and/or optical properties of transported dust through the Atlantic Ocean.

A great improvement in the detection of dust in terms of spatial and temporal coverage has been reached after the development of specific algorithms applied to the thermal infrared (TIR) channels of satellite sensors, such as Meteosat (Legrand et al., 2001). More recently, the observations from multichannel sensors, such as MSG-SEVIRI (Schepanski et al., 2007; Brindley and Russell, 2009), high resolution spectrometers like Aqua-AIRS (De Souza-Machado et al., 2006), or interferometers like MetOp-IASI (Peyridieu et al., 2013) have been used to derive dust optical and microphysical properties, taking advantage of the spectral signature of dust in the IR (Clarisse et al., 2013; Cuesta et al., 2015~~; Sellitto et al., 2016~~). However, the algorithms developed to infer dust properties from measured ~~brightness temperatures (~~BT~~)~~ require that the spectral variation of aerosol extinction, which depends on the spectral complex ~~refractive index (~~RI~~)~~ and the particles' ~~size distribution (~~SD~~)~~ (Klüser et al., 2012), is known. Thus, understanding the impact of different aerosol optical properties (AOPs) on the infrared BT is crucial for the satellite retrieval. Similarly, IR aerosol optical properties are crucial in determining the LW dust radiative effects in the atmosphere and at the surface (e.g., Meloni et al., 2015).

The Mediterranean Sea is very often affected by dust intrusions from the close Sahara desert (Meloni et al., 2008; Israelevich et al., 2012; Gkikas et al., 2013) producing significant perturbations to the ~~SW~~ solar and the ~~LW~~ IR radiation balance (di Sarra et al., 2011; Perrone et al., 2012; Meloni et al., 2015).

Lampedusa island, in the southern portion of the Central Mediterranean, is close to the Tunisian coasts, and hosts the ENEA Station for Climate Observations (35.52° N, 12.63° E, 45 m above sea level), operational since 1997. Due to its position, the small area (22 km^2) and flat surface surrounded by open sea, Lampedusa is an ideal site for the monitoring of transported dust physical and chemical properties. Measurements of aerosol optical depth (AOD) and vertical distribution started in 1999 (Di Iorio et al., 2009; di Sarra et al., 2015); in 2000 Lampedusa became an AERONET (Holben et al., 2001) site. Measurements of downward broadband SW and LW irradiances were started in 2004 (di Sarra et al., 2008; Di Biagio et al., 2010), together with the collection of filters to derive PM10 concentration and chemical composition (Becagli et al., 2012; Marconi et al., 2014).

The Ground based and Airborne Measurements of Aerosol Radiative forcing (GAMARF) field campaign was focussed on the determination of the LW radiative effects of Saharan dust and took place in Lampedusa in spring 2008 (Meloni et al., 2015). The campaign took great advantage from the measured vertical profiles of aerosol SD and LW irradiance from an ultralight aircraft, allowing to derive vertically resolved ARF and aerosol heating rate (AHR) for a case of desert dust intrusion. Moreover, the sensitivity of the SW and LW ARF and AHR to different AOPs was examined.

More recently, Lampedusa also hosted one of the ground-based sites of the Aerosol Direct Radiative Impact on the regional climate in the MEDiterranean region (ADRIMED) field campaign within the Chemistry-Aerosol Mediterranean Experiment (ChArMEx, http://charmex.lsce.ipsl.fr). The ChArMEx/ADRIMED experiment was held from 11 June to 5 July 2013 (Mallet et al., 2016). It aimed at characterizing the different aerosol particles and their radiative effect using airborne and ground-based measurements collected in the western and central parts of the basin.

In particular, ChArMEx/ADRIMED deployed two aircrafts based at the Cagliari's airport (Italy), the ATR-42 and Falcon 20, operated by the Service des Avions Français Instrumentés pour la Recherche en Environnement (SAFIRE).

During the campaign, different Saharan dust intrusions were observed at Lampedusa, mainly from 22 to 28 June and from 2 to 4 July 2013.

In this paper, we present three case studies, selected to represent desert dust of different load and properties (mainly the vertical profile of the size distribution), and for which airborne measurements are available: 22 and 28 June, and 3 July.

This study contributes at understanding how AOPs determine the LW radiative effects at the surface, in the atmosphere and at the top of the atmosphere, based on the combination of remote sensing and *in situ* observations from the ground, from airborne sensors, and from space, and radiative transfer modelling.

The novel aspect of this study is that the closure experiment is carried out not only on LW irradiance, but also on infrared spectral BT. In particular, the impact of different AOPs on the nadir spectral radiances measured by the airborne Conveyable Low-Noise Infrared Radiometer for Measurements of Atmosphere and Ground Surface Targets (CLIMAT) on-board the ATR-42 and IASI and by a ground-based zenith pyrometer is investigated. To our knowledge, this is the first closure experiment carried out simultaneously modelling the observations of instruments with different spectral intervals and on different platforms.

This paper is organized as follows: an overview of the ground-based, airborne and satellite observations used in the study is given in Sect. 2. Section 3 describes the radiative transfer model set-up and output, with a focus on the choice of the adopted

aerosol optical properties, and the model sensitivity to the input parameters. The results of the model calculations and the comparison with measurements are presented in Sect. 4 in terms of surface irradiance and sky BT, airborne irradiance and BT profiles, and satellite spectral radiance at TOA, with associated uncertainties. Finally, the vertical profiles of ARF and AHR for the 22 June case are discussed.

2 Instruments and measurements

The complete list of the instruments deployed at Lampedusa during the campaign is provided by Mallet et al. (2016), while Denjean et al. (2016) describes the ATR- 42 airborne instruments. Here the instruments and measured parameters used for the radiative closure study are presented.

2.1 Surface observations

Measurements of AOD from the AERONET Cimel standard sunphotometer #172 are available after 17 June 2013, with some interruptions during the campaign. The Multi Filter Rotating Shadowband Radiometer (MFRSR) AOD measurements are also available for the whole time period. The Cimel sunphotometer was calibrated at the AERONET-EUROPE RIMA site in Valladolid just before the campaign, and again in January 2015. The MFRSR is regularly calibrated on site applying the Langley technique, and AOD measurements are corrected by means of empirical functions that take into account the forward scattering caused by desert dust particles, which were derived comparing about four years of simultaneous MFRSR and Cimel measurements at Lampedusa (di Sarra et al., 2015). Here the MFRSR AOD measurements are used because of their higher temporal resolution (about 1 minute) compared to that of the Cimel sunphotometer.

Figure 1 shows the time series of the MFRSR corrected AOD at 500 nm and of the Ångström exponent, α, calculated from the AOD at 500 and 870 nm. The first days of the campaign are characterized by low aerosol load (AOD at 500 nm below 0.15) and mainly small particles (most of the values of α ~~above 1.5~~between 0.7 and 1.75); since 20 June, the aerosol burden increases with a corresponding decrease in α, indicating the ~~arrival~~ intrusion of desert dust (Denjean et al., 2016). The peak AOD is reached on 22 June. In the following days the alternation of low and moderate AOD conditions occur, but with α values always below 1.5, suggesting a mixing of particles with different dimensions, including desert dust.

The estimated uncertainty on AOD from ~~a freshly calibrated and well maintained Cimel is ±0.01 for wavelengths larger than 440 nm and ±0.02 below 400 nm (Holben et al., 1998), while that of~~ the MFRSR is <0.02 for the typical conditions at Lampedusa (di Sarra et al., 2015).

The column volume SD is retrieved in 22 size bins between 0.05 and 15 µm (optically equivalent radius) from the Cimel sunphotometer radiance measurements by the inversion method of Dubovik and King (2000). The accuracy of the SD is estimated by Dubovik et al. (2002a) to be below 10% in the maxima and 35% in the minima for particle radii between 0.1 and 7 µm, increasing above 85% outside the interval. Level 2 quality assured inversion products are obtained only for AOD at 440 nm larger than 0.4: this is the case only for the Cimel SD retrieval on 3 July, while on 22 and 28 June Level 1.5 SDs are used.

Column-integrated water vapour (IWV) is obtained from the Humidity And Temperature PROfiler (HATPRO), a microwave radiometer developed by Radiometer Physics GmbH (Rose et al., 2005). The instrument measures the sky BT at the high and low-frequency wings of the absorption water vapour and oxygen complex, centred at 22.235 and 60

GHz, respectively. The IWV is derived from the observations in the vertical mode, carried out every second, with a ±0.2 mm uncertainty. Compared to Cimel sunphotometer, the HATPRO provides a much larger dataset with sensibly smaller uncertainties (±1.5 mm for the standard Cimel, according to Holben et al., 2001).

Direct, downward diffuse and global SW irradiance and downward LW irradiance are routinely monitored at Lampedusa. ~~The direct and downward global SW irradiances are measured with a Kipp&Zonen CHP1 pyrheliometer and a CMP21 pyranometer, respectively.~~ The ~~diffuse SW irradiance and the~~ downward LW irradiance ~~are~~ is measured with ~~an Eppley PSP pyranometer and~~ a Kipp&Zonen CGR4 pyrgeometer, mounted on a solar tracker with shading balls.

As additional instrumentation deployed during the campaign, the Arctic Radiation Budget Experiment (ARBEX) system from the Physikalisch-Meteorologisches Observatorium Davos/World Radiation Center (PMOD/WRC) was placed on the roof of the building. The ARBEX setup includes Kipp&Zonen CM22 and CM21 pyranometers for downward and upward SW irradiance and Eppley PIR and Kipp&Zonen CG4 pyrgeometers for downward and upward LW irradiance. A modified Kipp&Zonen CGR3 pyrgeometer only sensitive to the 8-14 µm band is also part of ARBEX. All radiometers were freshly calibrated: the modified pyrgeometer with the reference blackbody of the PMOD/WRC at Davos and the broadband ones by comparison with the respective World Standard Groups hosted by the PMOD/WRC in order to guarantee high quality measurements. The measurement uncertainties (one sigma) of a standard and of the modified pyrgeometer calibrated at the WRC are ±2.3 W m^{-2} and ±1 W m^{-2}, respectively (Gröbner et al., 2009). Considering the additional uncertainty associated to the data acquisition system (Meloni et al., 2012), an overall two sigma uncertainty on the broadband pyrgeometer measurements of ±5 W m^{-2} can be assumed. The CGR3 pyrgeometer was not shaded; laboratory tests have shown that solar leakage effects are negligible. ~~thus a correction was applied to the measurements in order to remove possible effects due to solar leakage, which was empirically estimated to be proportional to the SW irradiance. This correction causes and additional uncertainty to the CGR3 measurement, that was increased to ±3 W m^{-2} (one sigma)~~

The mean bias (with one standard deviation) between the ENEA and the PMOD/WRC pyrgeometers during nighttime periods between June and September 2013 is 1.4±1.2 W m^{-2}, i.e. within the threshold value of ±2 W m^{-2} defined by Philipona et al. (2001) for well-calibrated instruments.

A KT19.85 II Heitronics Infrared Radiation Pyrometer (IRP) measures the zenith sky BT in the 9.6-11.5 µm spectral interval with a narrow FOV (about 2.6°). The IRP accuracy is estimated as ±0.5 K plus 0.7% of the temperature difference between the instrument body and the observed target (IRP Operational Instructions, 2008). The total accuracy is estimated in ±1 K for the operational conditions of the campaign. The pyrometer is housed in a ventilated box to reduce the measurement degradation due to dirt deposition on the IRP window: for the same reason, the instrument looks at the zenith through a gold mirror. During the campaign the mirror was cleaned every day. The IRP measurements were started on 22 June.

Figure 2 shows the time evolution of the broadband LW irradiance, of the irradiance in the 8-14 µm interval (from now on the WINDOW irradiance), and the infrared zenith BT during the campaign. All quantities are modulated by the atmospheric temperature and humidity; large increases in the irradiance and BT values are due to clouds, whose radiative effect is much larger than that associated with aerosols. Although the LW and WINDOW curves follow similar paths, some differences exist due to the different sensitivity of the two instruments to water vapour: the broadband pyrgeometer is sensitive to both IWV and to the water vapour present in the lowest atmospheric layers, while the modified pyrgeometer is mostly sensitive to the IWV. The pyrometer has a minimum detection limit of 223 K, and lower BT values are cut. The BT behaviour

resembles that of the irradiances, although some differences are present and are attributed to the different instrumental FOVs, with a larger variability for the IRP BT.

Aerosol backscattering, depolarization, and colour ratio profiles at 532 and 1064 nm wavelengths ~~were~~ are obtained by a backscatter lidar developed by the University of Rome "La Sapienza" and ENEA, and operated at Lampedusa since 1998~~,~~. The source is a Nd:YAG solid state laser, while the receiving system is composed of various telescopes detecting different altitude ranges in order to retrieve the backscattered signal from about 50 m to the tropopause. The lidar system can be operated in full daylight conditions thanks to the use of narrowband filters and analog signal detection. The details about the instrument set up and the inversion technique are provided by Di Iorio et al. (2009).

Vaisala RS92 radiosondes were launched in conjunction with the flights (not available on 22 June). Top altitudes reached by the sondes were between 25.5 and 33 km.

2.2 Airborne observations

The ATR-42 and Falcon 20 flight tracks during the ADRIMED campaign are summarized in Mallet et al. (2016).

In particular, the ADRIMED flights reached Lampedusa during dusty conditions, on 22 and 28 June, and on 2 and 3 July. 22 June and 2 July were the days with the largest AOD values throughout the ADRIMED campaign. On 22 June a trough located between France and Italy caused the transport of dust aerosols over the central Mediterranean basin and to Lampedusa with southwesterly winds at 3 km height. In the following days an upper-level low developed over central Europe, inducing a westerly flow from Tunisia at 700 hPa, with near-surface northwesterly winds. On 3 July the well-established Azores anticyclone forced northwesterly winds over Lampedusa, thus contributing to dust transport in the area. The meteorological fields and the maps of dust concentration for the days of the flights are shown and discussed in Denjean et al. (2016), as well as the aircraft measurement strategy.

The ATR-42 sounded the atmosphere during ~~profile~~ descents and ascents to infer the vertical structure and composition and to identify layers with different properties; on 22 and 28 June the ATR-42 landed at Lampedusa airport where it refuelled prior to taking off. The Falcon 20 flew above the ATR-42, following paths at nearly constant altitudes. In this study, only data from the descent portions of the ATR-42 flights (respectively, profile F35 on 22 June, F38 on 28 June, and F42 on 3 July) are used, since during the ascents the aircraft attitude is seldom horizontal. The 2 July flight is not analysed since the altitude interval sounded by the ATR-42 is too small to allow radiative closure experiments.

Table 1 summarizes the time, average AOD and IWV, and altitudes of the ATR-42 descents and Falcon 20 flights around Lampedusa. The AOD at 500 nm and IWV are mean and standard deviation of the MFRSR and HATPRO measurements, respectively, within the time duration of the ATR-42 flights.

Aerosol microphysical and optical properties, thermodynamic state of the atmosphere, ozone concentration, downward and upward SW and LW irradiances are measured on-board the ATR-42. SW and LW radiation measurements are also available on-board the Falcon 20.

The aerosol SD at different altitudes in the diameter range 0.03-32 μm is obtained by combining measurements from the Ultra High Sensitivity Aerosol Spectrometer (UHSAS) in the 40-900 nm interval of the optical equivalent diameter, the Grimm 1.129 Optical Particle Counter for diameter sizes from 250 nm to 32 μm, and the Forward Scattering Spectrometer Probe (FSSP) model 300 in the size range 0.28-20 μm (see Denjean et al., 2016 for details). The UHSAS and FSSP spectrometers measure SDs in ambient RH conditions, thus accounting for the possible particle growth due to water uptake.

Denjean et al. (2016) used the measurements of the spectral scattering coefficient at 450, 550, and 770 nm and the derived scattering Ångström exponent calculated between 450 and 770 nm, together with the sub- and super-micron particles number concentrations, to show that dust particles were found in distinct layers, with variable concentrations of fine and coarse particles, mainly associated with airmass back-trajectories from Sahara (see discussion of Section 3.1.1).

The radiation instrumentation on-board the ATR-42 and the Falcon 20 includes ~~upward and downward looking~~ Kipp&Zonen CMP22 pyranometers and CGR4 pyrgeometers. The upward- and downward-~~-~~looking instruments are installed above and below the aircraft fuselage, respectively, and are aligned with the aircraft attitude, so that the instrument orientation is determined by the aircraft pitch, roll, and heading angle. The selection of the radiation measurements collected under horizontal position is described in Sect. 4.2. Instruments were calibrated in January 2013. On-board irradiance measurements have been corrected for ~~the aircraft attitude angles (pitch, roll, heading), taking into account also the solar zenith and azimuth angles and the aircraft latitude and longitude, according to Saunders et al. (1992). Other corrections account for the thermopile response time, the cosine effect, and~~ the temperature dependence of the radiometer's sensitivity (Saunders et al., 1992). The estimated expanded uncertainties for both components of the instantaneous LW irradiances is ±6 W m^{-2}, obtained taking into account the accuracy of the instrument's calibration and of the acquisition system, and the consistency of airborne measurements.

The airborne version of the CLIMAT infrared radiometer (Legrand et al., 2000; Brogniez et al., 2003; 2005; Sourdeval et al., 2012) is installed below the fuselage to measure the nadir BT in three channels centred at 8.7, 10.6, and 12 µm with about 1 µm Full Width at Half Maximum (FWHM) bandwidth and about 3° FOV. While the contribution of the O_3 absorption band at 9.6 µm should not affect the CLIMAT measurements in the three bands, the 12 µm channel may be influenced by water vapour and CO_2. The absolute accuracy of BT measurements derived from CLIMAT is about 0.1 K. The instrument was calibrated at the Laboratoire d'Optique Atmosphérique in Febraury 2013.

2.3 Satellite observations

The Infrared Atmospheric Sounder Interferometer (IASI) radiance spectra simultaneous to ground-based measurements have been selected. IASI (Hilton et al., 2012) flies on the two EUMETSAT MetOp A and B polar platforms, with an equator crossing local solar time for the descending node around 9:30 and 8:45, respectively. The interferometer measures the spectral interval from 645 to 2760 cm^{-1}, with a sampling interval of 0.25 cm^{-1} and an effective apodized resolution of 0.5 cm^{-1}, resulting in 8461 points per spectrum. The horizontal resolution at nadir is 12 km. The radiometric noise of IASI spectra is 0.123 K (in the band 780-980 cm^{-1}) and 0.137 K (in the band 1070-1200 cm^{-1}) (Serio et al., 2015).

Morning IASI spectra for the days of the campaign are selected in the region including Lampedusa, within the latitude/longitude range 35.0-36.0° N and 12.0-13.2° E. More details can be found in Liuzzi et al. (2017). Clear-sky FOVs are selected applying the Cumulative Discriminant Analysis approach (Amato et al., 2014); data contaminated by sun glint are removed.

3 Radiative transfer model

The MODTRAN release version 5.3 has been used to calculate spectral LW and WINDOW irradiances and BTs at the surface, at aircrafts altitudes, and up to the top of the atmosphere (TOA). The model band highest resolution is 0.2 cm^{-1},

allowing to generate accurate spectral transmittances, radiances, and irradiances from 0 to 55000 cm^{-1} (Berk et al., 2006; 2008; Anderson et al., 2009).

The DISORT (Stamnes et al., 1988) multiple scattering method with 8 streams with the fast and accurate correlated-k option is used for the simulations in the IR spectral region.

3.1 Model input parameters

Pressure, temperature, and relative humidity vertical profiles are obtained from the ATR-42 measurements. At altitudes above the aircraft flight, the radiosounding meteorological parameters and the AFGL standard midlatitude summer profile (Anderson et al., 1986) are used. The time corresponding to the radiosonde launch is reported in Table 1. AFGL profiles of the main absorbing gases (O_3, CH_4, N_2O, CO, CO_2,) are also adopted. The humidity profile is scaled according to the HATPRO IWV averaged over the flight portion, in order to take into account small differences in the radiosonde and the aircraft paths and time. Column ozone measured at the Station with a Brewer spectrophotometer is used to scale the vertical profile, while surface CO_2 mixing ratio measured with a Picarro G2401 analyser is input to translate the CO_2 AFGL profile.

The model vertical resolution used is 0.1 km from the surface to the ATR-42 top altitude (5.8 km on 22 June, 5.4 km on 28 June, 4.8 km on 3 July), 0.25 km up to 10 km, 1 km up to the radiosounding maximum altitude, and larger than 1 km above. Radiosoundings were not launched on 22 June, so data from the European Centre for Medium-Range Weather Forecasts (ECMWF) operational analyses are used, with a spatial resolution of 0.125° x 0.125°. The ECMWF profile closest to the flight F35 (12 UT) is used on 22 June above the ATR-42 altitudes.

The vertical aerosol extinction profile is derived from the lidar backscatter profile and AOD measurements as described in Di Iorio et al. (2009) and Meloni et al. (2015). Figure 3 shows the lidar extinction profile at 532 nm for the three selected cases and the layers identified by the *in situ* aerosol measurements (Denjean et al., 2016). Mineral dust was not detected in the boundary layer, but was found to be stratified in different layers, each one characterized by uniform spectral scattering coefficients and number concentrations of sub- and super-micron particles, so that a homogeneous SD in each layer can be supposed. For example, during flight F35 the vertical profiles show very distinct dust layers above and below 3.5 km, the upper one containing dust from central Algeria and the lower one carrying dust from the southeastern Morocco-southwestern Algeria region. During flight F38 the scattering Ångström exponent above 0.5 and below 1.0 suggests that dust is mixed with pollution particles from the Mediterranean Sea.

The infrared emissivity of the sea water from Masuda et al. (1988) has been assumed in the model simulations. The sea emissivity in the 3.5-~~18~~ 13 µm window region has been considered for a zenith view and for realistic wind speed. The value at ~~18~~ 13 µm is applied also at longer wavelengths. The average surface wind speed is 6.7 m/s for F35, 7.3 m/s for F38, and 4 m/s for F42, and the sea emissivity corresponding to the wind speed value of 5 m/s has been adopted for all days. The sea emissivity has a maximum at 11 µm (0.993) and minima at 4.0 and 13.0 µm (0.977).

Daily MODIS sea surface temperature (SST) data at 1 km resolution (Feldman and McClain, 2014) produced and distributed by the NASA Goddard Space Flight Centre's Ocean Color Data Processing System (OCDPS) have been used.

3.1.1 Aerosol optical properties

The AOPs required by the model are spectral extinction, single scattering albedo, and phase function at each layer. They have been computed by applying the Mie theory for spherical particles to the SD obtained from AERONET and from *in situ*

observations (Denjean et al., 2016), with different values of the complex RIs. ~~have been derived from AERONET observations, and from *in situ* measurements on the ATR-42 (Denjean et al., 2016).~~ Figure 4 presents the comparison of AERONET and *in situ* SDs for the three case studies, normalized to 1 particle cm^{-3}. The parameters of the log-normal SDs are reported in Table S1 in the Supplement. The *in situ* SDs within the dust layers (LAYER 3 for 22 June and LAYER2 for 3 July) are characterized by a larger number of particles in the largest mode (M4 in Table S1) compared with the AERONET SD. On 28 June the *in situ* SDs are characterized by lower radii compared to the AERONET SD. On all days the normalized number concentration corresponding to M4 mode increases with altitude. Dust particles from Algeria on 22 June (LAYER 3) and from Tunisia on 3 July (LAYER 2) present the largest median radius in M4 mode; however, the largest number concentration in found in the former day, thus having the dominant effect on the infrared radiation. On 28 June the median radii of the M4 mode on both layers are lower compared to those of the other two days, as expected when dust is mixed with pollution in the Mediterranean area.

It must be emphasized that a direct comparison of the different SDs is problematic as the AERONET SD is column averaged and is an optically effective distribution essentially derived in the visible spectral range. ~~–~~Moreover, there are limitations in the capability of correctly reproducing the behaviour of the large particles mode, which is primarily important in the desert dust case (see e.g., the smaller accuracy for large particles, Dubovik et al., 2002a). On the contrary, the *in situ* SD is vertically resolved, and thus takes into account differences in aerosol types. On the other hand, small scale effects related to the aircraft position and flight pattern may affect the applicability of the retrieved SD to a somewhat larger scale. Notwithstanding this possible limitation, the vertically resolved SD derived from *in situ* observations is assumed to the one better representing the real atmospheric aerosol, and is used as a reference in the model calculations.

Particles' sphericity is assumed in the analysis by Denjean et al. (2016), while the AERONET inversion algorithm that derives the aerosol SD includes spheroid-based parameterization of light scattering (Dubovik et al., 2002b).

No information about the infrared complex RI is available from direct measurements. The Optical Properties of Aerosol and Clouds (OPAC) database (Hess et al., 1998) is widely used as a reference of AOP in the solar and infrared spectral regions for the estimation of aerosol radiative effects (e.g. Gómez-Amo et al., 2014), as well as in the inversion of satellite observations (Klüser et al., 2012). The dust RI from Volz (1973) (Volz1973 from now on) is adopted in various climate models used to evaluate the global dust radiative effect (e.g. Balkanski et al., 2007; Miller et al., 2014).

Recent estimates of the complex refractive index of mineral dust in the infrared spectral region were obtained by Di Biagio et al. (2014a, 2014b; 2017) for different source regions of the world, including Sahara and Sahel deserts. In particular, Di Biagio et al. (2017) (from now on DB2017) retrieved the RI in the 2-16 μm interval for various samples of natural soil collected in Tunisia, Algeria, and Morocco, which are the most probable source regions of the dust particles detected during the ChArMex flights of this study. Indeed, by comparing air mass back trajectories and dust concentration maps, Denjean et al. (2016) have shown that dust particles were transported from these regions at different altitudes (for details see Table 1 of Denjean et al., 2016). More specifically, for flight F35 the dust layer above-3.5 km originated from southern Algeria, while the dust layer between 1.5 and 3.5 km was transported from southern Morocco. On 28 June (F38) dust came from Tunisia. On 3 July (F42) dust arriving at Lampedusa above 3 km altitude originated from Tunisia, while dust below 3 km altitude came from southern Morocco. For F35 the RI of Algerian dust from DB2017 is used in LAYER 3 and up to the top of the aerosol profile (see Figure 3), that of Moroccan dust in LAYER 2, and the OPAC water soluble RI for LAYER 1, i.e., below the dust layer, down to the surface. Similarly, the Tunisian dust RI from DB2017 is used for F38 flight in LAYER 2

and the OPAC water soluble one in LAYER 1. For F42 the Tunisian and the Moroccan dust RIs from DB2017 are used in LAYER 2 (and to the top of the aerosol profile) and LAYER1, respectively, and the OPAC water soluble RI below LAYER 1.

The methodology applied in DB2017 allows to estimate the dust RI with an accuracy of about 20% and for conditions resembling the sandblasting process responsible for the generation of dust in the real environment. Moreover, DB2017 suggest that the LW RI does not change due to loss of coarse particles during the transport of dust from the source region, thus enabling its applicability also to transported dust.

~~The infrared AOPs of dust are henceforth calculated by applying the Mie theory for spherical particles to SD obtained from the AERONET retrieval and the *in situ* observations, and the different RIs from OPAC, Volz1973, and DB2017.~~ The differences in the complex RI from OPAC, Volz1973, and the ~~full~~ group of dust particles studied in DB2017 and used in this study can be found in Fig. ~~12 of DB2017~~S1 in the Supplement. Moreover, the spectral AOPs (extinction coefficients normalized to the value at 550 nm, single scattering albedoes, and asymmetry factors) computed using the combination of SDs and RIs for each layer of the three profiles have been shown in the Supplement (Figures S2, S3, and S4).

~~Below the dust layer (i.e., below 1400 m for F35, below 1000 m for F38, and below 1600 m for F42), the AOPs are calculated using the AERONET and the *in situ* SD and the OPAC water soluble RI.~~

Table 2 summarizes the combination of SD (AERONET and *in situ*) and RI (OPAC, Volz1973, and DB2017) used to obtain the LW AOPs. The different combinations of SD and RI produce different values of the infrared AOD, reported also in Table 2 at 8.6 μm. The AOD at 8.6 μm is calculated from the MFRSR AOD at 500 nm and the ratio between the extinction coefficient at 8.6 μm and 500 nm obtained from the Mie calculations for each aerosol layer in Fig. 3. On F35 the AOD derived from the *in situ* SDs largely exceeds the AOD obtained with the AERONET SD (for example, by +151% for the OPAC RI). For a fixed SD, the AOD decreases when passing from OPAC to Volz1973 to DB2017 RI. The increase in AOD calculated with the *in situ* SD with respect to the AOD from AERONET SD is also evident for F38 and F42, corresponding to +126% and +81%, respectively.

3.2 Model outputs

The downward and upward broadband LW irradiances are calculated at the surface, at the different atmospheric levels, and at TOA for the different AOPs reported in Table 2. They are compared with the ATR-42, Falcon 20, and ground-based measurements~~, and with IASI satellite observations~~.

The CGR3 downward WINDOW irradiance is simulated by integrating the spectral irradiance over the 8-14 μm interval.

The IRP and CLIMAT BTs are obtained integrating the modelled spectral BTs in the respective channel intervals, while IASI BT at the TOA are simulated in the 645-2760 cm^{-1} (approximately 3.6-15.5 μm) spectral range.

The aerosol direct radiative forcing and aerosol heating rates profiles are calculated after simulation of net (downward minus upward) irradiances and heating rates with and without aerosols for each model vertical layer, as in Meloni et al. (2015):

$$ARF(z) = NET_{AER}(z) - NET_{NOAER}(z) \quad (1)$$

$$AHR(z) = -\frac{g}{C_p}\left[\frac{\Delta NET(z)}{\Delta p(z)}_{AER} - \frac{\Delta NET(z)}{\Delta p(z)}_{NOAER}\right] \quad (2)$$

where z is the altitude, NET is the net flux ~~(either SW and LW)~~ with and without aerosols, p is the atmospheric pressure, g the gravitational acceleration, C_p is the specific heat of dry air at constant pressure, ΔNET and Δp are vertical variations of NET and P, respectively.

The ARF of the atmosphere is defined as the difference of the ARF at TOA and at the surface.

ARF and AHR are estimated only for F35 case, which is characterized by the largest AOD at 500 nm, and thus by the largest LW radiative effects.

The aerosol dust forcing efficiency, ARFE, defined as the ARF per unit AOD at 500 nm, is also calculated at the surface, TOA, and in the atmosphere.

3.3 Uncertainty analysis

The sensitivity of the modelled infrared quantities to the main model input parameters has been investigated for aerosol-free and aerosol laden conditions with the aim of assessing the model uncertainty. The main model input parameters affecting infrared radiation in aerosol-free conditions have been considered (i.e., IWV, atmospheric temperature profile, SST, and surface emissivity). Each quantity has been perturbed one at a time by the amount of its uncertainty (+0.2 mm for IWV, +0.3 K for the temperature from the radiosonde, +0.4 K for the surface temperature). The total model uncertainty has been calculated as the quadratic sum of uncertainties associated with the variation of each parameter. When considering the uncertainty associated with model simulations which include aerosol, the aerosol optical properties that have been varied are the AOD at 550 nm and the dust RI. Flight F35 has been selected as reference case, with INSU3 AOPs. The AOD at 550 nm has been increased by +0.02 while the dust imaginary part of the dust refractive index has been increased by 20%, whatever the dust origin (either Algeria or Morocco).

The model LW irradiance uncertainty decreases with increasing altitude for both the downward and upward components. The estimated model uncertainty on the downward and upward LW irradiances at the surface is 2.2 and 2.0 W m^{-2} for simulations without and with aerosols, respectively. At the Falcon 20 altitude (about 10 km) the uncertainties are 0.6 and 1.5 W m^{-2} for the downward and upward component, respectively, for both simulations with and without aerosol. The upward LW irradiance uncertainty is 1.4 W m^{-2} at TOA, for simulations with and without aerosol. The estimated uncertainty on ARF is obtained by the combination of the above values, and is 4.2 W m^{-2} at the surface and 2.0 W m^{-2} at the TOA. The uncertainty on AHR is largest at about 4.5 km altitude (0.030 K day^{-1} with aerosol and 0.026 K day^{-1} without aerosol), and close to the surface (0.050 K day^{-1} with and without aerosol).

The uncertainty on the downward WINDOW irradiance is 0.9 and 0.6 W m^{-2}, with and without aerosol, respectively. The estimated uncertainty on the modelled zenith BT is 0.7 and 0.3 K, with and without aerosol, respectively.

The aerosol-free CLIMAT BT is much sensitive to SST and surface emission, with slightly larger values at 600 m (0.3 K) than at 5670 m (0.28 K). The overall uncertainty for the case with aerosol is 0.31 K at 600 m and 0.37 K at 5670 m.

The uncertainty on the spectral BT at TOA in the atmospheric window varies between 0.25 and 0.29 K in aerosol-free conditions, and between 0.32 and 0.50 K with aerosol.

4 Results and discussion

4.1 Surface irradiance and BT

Ground-based measurements of downward irradiance and BT have been averaged over a 10 minute interval around the time in which the ATR-42 reached the bottom atmospheric layers (see Table 1) or for the duration of the flight above Lampedusa on 3 July (14 minutes). The obtained LW and WINDOW irradiances and zenith sky BT in the 9.6-11.5 μm band are reported in Table 3. It is worth noting that the variability of the measured variables during the chosen time interval is much smaller than the measurement uncertainties. For example, on 22 June the standard deviation values are 0.2 Wm^{-2} for the LW irradiance, 0.3 Wm^{-2} for the WINDOW irradiance, and 0.1downward LW irradiances obtained in the aerosol-free simulations (NOAER) for the three days agree with measurements within their uncertainties: this is caused by the moderate AOD measured during the campaign and by the uncertainty associated with the measurement. The magnitude of the aerosol perturbation with respect to NOAER increases with the AOD. For the 22 June case (AOD at 500 nm of 0.36), the increase in LW irradiance at the surface due to dust is +4.8, 4.7, 3.3, 10.9, 10.6, and 8.1 W m^{-2} with COL1, COL2, COL3, INSU1, INSU2, and INSU3, respectively. For the 28 June case (AOD at 500 nm of 0.21) the values are +3.2, 1.7, 6.3, 5.1 W m^{-2} with COL1, COL3, INSU1, and INSU3.

The reasons for the largest (lower) perturbation of INSU1 (COL3) AOPs are twofold: the *in situ* SD of dust has generally a larger number or a larger median radius of the coarse fraction with respect to AERONET which implies a stronger infrared emission. On the other hand, the DB2017 RI is characterized by a smaller absorption than OPAC and Volz1973, which produces a smaller dust IR emission (see Table 2).

In all cases the AERONET SD is able to reproduce the downward LW irradiance with all RIs (COL1, COL2 and COL3). With the *in situ* SD all RIs produce larger irradiances than measurements on 22 June, while on 3 July the agreement with observations depends on the adopted dust RI: measurements are reproduced with DB2017 RI and overestimated with OPAC RI. On 28 June, the low AOD makes the model results coherent with measurements regardless of the aerosol properties, and the modelled quantities including aerosols are equivalent whatever the AOP.

The modelled WINDOW irradiance with aerosol is always overestimated, with the largest effect produced by the *in situ* SD. It is worth noting that the amount of the aerosol perturbation compared to the aerosol-free simulation is equal to that found for the LW irradiance for each AOP. As for the broadband LW, the WINDOW irradiance on 22 June can be reproduced with the AERONET SD: the RI yielding the largest (lowest) radiative effect is OPAC (DB2017). On 28 June the modelled WINDOW irradiance is within the measurement uncertainty for the NOAER and the COL3 AOPs, i.e. that providing the lowest radiative perturbation. On 3 July the modelled WINDOW irradiance is overestimated with all AOPs and measurements are reproduced only for the NOAER simulations. It should be pointed out that the irradiance in the 8-14 μm interval is very sensitive to the shape of the filter. A sensitive study has been performed reducing the spectral integration by 0.4 μm in different parts of the interval, i.e. considering the 8.2-13.8 μm, the 8.4-14 μm, and the 8-13.6 μm ranges. The INSU3 AOPs have been used for all cases. In all three cases the resulted WINDOW irradiances are considerably reduced (by 8.1, 7.1, and 9.3 W m^{-2}, respectively) with respect to the simulations in the 8-14 μm interval, and are close to the measured values within measurement uncertainty. These results show that for the atmospheric conditions met during the campaign the choice of the spectral interval for the CGR3 calibration may be critical. This aspect surely deserves a dedicated study, which is beyond the scope of the paper.

On 22 June the zenith BT estimated by the model with the AERONET SD is lower than observations, while is generally higher when calculations are made with the *in situ* SD. The combination of *in situ* SD and DB2017 refractive indices produces the best agreement with observations. A similar behaviour is found for 28 June.

The best agreement on 3 July for the zenith BT is obtained using the AERONET SD: the reason may be connected with the absence of *in situ* information on the SD below 1600 m. The same SD as in the 1600-3500 m layer has been assumed in the lowest layers. This assumption may imply inaccurate model simulations using the *in situ* SD. However, as for the first two cases, the simulation with the *in situ* SD with DB2017 RI (INSU3) is sufficiently compliant with the measured LW irradiance and is close to the IRP BT.

Meloni et al. (2015) compared measured and modelled LW irradiances at the surface for a case with low (0.14 on 5 May 2008) and a case with high (0.59 on 3 May 2008) AOD at 500 nm during the GAMARF campaign. Similarly to this work, the simulations were made using SDs derived from AERONET and from *in situ* airborne measurements. For both cases the differences between LW irradiance measurement and model calculations are within measurement uncertainty either without aerosols, and accounting for the aerosol effect with the AERONET and the *in situ* SD. The results of the comparison shown in Table 3 are consistent with those by Meloni et al. (2015): in fact, congruity with measurements is obtained either disregarding the aerosol presence, or including aerosols with the AERONET SD (whichever the RI) and with the *in situ* SD, but only on 28 June (all RI) and 3 July (DB2017 RI).

The final results of the analysis of the surface measurements show that irradiances, either broadband and in the 8-14 μm spectral interval, are not useful to reduce the uncertainty on the dust RI, since the impact of different RIs is below the measurement and model uncertainty. On the contrary, narrowband zenith BT seems to be suitable to constrain the dust RI which better represents the dust optical properties either in moderate and in low dust loading conditions. These results apply also taking into account the model uncertainty discussed in Section 3.1.1. Under the assumption that the *in situ* SD is the most representative of the real aerosol dimensions, the DB2017 RI provides the best agreement between model and measurements, for LW and WINDOW irradiances and sky BT in the two cases where the atmospheric meteorological profiles and the *in situ* SD are measured down to the surface level (22 and 28 June).

~~Ground-based measurements of downward irradiance and BT have been averaged over a 10-minute interval around the time in which the ATR-42 reached the bottom atmospheric layers (see Table 1). The obtained LW and WINDOW irradiances and zenith sky IR BT in the 9.6-11.5 μm band are reported in Table 3.~~

~~Compared to the aerosol-free simulations (NOAER), the smallest perturbation to the surface irradiance and sky BT is produced by the AERONET SD and DB2017 RI (COL3), while the largest effect is produced by INSU1 for all cases.~~ ~~In the two cases with larger AOD (22 June and 3 July) the AERONET SD is able to reproduce LW irradiance with all RIs (COL1, COL2 and COL3). With the *in situ* SD all RI produce larger irradiances than measurements on 22 June, while on 3 July the agreement with observations depends on the adopted dust RI. The OPAC and Volz1973 RIs (INSU1 and INSU2) produce an overestimate of the irradiances, larger than the measurement uncertainty. The model-measurement difference is within the measurement uncertainty when the DB2017 RI (INSU3) is used. The reasons are twofold: the *in situ* SD of dust has generally a larger number or a larger modal radius of the coarse fraction with respect to AERONET; this implies a stronger infrared emission. On the other hand, the DB2017 RI is characterized by a smaller absorption than OPAC and Volz1973, which produces a smaller dust emission (see Table 2).~~

~~On 28 June, the low AOD makes the model results coherent with measurements regardless of the aerosol properties.~~

~~Compared to the aerosol free simulations (NOAER), the smallest perturbation to the surface irradiance and sky BT is produced by the AERONET SD and DB2017 RI (COL3), while the largest effect is produced by INSU1 for all cases.~~

~~The modelled WINDOW irradiance with aerosol is always overestimated, with the largest overestimate corresponding with the *in situ* SD. As for the broadband LW, the WINDOW irradiance on 22 June can be reproduced with the AERONET SD: the RI yielding the largest (lowest) radiative effect is OPAC (DB2017). On 28 June the modelled WINDOW irradiance is within the measurement uncertainty for the NOAER and the COL3 AOP, i.e. that providing the lowest radiative perturbation. On 3 July the modelled WINDOW irradiance is overestimated with all AOPs and measurements are reproduced only for the NOAER simulations. It should be pointed out that the irradiance in the 8-14 μm interval is very sensitive to the shape of the filter. A sensitive study has been performed reducing the spectral integration by 0.4 μm in different parts of the interval, i.e. considering the 8.2-13.8 μm, the 8.4-14 μm, and the 8-13.6 μm ranges. The INSU3 AOPs have been used for all cases. In all three cases the resulted WINDOW irradiances are considerably reduced (by 8.1, 7.1, and 9.3 W m^{-2}, respectively) with respect to the simulations in the 8-14 μm interval, and are close to the measured values within measurement uncertainty. These results show that for the atmospheric conditions met during the campaign the choice of the spectral interval for the CGR3 calibration may be critical. This aspect surely deserves a dedicated study, which is beyond the scope of the paper.~~

~~On 22 June the zenith sky BT estimated by the model with the AERONET SD is lower than observations, while is generally higher when calculations are made with the *in situ* SD. The combination of *in situ* SD and DB2017 refractive indices produces the best agreement with observations. A similar behaviour is found for 28 June.~~

~~The best agreement on 3 July is obtained using the AERONET SD, either for the LW irradiance or for the BT: one possible reason is the absence of *in situ* information on the SD below 1600 m. The same SD as in the 1600-3500 m layer has been assumed in the lowest layers. This assumption may imply inaccurate model simulations using the *in situ* SD. However, as for the first two cases, the simulation with the *in situ* SD with DB2017 RI (INSU3) is sufficiently compliant with the measured LW irradiance and is close to the IRP BT.~~

~~Meloni et al. (2015) compared measured and modelled LW irradiances at the surface for a case with low (0.14 on 5 May 2008) and high (0.59 on 3 May 2008) AOD at 500 nm during the GAMARF campaign. Similarly to this work, the simulations were made using SDs derived from AERONET and from *in situ* airborne measurements. For both cases the differences between LW irradiance measurement and model calculations are within measurement uncertainty either without aerosols, and accounting for the aerosol effect with the AERONET and the *in situ* SD. The results of the comparison shown in Table 3 are consistent with those by Meloni et al. (2015): in fact congruity with measurements is obtained either disregarding the aerosol presence, or including aerosols with the AERONET SD (whichever the RI) and with the *in situ* SD, but only on 28 June (all RI) and 3 July (DB2017 RI).~~

4.2 Airborne irradiance and BT

4.2.1 Flight F35

F35 is the descending phase of the ATR-42 flight towards the Lampedusa airport on 22 June. From the flight top (5800 m) down to 3700 m the flight path is above Lampedusa, then the ATR-42 moves East above the open sea while descending

close to the surface, down to about 100 m above sea level (see Fig. 5a). Successively, it moves again towards the island before landing: this last part of the descent is not used in the analysis, and only data over the sea are considered.

The comparison of the measured and modelled irradiances has been restricted to the 100-5800 m altitude range. Figure 6 shows the measured LW irradiances, selected for pitch and roll angles lower than 1° and 1.5°, respectively, and the model results without aerosol contribution and with all the AOPs. The average AOD during the descent is assumed as model input. The model-measurement comparison is provided in Table 4. The agreement is good for both downward and upward LW irradiances with the AERONET SD, and is best with~~for~~ COL1 and COL2 (RMSD of ~~–~~both components 4.1 W m^{-2}). However the modelled upward component is not sensitive to different AOPs.

The NOAER downward LW irradiance profile agrees with observations throughout most of the altitude range, mainly due to the relatively low AOD value. Significant differences are found in the lowest atmospheric layer, where the model including aerosols better fits with observations. Similarly, the aerosol effect on the upward LW irradiance is apparent mainly in the upper altitude range. The aerosol contribution in the LW spectral region due to dust is an increase in the downward LW irradiance at lower altitudes and a decrease in the upward LW irradiances for increasing altitudes.

The upward and downward LW irradiances at the Falcon 20 altitude are also reproduced with all AOPs, as shown in Table 5. The downward LW irradiance at the Falcon 20 altitude is not affected by the aerosol AOPs, since the flight altitude is above the aerosol layer top (see Fig. 3). The upward irradiance calculated with the model is within the measurement uncertainties for both AERONET and *in situ* SD, and is sensitive to the different SDs, the model uncertainty at the Falcon 20 altitude being 1.5 W m^{-2}. The results~~is~~ confirms~~s~~ what~~the results~~ found for the surface irradiance, i.e. that the broadband irradiance alone cannot help discriminating which SD and RI provide the best representation of the dust optical properties.

The CLIMAT BT profiles are plotted in Fig. 7. BT spikes are associated with ATR-42 passages over the island, where the surface temperature is larger than for the sea. The BT in the upper altitude range is less sensitive to SST, but more affected by the absorption and emission of the bottom layers, including aerosol. Moreover, while SST equally influences the BT at all CLIMAT channels, the spectral variation of the aerosol and atmospheric optical properties produces differences in BT above ~~2~~ 4 km altitude. BTs calculated at selected altitudes (600, 3300, 5670 m), corresponding to a nearly horizontal attitude of the ATR-42, are also shown in Fig. 7. A good agreement at all altitudes is observed when aerosols are included, while an overestimation is observed at the highest altitude (5670 m) in the aerosol-free simulation, as also summarized by Table 6. Within the dust layer (LAYER 3 in Fig. 3) the occurrence of dust induces a significant decrease of BT with respect to the aerosol-free cases, with comparable effects for COL1, COL2 and INSU3 (Fig. 7b), and minor effects for COL3 (Fig. 7a).Conversely, the relevant BT reduction obtained with INSU1 and INSU2 cause a model underestimation compared to measurements (not shown) ~~A good agreement at all altitudes is observed when aerosols are included, while an overestimation is observed at the highest altitude (5670 m) in the aerosol-free simulation, as also summarized by Table 6. However, while the model measurement agreement is very good at 600 and 3300 m, where the aerosol impact is small, a systematic overestimation is obtained at 5670 m. The deviation is smaller and not far from the measurement uncertainty for COL1, COL2, and INSU3.~~

~~These results show that exploring the BT in the thermal infrared is a useful tool to infer dust optical properties if the SD is provided.~~

Similarly to the upward LW irradiance, the largest CLIMAT BTs reduction with respect to aerosol-free conditions occurs above 4 km. The differences in BTs have been calculated for each channel with and without the aerosol contribution: the

INSU1 AOPs produce the largest BT reduction at 5650 m (-1.7, -2.0, and -1.7 K at 8.7, 10.6, and 12 µm, respectively), while the lowest reduction is found for –COL3 (-0.6, -0.7, and -0.2 K at 8.7, 10.6, and 12 µm, respectively). The perturbation caused by INSU3 AOPs are -1.1 K at 8.7 µm, -1.6 K at 10.6 µm, and -0.8 K at 12 µm: such differences are larger than the modelled BT uncertainty (0.37 K).

These results show the better sensitivity of BT to dust optical properties than broadband irradiance. When considering that *in situ* SD better represents the local aerosol distribution, the DB2017 RI from Algeria and Morocco provide the best model-measurement agreement.

The combination of SD and RI giving the best model-measurement match for the overall set of LW irradiances (downward at surface, upward and downward components on the ATR-42 and Falcon 20) have been evaluated by calculating the RMSD of all model-measurement absolute differences, and selecting only those AOPs for which the RMSD is below the ±5 W m^{-2} threshold value. For the AERONET SD all the three RIs meet the requirement (RMSD between 3.2 and 3.3 W m^{-2}), while for the *in situ* SD only the DB2017 (RMSD 4.7 W m^{-2}).

For a given SD, the model results obtained with the OPAC and Volz1973 RIs are very similar. Thus, the model simulations for the other two profiles will be made only with the OPAC RI.

4.2.2 Flight F38

As for F35, the F38 profile ends at the Lampedusa airport on 28 June. The descent path to Lampedusa is rather complex (Fig. 5b), with a descending phase from 5420 m down to 3800 m, where the aircraft performed a large circle over the sea (with Lampedusa in the centre) at constant altitude, then continuing the descent. The ATR-42 path overpasses the island at different altitudes (between 600 and 900 m, and between 3500 and 5400 m), and the effect of land emissivity on the upward LW irradiance can be explored.

The AOD at 500 nm measured during the descent is the lowest of the group of three flights (Table 1).

Model simulations coded as NOAER, COL1, COL3, INSU1, and INSU3 have been made for this profile.

The downward and upward LW irradiances are plotted in Fig. 8. Overall, the modelled downward LW irradiance follows very well the measured profile. Due to the low AOD, the modelled aerosol effect is small, similar to the irradiance measurement uncertainty. Conversely, a~~A~~ large upward LW irradiance variability is observed particularly below 2000 m: for example, the 10 W m^{-2} increase occurring between 1500 and 1700 m cannot be reproduced by the model taking into account the measured atmospheric profiles, nor it can be attributed to the presence of thin clouds, since the humidity is very low (below 20%) in that layer. The ATR-42 flight path shows that at 1700 m the aircraft is close to the West coast of Lampedusa, and the downward-looking pyrgeometer is influenced by the island emission. Similarly, the upward LW irradiance profile shows altitude intervals with sensibly larger values (by about 16-18 W m^{-2}) than the local minima, as those around 900 m. The large irradiances correspond to ATR-42 passes over Lampedusa. Model simulations accounting for the island emissivity corroborate this hypothesis. Indeed, the red curve in Fig. 8 is obtained assuming that the surface is a mix of sea (50%) and land (50%), with their respective temperatures. The land temperature is derived from Level 2 MODIS Land Surface Temperature and Emissivity products with 1 km spatial resolution (MOD11_L2). The agreement with measurements at 900 m and at 1700 m confirms that the peak can be attributed to land contribution to the surface emission. A small peak is visible around 4100 m, suggesting that at this altitude the portion of land surface in the pyrgeometer's FOV is smaller than at lower altitudes.

In addition, differences between model and observations are present in the upward LW irradiance profile, in particular in the ~~2600~~2500-3200 m height range, where the model overestimates measurements by up to 14 W m^{-2} around 2600 m. These differences can not be explained with changes in the temperature and/or humidity profiles, that would have been captured by the airborne instrumentations. In addition, while the upward LW irradiance may be influenced by inhomogeneity in SST or surface emissivity, the SST shows very little variability within the region spanned by the ATR-42 (two sigma standard deviation less than 1 K in the entire area shown in Fig. 5b and less than 0.3 K in the surface area corresponding to the 2600-3200 m aircraft altitude range). The model-measurement disagreement in this height region may be related with the pyrgeometer response to rapid altitude (and consequently temperature) changes. The nominal CGR4 response time is about 6 seconds; however, a significantly longer time may be needed by an airborne instrument to attain the thermal equilibrium with ambient air, as reported by previous studies (e.g. Ehrlich and Wendisch, 2015 and references therein). Consequently, during fast descents the pyrgeometer's measurements may be negatively biased. The vertical velocities during the descent sections of the 22 and 28 June profiles were calculated and compared. The average descent rates in the altitude ranges where model and measurements are in agreement are small: on 22 June between 3500 and 500 m is 2.8 m/s, and is 2.6 m/s on 28 June from 5400 to 4000 m. On the contrary, the average vertical velocity is 5.5 m/s from 3500 to 2000 m on 28 June. So the larger vertical velocities on 28 June might produce a possible underestimation of the upward LW irradiance.

~~A large upward LW irradiance variability is observed particularly below 2000 m: for example, the 10 W m^{-2} increase occurring between 1500 and 1700 m cannot be reproduced by the model taking into account the measured atmospheric profiles, nor it can be attributed to the presence of thin clouds, since the humidity is very low (below 20%) in that layer. The ATR-42 flight path shows that at 1700 m the aircraft is close to the West coast of Lampedusa, and the downward looking pyrgeometer is influenced by the island emission. Similarly, the upward LW irradiance profile shows altitude intervals with sensibly larger values (by about 16-18 W m^{-2}) than the local minima, as around 900 m. The large irradiances correspond to ATR-42 passes over Lampedusa. Model simulations accounting for the island emissivity corroborate this hypothesis. Indeed, the red curve in Fig. 8 is obtained assuming that the surface is a mix of sea (50%) and land (50%), with their respective temperatures. The land temperature is derived from Level 2 MODIS Land Surface Temperature and Emissivity products with 1 km spatial resolution (MOD11_L2). The agreement with measurements at 900 m and at 1700 m confirms that the peak can be attributed to land contribution to the surface emission. A small peak is visible around 4100 m, suggesting that at this altitude the portion of land surface in the pyrgeometer's FOV is smaller than at lower altitudes.~~

The Falcon 20 path is described in Fig. 5b, while the model-measurement comparison is shown in Table 5. The best agreement between modelled and measured upward LW irradiance is obtained with the *in situ* SD. A good agreement is found also with the AERONET SD.

The CLIMAT BTs have been simulated at three different altitudes (700, 3000, and 5200 m) where the ATR-42 is horizontal (Fig. 9). The best agreement between model and measurement is found with the *in situ* SD with minor differences between OPAC and DB2017 RI (INSU1 and INSU3), and with COL1. This is confirmed in Table 6, where the RMSD is below the CLIMAT uncertainty for INSU1. However, the aerosol perturbation to the BT is not significant (even at the highest altitude) compared to the aerosol-free case, as shown in Fig. 9 (differences of -0.4, -0.6, -0.4 K at 8.7, 10.6, and 12 µm, respectively, with INSU3). A slight overestimation (0.17 K RMSD with INSU1) of the model is observed at 3000 m, in agreement with the results for the upward LW irradiance in Fig. 8. Assuming that the differences in BT between model and measurement could be attributed to the SST, their small amount is not sufficient to explain the disagreement in upward LW irradiance. It

is important to underline that the CLIMAT response time is much lower (160 ms) than that of the pyrgeometer, so we do not expect that BT measurements are affected by the descent velocity of the ATR-42. BT simulations without aerosol show that the measured BTs spectral dependence, with nearly equidistant values, is well reproduced by the model. The spikes at 900 m and around 1700 m indicates that also CLIMAT captures the island emission~~, while no BT increase is detected at 1700 m, suggesting that while the pyrgeometer 180° FOV collects the signal emitted by the island, the narrow CLIMAT FOV does not~~.

4.2.3 Flight F42

During flight F42 on 3 July the ATR-42 arrived from north, performed a descent above Lampedusa, at altitudes between 4800 and 1600 m, and left southward (Fig. 5c). The short time period of the descent implies negligible AOD variations. As mentioned above, no *in situ* information on the aerosol properties below 1600 m is available.

Figure 10 shows the ATR-42 and the simulated LW irradiance profiles. The agreement between model and measurements for the downward component is good, except for the *in situ* SD and OPAC RI (INSU1), as also shown by the results in Table 4. The model overestimates the upward LW irradiance profile, except at 2000 m~~, where the aircraft overpassed Lampedusa~~ (see Fig. 5c), and around 4500 m, as also shown by Table 4. On the contrary, a good agreement with all AOPs is found when simulating the Falcon 20 irradiance. This may be a clue for possible inconsistencies in the description of the atmospheric thermodynamic state below the ATR-42 lower altitude, that affect more the simulations at lower altitudes and less those at higher altitudes. Nonetheless, the CLIMAT BTs (Fig. 11) are well reproduced by the model also at 3000 m, where the upward irradiance is overestimated. ~~Moreover, the underestimation of the CLIMAT BTs at 1600 m is not consistent with the overestimation of the upward irradiance.~~ For these reasons the hypothesis of a bad representation of the thermodynamic profiles in the model is not acceptable. Additionally, non-homogeneities in SST are not evident in the area (two sigma standard deviation of 0.4 K on the whole area of Fig. 5c), which may explain the disagreement of the upward LW irradiance with the model simulations. As for the flight F38, the calculated average vertical velocity between 4800 and 1600 m is 5.3 m/s, thus the hypothesis of a LW irradiance underestimation due to the slow response time of the CGR4 pyrgeometer may be valid also for this case, and may affect both the upward and the downward components.

The results of Table 6 show that a good model-measurement agreement is found for the AERONET SD and the OPAC RI (COL1), and for the *in situ* SD and DB2017 RI (INSU3). This supports the conclusions of Section 4.2.1, that different combinations of SD and RI may lead to the same values of BT. On the other hand, also in this case the DB2017 RIs appear to produce the best match with observations when the directly measured SD is used. However, according to the estimated uncertainty, the simulated BT including aerosol is not significantly different from that in aerosol-free conditions (differences of -0.3, -0.4, -0.3 K at 8.7, 10.6, and 12 µm, respectively, with INSU3).

As a conclusion of the simulation of airborne irradiance and BT for all the cases, it is worth remarking that irradiance is not sufficiently sensitive to the different AOPs, while the aerosol perturbation to the nadir infrared BT can be appreciated only at altitudes above the bulk aerosol emission, like for the flight F35.

~~The combination of SD and RI giving the best model-measurement match for the overall set of LW irradiances (downward at surface, upward and downward components on the ATR-42 and Falcon-20) have been evaluated by calculating the RMSD of all model-measurement absolute differences, and selecting only those AOPs for which the RMSD is below the ±5~~

~~W m^{-2} threshold value. For the AERONET SD all the three RIs meet the requirement (RMSD between 3.2 and 3.3 W m^{-2}), while for the *in situ* SD only the DB2017 (RMSD 4.7 W m^{-2}).~~

4.3 IASI radiance simulations

The IASI ~~radiance~~ spectra measured during the morning of 22 and 28 June and 3 July have been considered for the comparison with model simulations, with the aim of assessing the dust perturbation of the TOA infrared BT. IASI spectra are averaged in a region 1° latitude x 1.2° longitude centred at Lampedusa. The resulting standard deviation on the TOA spectral ~~radiance~~ BT is around ~~1%~~0.6 K (0.2%) for 22 and 28 June, and ~~0.5%~~0.3 K (0.1%) for 3 July. A triangular slit function of 0.5 cm^{-1} FWHM has been applied to the simulated spectra in order to reproduce the measured TOA radiances. The AOD at 500 nm and I~~V~~WV model input have been sampled in a 30-minute interval centred at the time of the IASI observation (8:45 AM for 22 June, 9:06 AM for 28 June, and 9:03 AM for 3 July). Model-measurement differences are calculated in the 8-14 µm interval (714-1250 cm^{-1}), the most significant for evaluating the aerosol effect; the regions of the O_3 (980-1070 cm^{-1}) and CO_2 (below 780 cm^{-1}) absorption bands have been excluded and the comparison has been evaluated in the 780-980 cm^{-1} and 1070-1200 cm^{-1} intervals, as in Liuzzi et al. (2017), in terms of BT~~brightness temperature~~. The measured and simulated radiance spectra have been resampled at 15 cm^{-1} to reduce the differences due to their respective spectral resolution.

The results of the comparison, presented as spectral differences in Fig. 12 and as RMSD in the two intervals in Table 7, ~~(Fig. 12)~~ show that differences between model and measurements are larger on 22 June than on 28 June and 3 July. The model shows that dust produces a decrease of the TOA BT~~radiance~~ with respect to aerosol-free conditions. On 22 June ~~T~~the *in situ* SD causes the larger effect compared to the AERONET SD: the maximum reduction of BT in the 780-980 cm^{-1} interval is 1.3 K with COL2 and 2.6 K with INSU2, while in the 1070-1200 cm^{-1} the aerosol-free TOA BT is reduced by 1.1 K with COL2 and by 2.3 K with INSU2. The reduction tends to cancel below 8.5 µm (i.e. above 1176 cm^{-1}) and above 12.5 µm (i.e. below 800 cm^{-1}) because water vapour and carbon dioxide absorption becomes dominant and hides the aerosol effects. The best match with the measured spectra is obtained with COL1 (INSU3) in the 780-980 cm^{-1} (1070-1200 cm^{-1}) interval. On 28 June no significant perturbation is produced by the inclusion of the aerosol; ~~.On 28 June~~ the BT reduction is less than ~~1~~ 0.8 K, the largest ~~(lowest)~~ residual obtained with INSU1 ~~(COL3)~~. The average residual in the 780-980 cm^{-1} interval is lowest with COL3 AOPs, ~~decreases~~, below the IASI radiometric noise (0.123 K) ~~with COL3 AOPs. Similarly to the previous case, o~~On 3 July the perturbation to the TOA aerosol-free BT~~radiance~~ reaches 1.1 K with INSU1 in both intervals, and the best match with the measured BTs between 780 and 980 cm^{-1} is found with INSU1. ~~Table 7 summarizes the results of the comparison for the two spectral intervals: significant differences with respect to the aerosol free simulations are obtained with COL1 on 22 June for both intervals, while the best match with the measured spectra is achieved with INSU3 in the 1070-1200 cm^{-1} interval. On 28 June no significant perturbation is produced by the inclusion of the aerosol. The average residual in the 780-980 cm^{-1} interval decreases below the IASI radiometric noise (0.123) with COL3 AOPs. Finally, a significant difference with respect to the aerosol free simulation is equivalently obtained with COL1 and INSU3, although the best match with the measured BTs between 780 and 980 cm^{-1} is achieved with INSU1.~~ The results in Table 7 suggest that, although the radiative closure at the TOA does not enable the univocal retrieval of the aerosol RI, the perturbation due to the aerosol effect is significant when the AOD is sufficiently large and that the inclusion of aerosol in the radiative transfer simulations produces a non-marginal improvement of the results.

~~**The model simulations with and without aerosol contribution are very similar for 28 June, due to the low AOD. The aerosol radiative effect is largest on 22 June, either because of the larger AOD and of the aerosol vertical distribution which reaches higher altitudes (Meloni et al., 2005).**~~

Liuzzi et al. (2017) simulated the IASI TOA BT with the σ-IASI-as radiative transfer model using the *in situ* SD and two sets of dust RI, the one from Shettle and Fenn (1979) and those from DB2017. ~~The Shettle and Fenn (1979) RI is very different from the other computed RIs used in this study, especially for the imaginary part, which is considerably lower than that for OPAC and Volz1973, implying lower emission. The real part is also generally lower or Shettle and Fen (1979) compared to OPAC and Volz1973, except for small spectral intervals, like 7-9 μm and 11-19 μm. On the contrary, the~~The AOPs of Liuzzi et al. (2017) using the *in situ* SD and DB2017 RI are equivalent to INSU3 used here. ~~Other~~ Some differences in the choice of the model setup and input parameters exist with respect to the present study. First of all, the σ-IASI-as has a finer (0.01 cm^{-1}) resolution than MODTRAN5 (0.1 cm^{-1}). The~~is~~ limitation in the MODTRAN5 resolution does not allow to reproduce the high resolution IASI spectra: however, the scope of simulating the IASI measurements in this work is to show that TOA BTs are sensitive to the dust occurrence and to its AOPs, and that they can be reproduced with the same input parameters that allow to simulate irradiance and BT at the surface and in the atmosphere. Liuzzi et al. (2017) results show that the best agreement is found with INSU3 for all cases in the 780-980 cm^{-1} band, while Shettle and Fenn (1979) RI seems to perform better in the 1070-1200 cm^{-1} spectral range on 28 June and 3 July.

~~t~~The perturbation to the aerosol-free BT on 22 June with INSU3 AOP (2.3 K at 980 cm^{-1} and 1.9 K at 1100 cm^{-1}) is comparable to that found in Liuzzi et al. (2017). ~~Furthermore, in Liuzzi et al. (2017) temperature, humidity, and ozone mixing ratio profiles, as well as the sea surface temperature, were taken from the ECMWF reanalyses; in addition, the sea temperature and column water vapour were slightly tuned in order to achieve a better match of the model with IASI spectra. Liuzzi et al. (2017) results show that the best agreement is found with INSU3 for all cases in the 780-980 cm^{-1} band, while Shettle and Fenn (1979) RI seems to perform better in the 1070-1200 cm^{-1} spectral range on 28 June and 3 July. In our case, the MODTRAN spectral resolution impacts the standard deviations of the model measurement differences, making the results obtained with different AOPs equivalent.~~ It must be ~~however~~ highlighted that our results are obtained without tuning any parameter, by including in the simulations all the available (and significant) observed quantities, and by obtaining a good agreement also along the vertical profile, and at the surface. The good agreement between model and measurement is thus a quite robust result.

4.4 Radiative forcing and heating rate

The dust LW radiative forcing and heating rate profiles have been estimated for 22 June, which is the case with largest AOD, according to Eq. (1) and (2), with the AOPs that give the model-measurement match for the overall set of LW irradiances with RMSD below ±5 W m^{-2}, i.e. COL1, COL2, COL3, and INSU3.

~~The combination of SD and RI giving the best model-measurement match for the overall set of LW irradiances (downward at surface, upward and downward components on the ATR-42 and Falcon-20) have been evaluated by calculating the RMSD of all model-measurement absolute differences, and selecting only those AOPs for which the RMSD is below the ±5 W m^{-2} threshold value. For the AERONET SD all the three RIs meet the requirement (RMSD between 3.2 and 3.3 W m^{-2}), while for the *in situ* SD only the DB2017 (RMSD 4.7 W m^{-2}).~~ Moreover, the results obtained with INSU1 AOPs, i.e. those

causing the largest aerosol radiative perturbation on LW irradiance, are presented to assess the radiative effect of different AOPs (Fig. 13).

~~The ARF and AHR vertical profiles are then calculated with COL1, COL2, COL3, and INSU3 and are shown in Fig. 13.~~

ARF is positive at the surface and at TOA, which corresponds to a higher IR irradiance reaching the surface, and lower irradiance leaving the atmosphere with respect to aerosol-free conditions. A common feature of all profiles is the maximum radiative effect around 3800 m altitude, i.e. below the thickest dust layer (LAYER 3 in Fig. 3), as expected due to dust emission (e.g. Meloni et al., 2015). Very different ARF values are obtained depending on the AOPs, as shown in Table 8. The largest ARF is produced by INSU1, followed by INSU3 AOP. The lower DB2017 absorption is evident compared to OPAC and Voltz RIs in the simulations with the AERONET SD. At the surface the ARF for INSU3 is 74% larger than for COL2, and 146% larger than COL3; the ARF for INSU1 is 33% larger than for INSU3. At TOA the ARF for INSU3 is about 71% larger than for COL2, and 172% larger than for COL3; the ARF for INSU1 is 47% larger than for INSU3. The~~se~~ large differences in ARF for COL1, COL2, COL3, and INSU3 show that different combination of SD and RI may all lead to reasonably simulated LW irradiances, but may also produce very different radiative effects. This behaviour underlines the importance of determining accurate AOPs to correctly infer the aerosol radiative effects.

The aerosol dust forcing efficiency ARFE has been calculated at the surface, TOA, and in the atmosphere. This quantity is relevant because it gives an estimation of the aerosol radiative effect for large aerosol burden, i. e. for AOD at 500 nm equal to one. The estimated ARFE values are reported in Table 8. INSU1 AOPs produce the largest ARFE absolute values. Among the ~~The~~ AOPs obtained with the measured SD and the RI giving ~~the best~~ agreement with measured irradiances, ~~which is~~ INSU3~~,~~ produce the largest ARFE absolute values at the surface, in the atmosphere and at TOA. The ARFE at the surface, +23.7 W m^{-2}, is comparable with the one determined at Lampedusa for the dust event occurring on 3 May 2008 during the GAMARF campaign (Meloni et al., 2015). The ARFE at TOA is nearly doubled with respect to that found during GAMARF, while the atmospheric ARFE is lower. COL1, COL2, and COL3 AOPs provide similar ARFE values, although significantly smaller than for INSU3, at the surface, in the atmosphere and at TOA. The COL3 AOP produces the lowest ARFE at the surface and at TOA, due to the smaller absorption associated with the DB2017 RI compared to OPAC and Volz1973. If the ARF calculated with the moderate AOD of 22 June is not sensitive to the different AOPs according to the model uncertainties, when the aerosol loading is large the ARF notably increases and the effect of the various AOPs becomes significant.

The AHR profile is negative within LAYER3, due to cooling caused by dust emission, and becomes positive just below the altitude of the maximum ARF. The layers below 200 m are locally heated by surface emission. Similarly to ARF, the local heating/cooling is very different when considering the various AOPs. For example, the maximum cooling reached at 4400 m is -0.28 K day^{-1} with INSU1, -0.17 K day^{-1} with INSU3, -0.13 K day^{-1} with COL1, -0.12 K day^{-1} with COL2, and -0.08 K day^{-1} with COL3. Larger differences are observed at the top of LAYER3, around 6200 m, where the AHR with INSU1 is -0.20 K day^{-1}, with INSU3 is -0.14 K day^{-1} and decreases to -0.06 K day^{-1} with COL1 and COL2, and to -0.04 K day^{-1} with COL3.

5 Conclusions

Three cases of Saharan dust occurring during the summer 2013 ChArMex/ADRIMED campaign have been selected to perform a radiative closure study and to assess how different aerosol optical properties may affect the simulations of various radiation quantities in the infrared spectral interval. The average AOD at 500 nm for the selected cases were moderate: 0.36 on 22 June, 0.21 on 28 June, and 0.26 on 3 July.

Downward surface broadband LW irradiance, irradiance in the 8-14 μm range, and zenith sky BT in the 9.6-11.5 μm band were measured at the ENEA Station for Climate Observations in Lampedusa. Simultaneously, instruments on board the SAFIRE ATR-42 and Falcon 20 aircrafts flying around the island collected vertical profiles of LW irradiance (upward and downward components) and nadir BT in three narrowband channels centred at 8.7, 10.6, and 12 μm. The IASI spectra closest in space and time to the flights have also been selected. In parallel, all parameters influencing the IR radiation were measured or, in some cases, inferred from satellite observations. These include in particular the atmospheric thermodynamic vertical profiles, and the aerosol size distribution.

The MODTRAN5.3 radiative transfer model has been initialized with all the available information. The sensitivity of the computed irradiances and BTs on different aerosol size distributions (columnar from AERONET and *in situ* from airborne observations) and infrared refractive indices (OPAC, Volz1973, and DB2017) has been investigated. Vertically resolved in situ measurements of the aerosol SD are used as reference because they provide the most detailed description of the atmospheric aerosol distribution. The computed IR AOD (at 8.6 μm) strongly depends on the size distribution: for example, on 22 June the AOD with the *in situ* size distribution increases by a factor of 2.5-2.8 compared to the AOD with the AERONET size distribution, depending on the dust refractive index. The radiative closure has been carried out simultaneously using radiances and irradiances measured at the ground, airborne, at different atmospheric levels, and from space. This method constitutes a strong constraint on the aerosol properties and allows to identify key parameters also for low-to-moderate values of AOD, as is the case of this study.

The main results of the study can be summarized in the following points:

1. different combinations of SD and RI may produce similar LW and WINDOW irradiances; more specifically, column integrated SD may produce a good agreement between modelled and observed radiative fluxes with specific values of RI, which however do not necessarily correspond with the occurring value;
2. the integration of *in situ* radiation measurements at different levels in the atmosphere and in different IR bands helps in constraining the aerosol properties and the radiative effects; measurements of broadband LW irradiance are helpful for the determination of the dust properties and radiative effects, but alone do not permit reducing the uncertainty on the dust RI. In addition, the moderate AOD values measured during the campaign cause the measured irradiances to agree with simulations either in aerosol-free conditions and including aerosols with different AOPs, when uncertainties are taken into account;
3. knowledge of the dust SD, assumed to correspond with the *in situ* vertically resolved profiles, allows to constrain the RI, and consequently aerosol radiative forcing and heating rate. For the ADRIMED campaign, with dust particles originating from northern Algeria, Tunisia and Morocco, the dust RI from DB2017, derived for soil samples from the same regions, produces the best agreement with observations;
4. the use of inaccurate, although optically equivalent, size distributions and refractive indices, has a large impact on the ARF determination. The ARF may change by a factor as large as 2.5 at surface and 2.7 at TOA, depending on

the SD and RI, for cases producing a good agreement with observed irradiances. Thus, the knowledge of the SD is crucial for a correct estimate of ARF;

5. the values of ARFE retrieved on 22 June are +23.7 W m^{-2} at the surface, -7.9 W m^{-2} in the atmosphere, and +15.8 W m^{-2} at TOA. Significantly smaller ARFE are obtained when equivalent SDs and RIs are used;
6. similarly, the heating rate profile significantly depends on SD, RI, and vertical distribution;
7. knowledge of the whole vertical profile is important to obtain a good closure with respect to the radiative quantities; moreover, the dust vertical distribution appears to influence the derived ARF, primarily at TOA.

The dust radiative effects in the IR are thus non negligible, and their improper estimate may prevent a correct representation of processes acting on local and regional scales. Thus, it appears that specific efforts should be dedicated at determining reliable estimates of the dust vertical distribution and SD, and at implementing source-dependent RIs in regional and large scale models, with the aim of obtaining better determinations of the dust IR radiative effects at the regional scale.

6 Data availability

All the data used in this study are available upon request. Please contact the corresponding author.

The in situ distribution data from the ATR-42 aircraft are available on the ChArMEx database at http://mistrals.sedoo.fr/ChArMEx/. The user must register before having access to the data.

The authors declare that they have no conflict of interest.

Acknowledgements

This work has been supported by the Italian Ministry for University and Research project NextData. Measurements presented here are from the Chemistry-Aerosol Mediterranean Experiment project (ChArMEx, http://charmex.lsce.ipsl.fr), which is the atmospheric component of the French multidisciplinary program MISTRALS (Mediterranean Integrated Studies aT Regional And Local Scales). ChArMEx-France was principally funded by INSU, ADEME, ANR, CNES, CTC (Corsica region), EU/FEDER, Météo-France, and CEA.

The authors thank the Group of Atmospheric Optics, Valladolid University, for the provision of the CÆLIS tool (www.caelis.uva.es) used in this publication and the technicians, pilots and ground crew of SAFIRE (Service des Avions Français Instrumentés pour la Recherche en Environnement) for facilitating the instrument integration and conducting flying operations. We thank the AERONET, PHOTONS and RIMA staff for their support. The research leading to these results has received funding from the European Union's Horizon 2020 research and innovation programme under grant agreement No 654109~~European Union Seventh Framework Programme (FP7/2007-2013) under grant agreement Nr. 262254 [ACTRIS]~~.

ECMWF data used in this study have been obtained from the ECMWF Data Server.

The Level 2 MODIS Land Surface Temperature and Emissivity product was retrieved from the online Data Pool, courtesy of the NASA Land Processes Distributed Active Archive Center (LP DAAC), USGS/Earth Resources Observation and Science (EROS) Center, Sioux Falls, South Dakota, https://lpdaac.usgs.gov/data_access/data_pool.

The authors are grateful to Dr. Claudia Di Biagio for providing the dust infrared refractive indices of African soils and for the useful discussion about their use, and to Prof. Carmine Serio and Prof. Guido Masiello for providing the IASI spectra. Finally, thanks to the two reviewers' suggestions and questions the paper has improved and gained in readability.

References

Anderson, G. P., Clough, S. A., Kneizys, F. X., Chetwynd, J. H., and Shettle, E. P.: AFGL Atmospheric Constituent Profiles (0-120 km), AFGL-TR-86-0110, AFGL (OPI), Hanscom AFB, MA 01736, 1986.

Anderson, G.P., Berk, A., Acharya, P. K., Bernstein, L. S., Adler-Golden, S. M., Lee, J., and Muratov L.: Reformulated Atmospheric Band Model Method for Modeling Atmospheric Propagation at Arbitrarily Fine Spectral Resolution and Expanded Capabilities, U.S. Patent #7593835, issued September 22, 2009.

Ansmann, A., Petzold, A., Kandler, K., Tegen, I., Wendisch, M., Müller, D., Weinzierl, B., Müller, T., and Heintzenberg, J.: Saharan mineral dust experiments SAMUM-1 and SAMUM-2: What have we learned?, Tellus B, 63, 403–429, doi:10.1111/j.1600-0889.2011.00555.x, 2011.

Balkanski, Y., Schulz, M., Claquin, T., and Guibert, S.: Reevaluation of mineral aerosol radiative forcings suggests a better agreement with satellite and AERONET data, Atmos. Chem. Phys., 7, 81–95, doi:10.5194/acp-7-81-2007, 2007.

Becagli, S., Sferlazzo, D. M., Pace, G., di Sarra, A., Bommarito, C., Calzolai, G., Ghedini, C., Lucarelli, F., Meloni, D., Monteleone, F., Severi, M., Traversi, R., and Udisti, R.: Evidence for heavy fuel oil combustion aerosols from chemical analyses at the island of Lampedusa: a possible large role of ships emissions in the Mediterranean, Atmos. Chem. Phys., 12, 3479–3492, doi:10.5194/acp-12-3479-2012, 2012.

Berk, A., Anderson, G. P., Acharya, P. K., Bernstein, L. S., Muratov, L., Lee, J., Fox, M., Adler-Golden, S. M., Chetwynd, J. H., Hoke, M. L., Lockwood, R. B, Gardner, J. A., Cooley, T. W., Borel, C. C., Lewis, P. E., and Shettle, E. P.: MODTRAN5: 2006 Update, Proc. SPIE, Vol. 6233, 62331F, 2006.

Berk, A., Acharya, P. K., Bernstein, L. S., Anderson, G. P., Lewis, P., Chetwynd, J. H., and Hoke, M. L.: Band Model Method for Modeling Atmospheric Propagation at Arbitrarily Fine Spectral Resolution, U.S. Patent #7433806, issued October 7, 2008.

Brindley, H. E. and Russell, J. E.: An assessment of Saharan dust loading and the corresponding cloud-free longwave direct radiative effect from geostationary satellite observations, J. Geophys. Res.-Atmos., 114, D23201, doi:10.1029/2008jd011635, 2009.

Brogniez, G., Pietras, C., Legrand, M., Dubuisson, P., and Haeffelin, M.: A high-accuracy multiwavelength radiometer for in situ measurements in the thermal infrared. Part II: Behavior in field experiments, J. Atmos. Oceanic Technol., 20, 1023–1033, 2003.

Brogniez, G., Legrand, M., Damiri, B., Behnert, I., and Buis J.-P.: Multi-channel ground based and airborne infrared radiometers, in: NEWRAD Proc. Ninth Int. Conf. on New Developments and Applications in Optical Radiometry, Davos, Switzerland, Physikalisch- Meteorologisches Observatorium Davos, World Radiation Center, 173–174, 2005.

Clarisse, L., Coheur, P.-F., Prata, F., Hadji-Lazaro, J., Hurtmans, D., and Clerbaux, C.: A unified approach to infrared aerosol remote sensing and type specification, Atmos. Chem. Phys., 13, 2195–2221, doi:10.5194/acp-13-2195-2013, 2013.

Cuesta, J., Eremenko, M., Flamant, C., Dufour, G., Laurent, B., Bergametti, G., Hopfner, M., Orphal, J., and Zhou, D.: Three-dimensional distribution of a major desert dust outbreak over East Asia in March 2008 derived from IASI satellite observations, J. Geophys. Res., 120, 7099-7127, 2015.

DeSouza-Machado, S. G., Strow, L. L., Hannon, S. E., and Motteler, H. E.: Infrared dust spectral signatures from AIRS, Geophy. Res. Lett., 33(L03801), 1-5, 2006.

Denjean, C., Cassola, F., Mazzino, A., Triquet, S., Chevaillier, S., Grand, N., Bourrianne, T., Momboisse, G., Sellegri, K., Schwarzenbock, A., Freney, E., Mallet, M., and Formenti, P.: Size distribution and optical properties of mineral dust aerosols transported in the western Mediterranean, Atmos. Chem. Phys., 16, 1081-1104, doi:10.5194/acp-16-1081-2016, 2016.

Di Biagio, C., di Sarra, A., and Meloni, D.: Large atmospheric shortwave radiative forcing by Mediterranean aerosols derived from simultaneous ground-based and spaceborne observations and dependence on the aerosol type and single scattering albedo, J. Geophys. Res., 115, D10209, doi:10.1029/2009JD012697, 2010.

Di Biagio, C., Formenti, P., Styler ,S. A., Pangui, E., and Doussin, J.-F.: Laboratory chamber measurements of the longwave extinction spectra and complex refractive indices of African and Asian mineral dusts, Geophys. Res. Lett., 41, 6289–6297, doi:10.1002/2014GL060213, 2014a.

Di Biagio, C., Boucher, H., Caquineau, S., Chevaillier, S., Cuesta, J., and Formenti, P.: Variability of the infrared complex refractive index of African mineral dust: experimental estimation and implications for radiative transfer and satellite remote sensing, Atmos. Chem. Phys., 14, 11093-11116, doi:10.5194/acp-14-11093-2014, 2014b.

Di Biagio, C., Formenti, P., Balkanski, Y., Caponi, L., Cazaunau, M., Pangui, E., Journet, E., Nowak, S., Caquineau, S., Andreae, M. O., Kandler, K., Saeed, T., Piketh, S., Seibert, D., Williams, E., and Doussin, J.-F.: Global scale variability of the mineral dust longwave refractive index: a new dataset of in situ measurements for climate modelling and remote sensing, Atmos. Chem. Phys., 17, 1901–1929, doi:10.5194/acp-17-1901-2017 , 2017.

Di Iorio, T., di Sarra, A., Sferlazzo, D. M., Cacciani, M., Meloni, D., Monteleone, F., Fuà, D., and Fiocco, G.: Seasonal evolution of the tropospheric aerosol vertical profile in the central Mediterranean and role of desert dust, J. Geophys. Res., 114, D02201, doi:10.1029/2008JD010593, 2009.

di Sarra, A., Pace, G., Meloni, D., De Silvestri, L., Piacentino, S., and Monteleone, F.: Surface shortwave radiative forcing of different aerosol types in the central Mediterranean, Geophys. Res. Lett., 35, L02714, doi:10.1029/2007GL032395, 2008.

di Sarra, A., Di Biagio, C., Meloni, D., Monteleone, F., Pace, G., Pugnaghi, S., and Sferlazzo D.: Shortwave and longwave radiative effects of the intense Saharan dust event of 25–26 March 2010 at Lampedusa (Mediterranean Sea), J. Geophys. Res., 116, D23209, doi:10.1029/2011JD016238, 2011.

di Sarra, A., Sferlazzo, D., Meloni, D., Anello, F., Bommarito, C., Corradini, S., De Silvestri, L., Di Iorio, T., Monteleone, F., Pace, G., Piacentino, S., and Pugnaghi, S.: Empirical correction of MFRSR aerosol optical depths for the aerosol forward scattering and development of a long-term integrated MFRSR-Cimel dataset at Lampedusa, Appl. Optics, 54, 2725-2737, 2015.

Dubovik, O. and King, M. D.: A flexible inversion algorithm for retrieval of aerosol optical properties from sun and sky radiance measurements, J. Geophys. Res., 105, 20673–20696, 2000.

Dubovik, O., Holben, B., Eck, T. F., Smirnov, A., Kaufman, Y. J., King, M. D., Tanre, D., and Slutsker, I.: Variability of Absorption and Optical Properties of Key Aerosol Types Observed in Worldwide Locations, J. Atmos. Sci., 59, 590–608, 2002a.

Dubovik, O., Holben, B. N., Lapyonok, T., Sinyuk, A., Mishchenko, M. I., Yang, P., and Slutsker I.: Non-spherical aerosol retrieval method employing light scattering by spheroids, Geophys. Res. Lett., 29(10), 1415, doi:10.1029/2001GL014506, 2002b.

Dutton, E. G. and Long, C., with contributions by Wild, M., Ohmura, A., Gröbner, J., and Roesch, A.: Chapter 5: Long-Term In-Situ Surface Flux Data Products, in GEWEX Radiative Flux Assessment (RFA) Volume 1: Assessment, pp. 135-158, WCRP Report No. 19/2012, World Climate Research Programme, Geneva, Switzerland, 2012. (Available at http://www.wcrp-climate.org/documents/GEWEX%20RFA-Volume%201-report.pdf).

Ehrlich, A. and Wendisch, M.: Reconstruction of high-resolution time series from slow-response broadband terrestrial irradiance measurements by deconvolution, Atmos. Meas. Tech., 8, 3671–3684, doi:10.5194/amt-8-3671-2015, 2015.

Feldman, G. C. and McClain, C. R.: Ocean Color Web, MODIS Reprocessing 5, NASA Goddard Space Flight Center. Eds. Kuring, N., Bailey, S. W. October 2014. http://oceancolor.gsfc.nasa.gov/.

Formenti, P., Rajot, J. L., Desboeufs, K., Caquineau, S., Chevaillier, S., Nava, S., Gaudichet, A., Journet, E., Triquet, S., Alfaro, S., Chiari, M., Haywood, J., Coe, H., and Highwood, E.: Regional variability of the composition of mineral dust from western Africa: Results from the AMMA SOP0/DABEX and DODO field campaigns, J. Geophys. Res., 113, D00C13, doi:10.1029/2008JD009903, 2008.

Ginoux, P., Prospero, J. M., Gill, T. E., Hsu, N. C., and Zhao, M.: Global-scale attribution of anthropogenic and natural dust sources and their emission rates based on MODIS Deep Blue aerosol products, Rev. Geophys., 50, RG3005, doi:10.1029/2012RG000388, 2012.

Gkikas, A., Hatzianastassiou, N., Mihalopoulos, N., Katsoulis, V., Kazadzis, S., Pey, J., Querol, X., and Torres, O.: The regime of intense desert dust episodes in the Mediterranean based on contemporary satellite observations and ground measurements, Atmos. Chem. Phys., 13, 12135–12154, doi:10.5194/acp-13-12135-2013, 2013.

Gómez-Amo, J. L., di Sarra. A., and Meloni. D.: Sensitivity of the atmospheric temperature profile to the aerosol absorption in the presence of dust, Atmos. Environ., 98, 331-336, doi: 10.1016/j.atmosenv.2014.09.008, 2014.

Gröbner, J., Wacker, S., Vuilleumier, L., and Kämpfer, N.: Effective atmospheric boundary layer temperature from longwave radiation measurements, J. Geophys. Res., 114, D19116, doi:10.1029/2009JD012274, 2009.

Hansell, R. A., Tsay, S. C., Ji, Q., Hsu, N. C., Jeong, M. J., Wang, S. H., Reid, J. S., Liou, K. N., and Ou, S. C.: An assessment of the surface longwave direct radiative effect of airborne Saharan dust during the NAMMA field campaign, J. Atmos. Sci., 67, 1048–1065, doi:10.1175/2009JAS3257.1, 2010.

Hansell, R. A., Tsay, S.-C., Hsu, n. C., Ji,Q., Bell, S. W., Holben, B. N., Welton, E. J., Roush, T. L., Zhang, W., Huang, J., Li, Z., and Chen, H.: An assessment of the surface longwave direct radiative effect of airborne dust in Zhangye, China, during the Asian Monsoon Years field experiment (2008), J. Geophys. Res., 117, D00K39, doi:10.1029/2011JD017370, 2012.

Haywood, J. M., Johnson, B. T., Osborne, S. R., Mulcahy, J., Brooks, M. E., Harrison, M., Milton, S. F., and Brindley, H.: Observations and modelling of the solar and terrestrial radiative effects of Saharan dust: A radiative closure case-study over oceans during the GERBILS campaign, Q. J. R. Meteorol. Soc., 137, 1211–1226, doi:10.1002/qj.770, 2011.

Hess, M., Koepke, P., and Schult, I.: Optical properties of aerosols and clouds: the software package OPAC, Bull. Amer. Meteorol. Soc., 79, 831-844, 1998.

Highwood, E. J., Haywood, J. M., Silverstone, M. D., Newman, S. M., and Taylor, J. P.: Radiative properties and direct effect of Saharan dust measured by the C-130 aircraft during Saharan Dust Experiment (SHADE): 2. Terrestrial spectrum, J. Geophys. Res., 108(D18), 8578, doi:10.1029/2002JD002552, 2003.

Hilton, F., Armante, R., August, T., Barnet, C., Bouchard, A., Camy-Peyret, C., Capelle, V., Clarisse, L., Clerbaux, C., Coheur, P. F., Collard, A., Crevoisier, C., Dufour, G., Edwards, D., Faijan, F., Fourrié, N., Gambacorta, A., Goldberg, M., Guidard, V., Hurtmans, D., Illingworth, S., Jacquinet-Husson, N., Kerzenmacher, T., Klaes, D., Lavanant, L., Masiello, G., Matricardi, M., McNally, A., Newman, S., Pavelin, E., Payan, S., Péquignot, E., Peyridieu, S., Phulpin, T., Remedios, J., Schlüssel, P., Serio, C., Strow, L., Stubenrauch, C., Taylor, J., Tobin, D., Wolf, W., and Zhou, D.: Hyperspectral Earth Observation from IASI: five years of accomplishments, B. Am. Meteorol. Soc., 93, 347–370, doi:10.1175/BAMS-D-11-00027.1, 2012.

~~Holben B. N., Eck, T. F., Slutsker, I., Tanré, D., Buis, J. P., Setzer, A., Vermote, E., Reagan, J. A., Kaufman, Y. J., Nakajima, T., Lavenu, F., Jankowiak, I., and Smirnov, A.: AERONET – A federated instrument network and data archive for aerosol characterization, Rem. Sens. Environ., 66, 1-16, 1998.~~

Holben, B., et al.: An emerging ground-based aerosol climatology: Aerosol Optical Depth from AERONET, J. Geophys. Res., 106, 12067–12097, 2001.

INFRARED RADIATION PYROMETER KT 19 II, Operational Instruction, Heitronics Infrarot Messtechnik, Version 21/07/08e, pp 3-1.

Israelevich, P., Ganor, E., Alpert, P., Kishcha, P., and Stupp, A.: Predominant transport paths of Saharan dust over the Mediterranean Sea to Europe, J. Geophys. Res., 117, D02205, doi:10.1029/2011JD016482, 2012.

Jin, Z., Qiao, Y., Wang, Y., Fang, Y., and Yi, W.: A new parametrization of spectral and broadband ocean surface albedo, Optics, Express, 19, 26429-26443, 2011.

Klüser, L., Kleiber, P., Holzer-Popp, T., and Grassian, V. H.: Desert Dust Observation From Space – Application of Measured Mineral Component Infrared Extinction Spectra, Atmos. Environ., 54, 419-427, 2012.

Legrand, M., Pietras, C., Brogniez, G., and Haeffelin, M.: A high-accuracy multiwavelength radiometer for in situ measurements in the thermal infrared. Part I: Characterization of the instrument. J. Atmos. Oceanic Technol., 17, 1203–1214, 2000.

Legrand, M., Plana-Fattori, A., and N'doumé, A.: Satellite detection of dust using the IR imagery of Meteosat: 1. Infrared difference dust index, J. Geophys. Res., 106, 18,251 – 18,274, doi:10.1029/2000JD900749, 2001.

Liuzzi, G., Masiello, G., Serio, C., Meloni, D., Di Biagio, C., and Formenti, P.: Consistency of dimensional distributions and refractive indices of desert dust measured over Lampedusa with IASI radiances, Atmos. Meas. Tech., 10,599-615, doi:10.5194/amt-2016-256, 2017.

Mallet, M., Dulac, F., Formenti, P., Nabat, P., Sciare, J., Roberts, G., Pelon, J., Ancellet, G., Tanré, D., Parol, F., Denjean, C., Brogniez, G., di Sarra, A., Alados-Arboledas, L., Arndt, J., Auriol, F., Blarel, L., Bourrianne, T., Chazette, P., Chevaillier, S., Claeys, M., D'Anna, B., Derimian, Y., Desboeufs, K., Di Iorio, T., Doussin, J.-F., Durand, P., Féron, A., Freney, E., Gaimoz, C., Goloub, P., Gómez-Amo, J. L., Granados-Muñoz, M. J., Grand, N., Hamonou, E., Jankowiak, I., Jeannot, M., Léon, J.-F., Maillé, M., Mailler, S., Meloni, D., Menut, L., Momboisse, G., Nicolas, J., Podvin, T., Pont, V.,

Rea, G., Renard, J.-B., Roblou, L., Schepanski, K., Schwarzenboeck, A., Sellegri, K., Sicard, M., Solmon, F., Somot, S., Torres, B., Totems, J., Triquet, S., Verdier, N., Verwaerde, C., Waquet, F., Wenger, J., and Zapf, P.: Overview of the Chemistry-Aerosol Mediterranean Experiment/Aerosol Direct Radiative Forcing on the Mediterranean Climate (ChArMEx/ADRIMED) summer 2013 campaign, Atmos. Chem. Phys., 16, 455-504, doi:10.5194/acp-16-455-2016, 2016.

Marconi, M., Sferlazzo, D. M., Becagli, S., Bommarito, C., Calzolai, G., Chiari, M., di Sarra, A., Ghedini, C., Gómez-Amo, J. L., Lucarelli, F., Meloni, D., Monteleone, F., Nava, S., Pace, G., Piacentino, S., Rugi, F., Severi, M., Traversi, R., and Udisti, R.: Saharan dust aerosol over the central Mediterranean Sea: PM10 chemical composition and concentration versus optical columnar measurements, Atmos. Chem. Phys., 14, 2039–2054, doi:10.5194/acp-14-2039-2014, 2014.

Maring, H., Savoie, D. L., Izaguirre, M. A., Custals, L., and Reid, J. S.: Mineral dust aerosol size distribution change during atmospheric transport, J. Geophys. Res.-Atmos., 108, 8592, doi:10.1029/2002jd002536, 2003.

Markowicz, K. M., Flatau, P. J., Vogelmann, A. M., Quinn, P. K., and Welton, E. J.: Clear-sky infrared radiative forcing at the surface and the top of the atmosphere, Q. J. Roy. Meteor. Soc. 129, 2927–2947, 2003.

Masuda, K., Takashima, T., and Takayama, Y.: Emissivity of pure and sea waters for the model sea surface in the infrared window regions, Remote Sens. Environ., 24, 313–329, 1988.

~~Meloni, D., di Sarra, A., Di Iorio, T., and Fiocco, G.: Influence of the vertical profile of Saharan dust on the visible direct radiative forcing, J. Quant. Spectrosc. Radiat. Transfer, 93, 397–413, 2005.~~

Meloni, D., Di Biagio, C., di Sarra, A., Monteleone, F., Pace, G., and Sferlazzo, D. M.: Accounting for the solar radiation influence on downward longwave irradiance measurements by pyrgeometers, J. Atmos. Oceanic Technol., 29(11), 1629–1643, 2012.

Meloni, D., Junkermann, W., di Sarra, A., Cacciani, M., De Silvestri, L., Di Iorio, T., Estellés, V., Gómez-Amo, J. L., Pace, G., and Sferlazzo, D. M.: Altitude-resolved shortwave and longwave radiative effects of desert dust in the Mediterranean during the GAMARF campaign: Indications of a net daily cooling in the dust layer, J. Geophys. Res. Atmos., 120, 3386–3407, doi:10.1002/2014JD022312, 2015.

Miller, R. L., Knippertz, P., Pérez García-Pando, C., Perlwitz, J. P., and Tegen, I.: Impact of dust radiative forcing upon climate, in: Mineral Dust: A Key Player in the Earth System. P. Knippertz, and J.-B.W. Stuut, Eds. Springer, 327-357, doi:10.1007/978-94-017-8978-3_13, 2014.

Osborne, S. R., Baran, A. J., Johnson B. T., Haywood, J. M., Hesse, E., and Newman, S.: Short-wave and long-wave radiative properties of Saharan dust aerosol, Q. J. Roy. Meteorol. Soc., 137, 1149–1167, doi:10.1002/qj.771, 2011.

Otto, S., de Reus, M., Trautmann, T., Thomas, A., Wendisch, M., and Borrmann, S.: Atmospheric radiative effects of an in situ measured Saharan dust plume and the role of large particles, Atmos. Chem. Phys. 7, 4887–4903, doi:10.5194/acp-7-4887-2007, 2007.

Perrone, M. R., Tafuro, A. M., and Kinne, S.: Dust layer effects on the atmospheric radiative budget and heating rate profiles, Atmos. Environ., 59, 344-354, 2012.

Peyridieu, S., Chedin, A., Capelle, V., Tsamalis, C., Pierangelo, C., Armante, R., Crevoisier, C., Crepeau, L., Simeon, M., Ducos, F., and Scott, N. A.: Characterisation of dust aerosols in the infrared from IASI and comparison with PARASOL, MODIS, MISR, CALIOP, and AERONET observations, Atmos. Chem. Phys., 13, 6065–6082, doi:10.5194/acp-13-6065-2013, 2013.

Philipona, R., Dutton, E. G., Stoffel, T., Michalsky, J., Reda, I., Stifter, A., Wendling, P, Wood, N., Clough, S. A., Mlawer, E. J., Anderson, G., Revercomb, H. E., and Shippert, T. R.: Atmospheric longwave irradiance uncertainty: Pyrgeometers compared to an absolute sky-scanning radiometer, atmospheric emitted radiance interferometer, and radiative transfer model calculations, J. Geophys. Res. 106, 28129-28141, 2001.

Prospero, J. M., Ginoux, P., Torres, O., Nicholson, S. E., and Gill, T. E.: Environmental characterization of global sources of atmospheric soil dust identified with the Nimbus 7 Total Ozone Mapping Spectrometer (TOMS) absorbing aerosol product, Rev. Geophys., 40, 2-1–2-31, 2002.

Rose, T., Crewell, S., Löhnert, U., and Simmer, C.: A network suitable microwave radiometer for operational monitoring of the cloudy atmosphere, Atmos. Res., 75, 183-200, 2005.

Ryder, C. L., Highwood, E. J., Lai, T. M., Sodemann, H., and Marsham, J. H.: Impact of atmospheric transport on the evolution of microphysical and optical properties of Saharan dust, Geophys. Res. Lett., 40, 2433–2438, doi:10.1002/Grl.50482, 2013.

Saunders, R. W., Brogniez, G., Buriez, J. C., Meerkotter, R., and Wendling, P: A comparison of Measured and Modeled Broadband Fluxes from Aircraft Data during the ICE '89 Field Experiment, J. Atmos. Oceanic Technol., 9, 391–406, 1992.

Schepanski, K., Tegen, I., Laurent, B., Heinold, B., and Macke, A.: A new Saharan dust source activation frequency map derived from MSG-SEVIRI IRchannels, Geophys. Res. Lett., 34, L18803, doi:10.1029/2007GL030168, 2007.

Seinfeld, J. H., Carmichael, G. R., Arimoto, R., Conant, W. C., Brechtel, F. J., Bates, T. S., Cahill, T. A., Clarke, A. D., Doherty, S. J., Flatau, P. J., Huebert, B. J., Kim, J., Markowicz, K. M., Quinn, P. K., Russell, L. M., Russell, P. B., Shimizu, A., Shinozuka, Y., Song, C. H., Tang, Y., Uno, I., Vogelmann, A. M., Weber, R. J., Woo, J.-H., and Zhang, X. Y.: ACE-ASIA regional climatic and atmospheric chemical effects of Asian dust and pollution, B. Am. Meteorol. Soc., 85, 367–380, 2004.

~~Sellitto, P. and Legras, B.: Sensitivity of thermal infrared nadir instruments to the chemical and microphysical properties of UTLS secondary sulfate aerosols, Atmos. Meas. Tech., 9, 115–132, doi:10.5194/amt-9-115-2016, 2016.~~

Serio, C., Standfuss, C., Masiello, G., Liuzzi, G., Dufour, E., Tournier, B., Stuhlmann, R., Tjemkes, S., and Antonelli, P.: Infrared Atmospheric Sounder Interferometer radiometric noise assessment from spectral residuals, Appl. Opt., 54(19), 5924–5936, doi:10.1364/AO.54.005924, 2015.

Sicard, M., Bertolín, S., Mallet, M., Dubuisson, P., and Comerón, A.: Estimation of mineral dust longwave radiative forcing: Sensitivity study to particle properties and application to real cases in the region of Barcelona, Atmos. Chem. Phys., 14, 9213–9231, doi:10.5194/acp-14-9213-2014, 2014.

Slingo, A., et al.: Overview of observations from the RADAGAST experiment in Niamey, Niger: Meteorology and thermodynamic variables, J. Geophys. Res., 113, D00E01, doi:10.1029/2008JD009909, 2008.

Sokolik, I. and Toon, O.: Incorporation of mineralogical composition into models of the radiative properties of mineral aerosol from UV to IR wavelengths, J. Geophys. Res., 104, 9423–9444, 1999.

Sourdeval, O. and Brogniez, G.: Validation of IIR/CALIPSO Level 1 Measurements by Comparison with Collocated Airborne Observations during CIRCLE-2 and Biscay '08 Campaigns, J. Atmos. Oceanic Technol., 29, 653-667, 2012.

Stamnes, K., Tsay, S.-C., Wiscombe, W., and Jayaweera, K.: Numerically stable algorithm for discrete-ordinate-method radiative transfer in multiple scattering and emitting layered media, Appl. Optics, 27, 2502–2509, doi:10.1364/AO.27.002502, 1988.

Vogelmann, A., Flatau, P., Szczodrak, M., Markowicz, K., and Minnett, P.: Observations of large aerosol infrared forcing at the surface, Geophys. Res. Lett., 30, 1655, doi:10.1029/2002GL016829, 2003.

Volz, F. E.: Infrared optical constants of ammonium sulfate, Sahara dust, volcanic pumice and flyash, Appl. Optics, 12, 564-568, 1973.

Weinzierl, B., et al.: The Saharan Aerosol Long-Range Transport and Aerosol–Cloud-Interaction Experiment: Overview and Selected Highlights, Bull. Amer. Meteor. Soc., 98, 1427–1451, doi:10.1175/BAMS-D-15-00142.2, 2017.

Table 1. Summary of the time intervals, average (with standard deviation) AOD at 500 nm, IWV, and surface temperature during the descent portion of the three flights selected for this study. The altitude ranges of the ATR-42 and Falcon 20 observations are also shown.

Day/Flight	Time (UT)	Radiosonde launch time (UT)	AOD at 500 nm	IWV (cm)	Surface T (K)	ATR-42 altitude range (m)	Falcon 20 altitude range (m)
22/06 F35	10:23-11:18	n. a.	0.36±0.01	2.65±0.04	298.5±0.1	5800-15	10555-10565
28/06 F38	12:25-13:30	11:30	0.21±0.01	2.19±0.02	296.0±0.1	5420-15	9530-9560
03/07 F42	9:47-10:01	11:31	0.259±0.006	3.02±0.01	298.5±0.1	4830-1600	9280-9310

Table 2. Summary of the size distributions and complex refractive indices combinations used to calculate AOPs in the infrared spectral interval. The abbreviations for each combination and for aerosol-free conditions are reported in the first column. The column AOD at 8.6 μm is also shown. The upper table panel refers to the simulations for the flight F35, the middle panel for the flight F38, and the lower panel for the flight F42.

Abbreviation	Aerosol layer	Size distribution (SD)	Refractive index (RI)	AOD at 8.6 μm
NOAER		No aerosol		
COL1	3600-5800 m	AERONET	OPAC mineral (Hess et al., 1998)	0.058
	1400-3600 m	AERONET	OPAC mineral (Hess et al., 1998)	
	0-1400 m	AERONET	OPAC water soluble (Hess et al., 1998)	
COL2	3600-5800 m	AERONET	Saharan dust (Volz, 1973)	0.055
	1400-3600 m	AERONET	Saharan dust (Volz, 1973)	
	0-1400 m	AERONET	OPAC water soluble (Hess et al., 1998)	
COL3	3600-5800 m	AERONET	Algeria dust (Di Biagio et al., 2017)	0.040
	1400-3600 m	AERONET	Morocco dust (Di Biagio et al., 2017)	
	0-1400 m	AERONET	OPAC water soluble (Hess et al., 1998)	
INSU1	3600-5800 m	*in situ*	OPAC mineral (Hess et al., 1998)	0.146
	1400-3600 m	*in situ*	OPAC mineral (Hess et al., 1998)	
	0-1400 m	*in situ*	OPAC water soluble (Hess et al., 1998)	
INSU2	3600-5800 m	*in situ*	Saharan dust (Volz, 1973)	0.135
	1400-3600 m	*in situ*	Saharan dust (Volz, 1973)	
	0-1400 m	*in situ*	OPAC water soluble (Hess et al., 1998)	
INSU3	3600-5800 m	*in situ*	Algeria dust (Di Biagio et al., 2017)	0.110
	1400-3600 m	*in situ*	Morocco dust (Di Biagio et al., 2017)	
	0-1400 m	*in situ*	OPAC water soluble (Hess et al., 1998)	

Abbreviation	Aerosol layer	Size distribution (SD)	Refractive index (RI)	AOD at 8.6 µm
NOAER		No aerosol		
COL1	1000-5400 m	AERONET	OPAC mineral (Hess et al., 1998)	0.031
	0-1000 m	AERONET	OPAC water soluble (Hess et al., 1998)	
COL3	1000-5400 m	AERONET	Tunisia dust (Di Biagio et al., 2017)	0.023
	0-1000 m	AERONET	OPAC water soluble (Hess et al., 1998)	
INSU1	1000-5400 m	*in situ*	OPAC mineral (Hess et al., 1998)	0.070
	0-1000 m	*in situ*	OPAC water soluble (Hess et al., 1998)	
INSU3	1000-5400 m	*in situ*	Tunisia dust (Di Biagio et al., 2017)	0.061
	0-1000 m	*in situ*	OPAC water soluble (Hess et al., 1998)	

Abbreviation	Aerosol layer	Size distribution (SD)	Refractive index (RI)	AOD at 8.6 µm
NOAER		No aerosol		
COL1	3500-4800 m	AERONET	OPAC mineral (Hess et al., 1998)	0.043
	1600-3500 m	AERONET	OPAC mineral (Hess et al., 1998)	
	0-1600 m	AERONET	OPAC water soluble (Hess et al., 1998)	
COL3	3500-4800 m	AERONET	Tunisia dust (Di Biagio et al., 2017)	0.032
	1600-3500 m	AERONET	Morocco dust (Di Biagio et al., 2017)	
	0-1600 m	AERONET	OPAC water soluble (Hess et al., 1998)	
INSU1	3500-4800 m	*in situ*	OPAC mineral (Hess et al., 1998)	0.078
	1600-3500 m	*in situ*	OPAC mineral (Hess et al., 1998)	
	0-1600 m	*in situ*	OPAC water soluble (Hess et al., 1998)	
INSU3	3500-4800 m	*in situ*	Tunisia dust (Di Biagio et al., 2017)	0.064
	1600-3500 m	*in situ*	Morocco dust (Di Biagio et al., 2017)	
	0-1600 m	*in situ*	OPAC water soluble (Hess et al., 1998)	

Table 2. Summary of the size distributions and complex refractive indices combinations used to calculate AOPs in the infrared spectral interval. The abbreviations for each combination and for aerosol free conditions are reported in the first column. Average AOD at 8.6 μm for each profile (F35, F38, F42).

Abbreviation	Size distribution (SD)	Refractive index (RI)	AOD F35	AOD F38	AOD F42
NOAER	No aerosol				
COL1	AERONET	Dust layer: OPAC mineral (Hess et al., 1998) Below the dust layer: OPAC water soluble (Hess et al., 1998)	0.058	0.031	0.043
COL2	AERONET	Dust layer: Saharan dust (Volz, 1973) Below the dust layer: OPAC water soluble (Hess et al., 1998)	0.055		
COL3	AERONET	Dust layer: Algeria-Tunisia-Morocco dust (Di Biagio et al., 2017) Below the dust layer: OPAC water soluble (Hess et al., 1998)	0.040	0.023	0.032
INSU1	*in situ*	Dust layer: OPAC mineral (Hess et al., 1998) Below the dust layer: OPAC water soluble (Hess et al., 1998)	0.146	0.070	0.078
INSU2	*in situ*	Dust layer: Saharan dust (Volz, 1973) Below the dust layer: OPAC water soluble (Hess et al., 1998)	0.135		
INSU3	*in situ*	Dust layer: Algeria-Tunisia-Morocco dust (Di Biagio et al., 2017) Below the dust layer: OPAC water soluble (Hess et al., 1998)	0.110	0.061	0.064

Table 3. Measured and simulated downward LW and WINDOW irradiance and sky BT at the surface for the three analysed cases; model calculations are performed with different AOPs. The expanded ~~measurement~~ uncertainty associated to the measurements is shown in parentheses together with the measured values. The model-measurement difference is shown in parentheses together with the modelled values. Differences within the measurement uncertainty are in bold.

AOP	NOAER	COL1	COL2	COL3	INSU1	INSU2	INSU3	Measurement
				22 June				
LW (W m^{-2})	356.3 **(-2.3)**	361.1 **(+2.5)**	361.0 **(+2.4)**	359.6 **(+1.0)**	367.2 (+8.6)	366.9 (+8.3)	364.4 (+5.8)	358.6 (±5)
WINDOW (W m^{-2})	82.5 (-3.4~~+1.2~~)	87.3 **(+~~6.0~~1.4)**	87.2 **(+~~5.9~~1.3)**	85.8 **(~~+~~(-0.14~~.5~~)**	93.4 (+~~12.1~~7.5)	93.1 (+~~11.8~~7.2)	90.5 (+~~9.2~~4.6)	~~81.3~~85.9 (±~~6~~2)
IR BT (K)	224.2 (-7.7)	228.4 (-3.5)	229.1 (-2.8)	227.5 (-4.4)	234.2 (+2.3)	234.6 (+2.7)	232.5 **(+0.6)**	231.9 (±1)
				28 June				
LW (W m^{-2})	335.2 **(-2.7)**	338.6 **(+0.5)**		336.9 **(-1.0)**	341.5 **(+3.6)**		339.3 **(+2.4)**	337.9 (±5)
WINDOW (W m^{-2})	73.4 **(-0.5~~+2.8~~)**	76.7 (+~~6.1~~2.8)		75.1 **(+~~4.5~~1.2)**	79.5 (+~~8.9~~5.6)		77.4 (+~~6.8~~3.5)	~~70.6~~73.9 (±~~6~~2)
IR BT (K)	219.9 (-4.9)	223.0 (-1.8)		221.6 (-3.2)	225.9 (+1.1)		224.2 **(-0.6)**	224.8 (±1)
				3 July				
LW (W m^{-2})	362.4 **(-1.3)**	367.4 **(+3.7)**		365.6 **(+1.9)**	370.8 (+7.1)		368.0 **(+4.3)**	363.7 (±5)
WINDOW (W m^{-2})	92.0 **(+~~5.2~~1.4)**	96.9 (+~~10.1~~6.3)		95.1 (+~~8.3~~4.5)	100.1 (+~~13.3~~9.5)		97.4 (+~~10.6~~6.8)	~~86.8~~90.6 (±~~6~~2)
IR BT (K)	233.6 (-3.4)	237.4 **(+0.4)**		236.1 **(-0.9)**	240.5 (+3.5)		238.2 (+1.2)	237.0 (±1)

Table 4. RMSD in W m^{-2} between modelled and measured downward and upward LW irradiances for the ATR-42 profiles in the three analysed cases. Model calculations are made with different AOPs. The measurement uncertainty is ±6 W m^{-2}. Values within the measurement uncertainty are in bold.

AOP	NOAER	COL1	COL2	COL3	INSU1	INSU2	INSU3
			22 June				
LW↓	**3.4**	**3.2**	**3.0**	**2.2**	9.3	8.8	**5.6**
LW↑	**5.9**	**4.9**	**4.9**	**5.2**	**3.9**	**4.0**	**4.4**
			28 June				
LW↓	**3.8**	**3.2**		**3.5**	**3.4**		**3.2**
LW↑	7.7	7.2		7.4	6.8		7.0
			3 July				
LW↓	**4.0**	**5.9**		**4.8**	7.2		**5.6**
LW↑	10.9	9.2		9.6	8.6		9.1

Table 5. Downward and upward LW irradiances measured on-board the Falcon 20 and modelled for on the three analysed cases. Model calculations are made with different AOPs. The measurements uncertainty is ±6 W m^{-2}. Differences with respect to measurements are shown in parentheses and are in bold if lower than the measurement uncertainty.

AOP	NOAER	COL1	COL2	COL3	INSU1	INSU2	INSU3	Measurement
				22 June				
LW↓	41.0 **(-1.7)**	41.0 **(-1.7)**	41.0 **(-1.7)**	41.0 **(-1.7)**	41.0 **(-1.7)**	41.0 **(-1.7)**	41.0 **(-1.7)**	42.7
LW↑	298.0 **(+4.8)**	294.1 **(+0.9)**	294.3 **(+1.1)**	295.6 **(+2.4)**	288.9 **(-4.3)**	289.2 **(-4.0)**	291.7 **(-1.5)**	293.2
				28 June				
LW↓	51.2 **(-5.0)**	51.2 **(-5.0)**		51.2 **(-5.0)**	51.2 **(-5.0)**		51.**2** **(-5.0)**	56.2
LW↑	300.0 (+6.9)	298.6 **(+5.5)**		299.2 (+6.1)	297.2 **(+4.1)**		298.0 **(+4.9)**	293.1
				3 July				
LW↓	57.0 **(+0.2)**	57.0 **(+0.2)**		57.0 **(+0.2)**	57.0 **(+0.2)**		57.0 **(+0.2)**	56.8
LW↑	306.6 **(+4.7)**	304.9 **(+3.0)**		305.7 **(+3.8)**	303.6 **(+1.7)**		304.8 **(+2.9)**	301.9

Table 6. Comparison of the measured and modelled CLIMAT BTs. Model calculations are made with different AOPs. Differences are expressed as RMSD (K) from data at three different altitudes and for the three CLIMAT channels (see text). The RMSD at the maximum altitude is shown in parentheses.

AOP	NOAER	COL1	COL2	COL3	INSU1	INSU2	INSU3
22 June	0.36 (0.61)	0.10 (0.15)	0.11 (0.17)	0.19 (0.32)	0.27 (0.47)	0.25 (0.43)	0.10 (0.16)
28 June	0.27 (0.36)	0.14 (0.15)		0.21 (0.27)	0.09 (0.09)		0.12 (0.11)
3 July	0.22 (0.23)	0.17 (0.02)		0.19 (0.14)	0.21 (0.16)		0.18 (0.03)

Table 7. Differences (K) between modelled and measured IASI BT spectra in the 780-980 cm^{-1} and 1070-1200 cm^{-1} spectral intervals of the atmospheric window. Model calculations with different AOPs are shown. Differences are expressed as ~~percent~~ RMSD and standard deviation. In bold the significant differences with respect to the NOAER simulations.

AOP	NOAER	COL1	COL2	COL3	INSU1	INSU2	INSU3
				22 June			
780-980 cm^{-1}	1.0±0.3	**0.4±0.3**	0.5±0.5	0.7±0.3	1.1±0.4	1.5±0.8	0.8±0.6
1070-1200 cm^{-1}	1.3±0.3	**0.6±0.1**	**0.6±0.2**	**0.8±0.1**	**0.4±0.3**	0.8±0.7	**0.2±0.2**
				28 June			
780-980 cm^{-1}	0.2±0.1	0.2±0.1		0.1±0.1	0.5±0.1		0.3±0.1
1070-1200 cm^{-1}	0.5±0.2	0.3±0.2		0.4±0.2	0.2±0.2		0.2±0.2
				3 July			
780-980 cm^{-1}	0.8±0.1	**0.4±0.2**		0.6±0.2	**0.2±0.2**		**0.4±0.2**
1070-1200 cm^{-1}	0.9±0.1	**0.6±0.2**		0.7±0.2	0.5±0.4		**0.6±0.2**

Table 8. LW ARF and ARFE at the surface, TOA, and in the atmosphere (in W m^{-2}) on 22 June calculated with the AOPs which produce the best agreement with respect to the irradiance profiles (COL1, COL2, COL3, and INSU3) and with INSU1 AOP in addition.

	ARF					ARFE				
AOP	COL1	COL2	COL3	INSU1	INSU3	COL1	COL2	COL3	INSU1	INSU3
Surface	5.0	4.9	3.5	11.3	8.5	13.9	13.6	9.6	31.5	23.7
TOA	3.5	3.3	2.1	8.3	5.7	9.7	9.2	5.8	23.1	15.8
Atmosphere	-1.5	-1.6	-1.4	-3.0	-2.8	-5.8	-5.6	-3.8	-8.4	-7.9

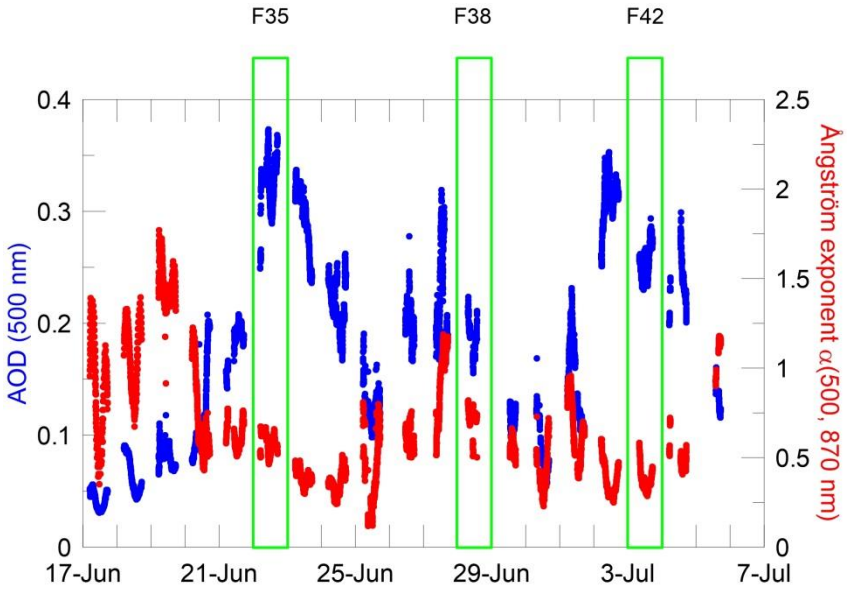

Figure 1: AOD at 500 nm (blue dots) and Ångström exponent (red dots) measured by the MFRSR during the campaign.

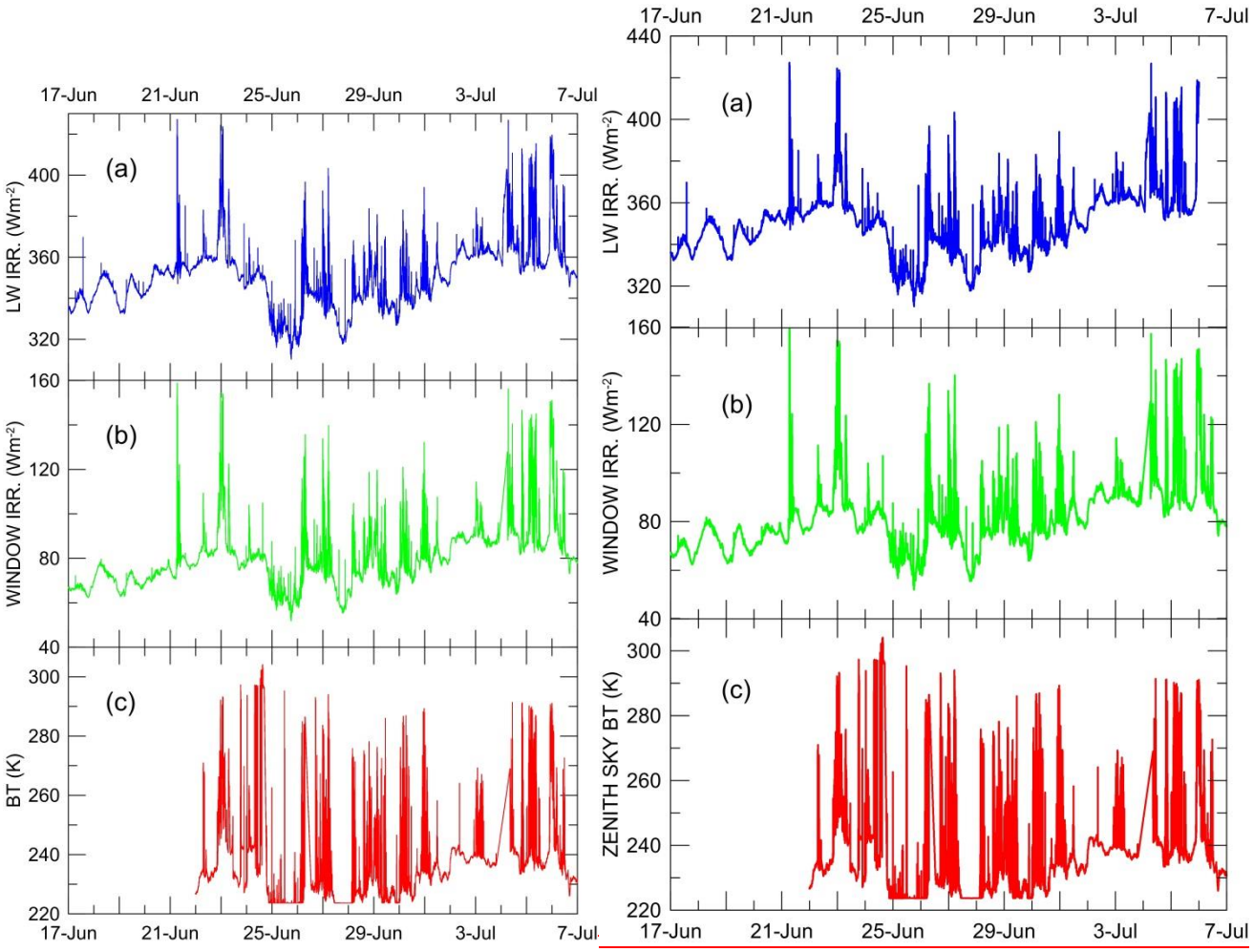

Figure 2: Time evolution of (a) the downward broadband LW irradiance, (b) the WINDOW irradiance, and (c) the zenith sky BT during the ADRIMED campaign.

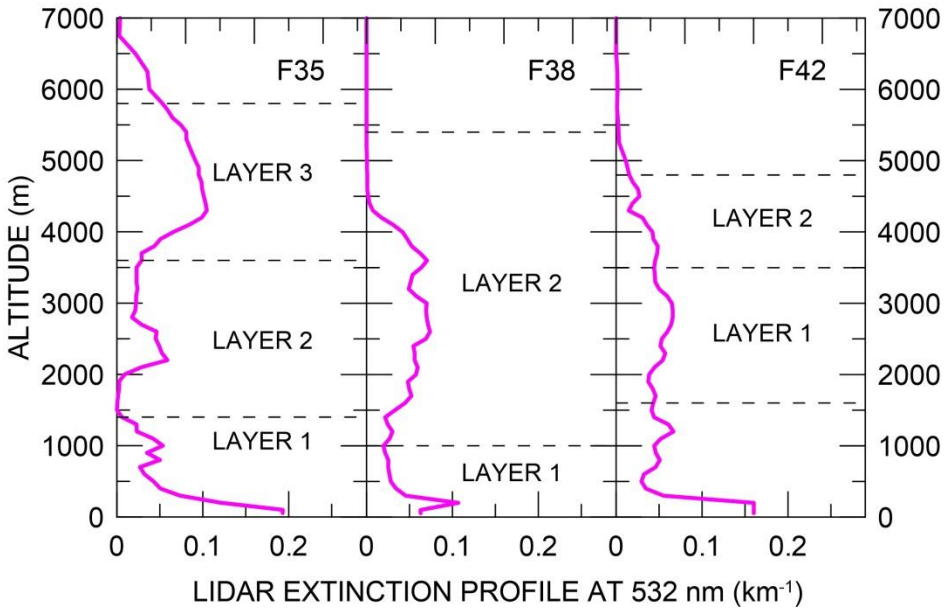

Figure 3: Lidar extinction profiles at 532 nm averaged during the three ATR-42 descents. From left to right, on 22 and 28 June, and on 3 July. The aerosol layers identified by different optical properties from the *in situ* airborne measurements are also evidenced. Note that on 3 July the *in situ* profiles end at the bottom of layer 1.

5

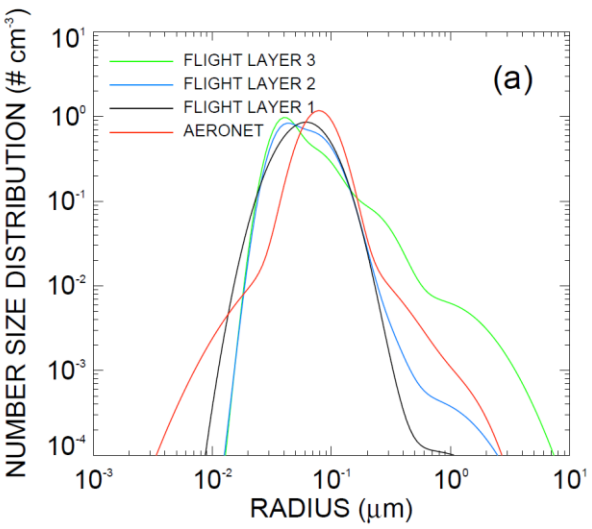
FLIGHT LAYER 3
FLIGHT LAYER 2
FLIGHT LAYER 1
AERONET
(a)
NUMBER SIZE DISTRIBUTION (# cm-3)
RADIUS (μm)

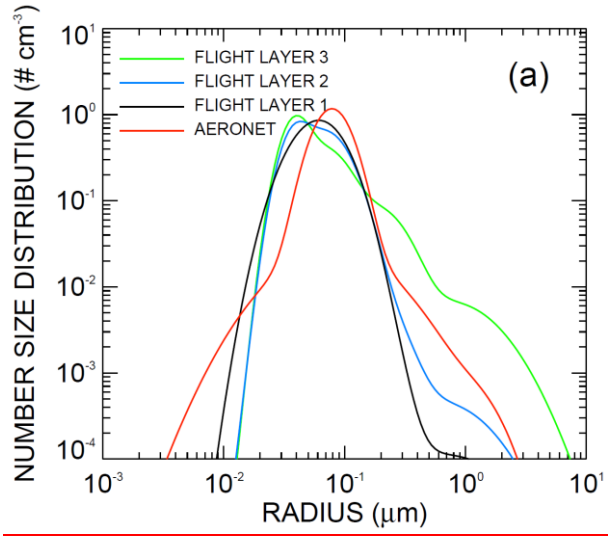
FLIGHT LAYER 3
FLIGHT LAYER 2
FLIGHT LAYER 1
AERONET
(a)
NUMBER SIZE DISTRIBUTION (# cm-3)
RADIUS (μm)

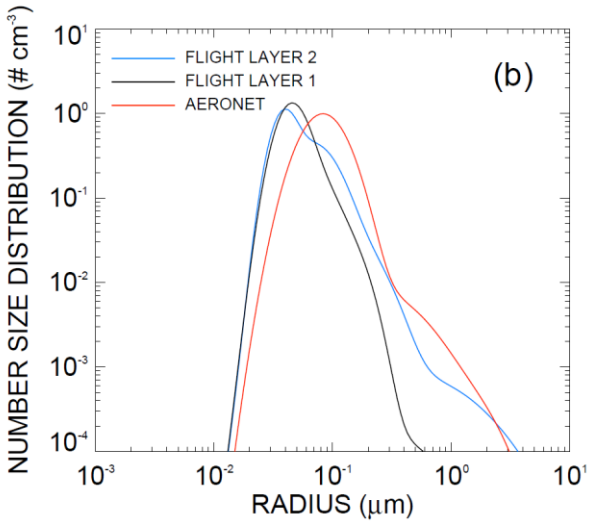
FLIGHT LAYER 2
FLIGHT LAYER 1
AERONET
(b)
NUMBER SIZE DISTRIBUTION (# cm-3)
RADIUS (μm)

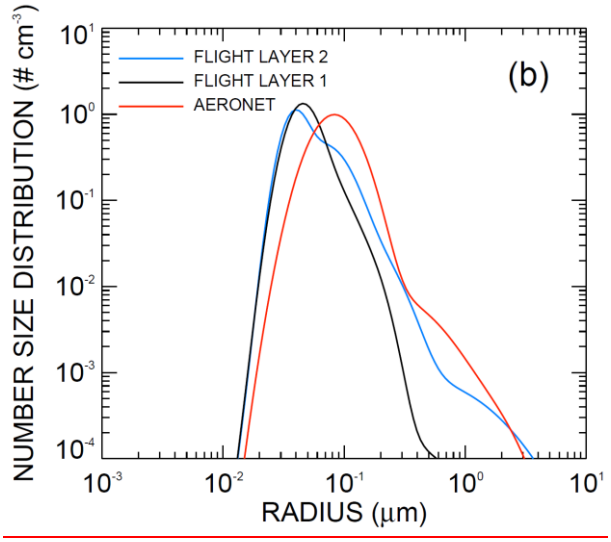
FLIGHT LAYER 2
FLIGHT LAYER 1
AERONET
(b)
NUMBER SIZE DISTRIBUTION (# cm-3)
RADIUS (μm)

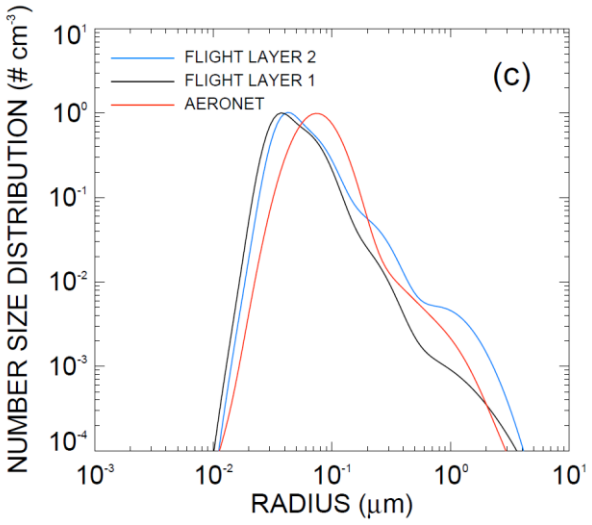
FLIGHT LAYER 2
FLIGHT LAYER 1
AERONET
(c)
NUMBER SIZE DISTRIBUTION (# cm-3)
RADIUS (μm)

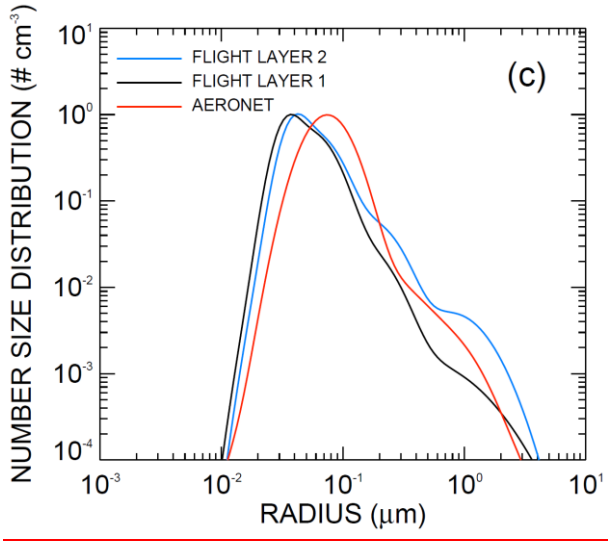
FLIGHT LAYER 2
FLIGHT LAYER 1
AERONET
(c)
NUMBER SIZE DISTRIBUTION (# cm-3)
RADIUS (μm)

Figure 4: Normalized aerosol number size distribution derived from AERONET measurements (red curve) and from the airborne in situ measurements for the layers of figure 3 for (a) F35, (b) F38, and (c) F42.

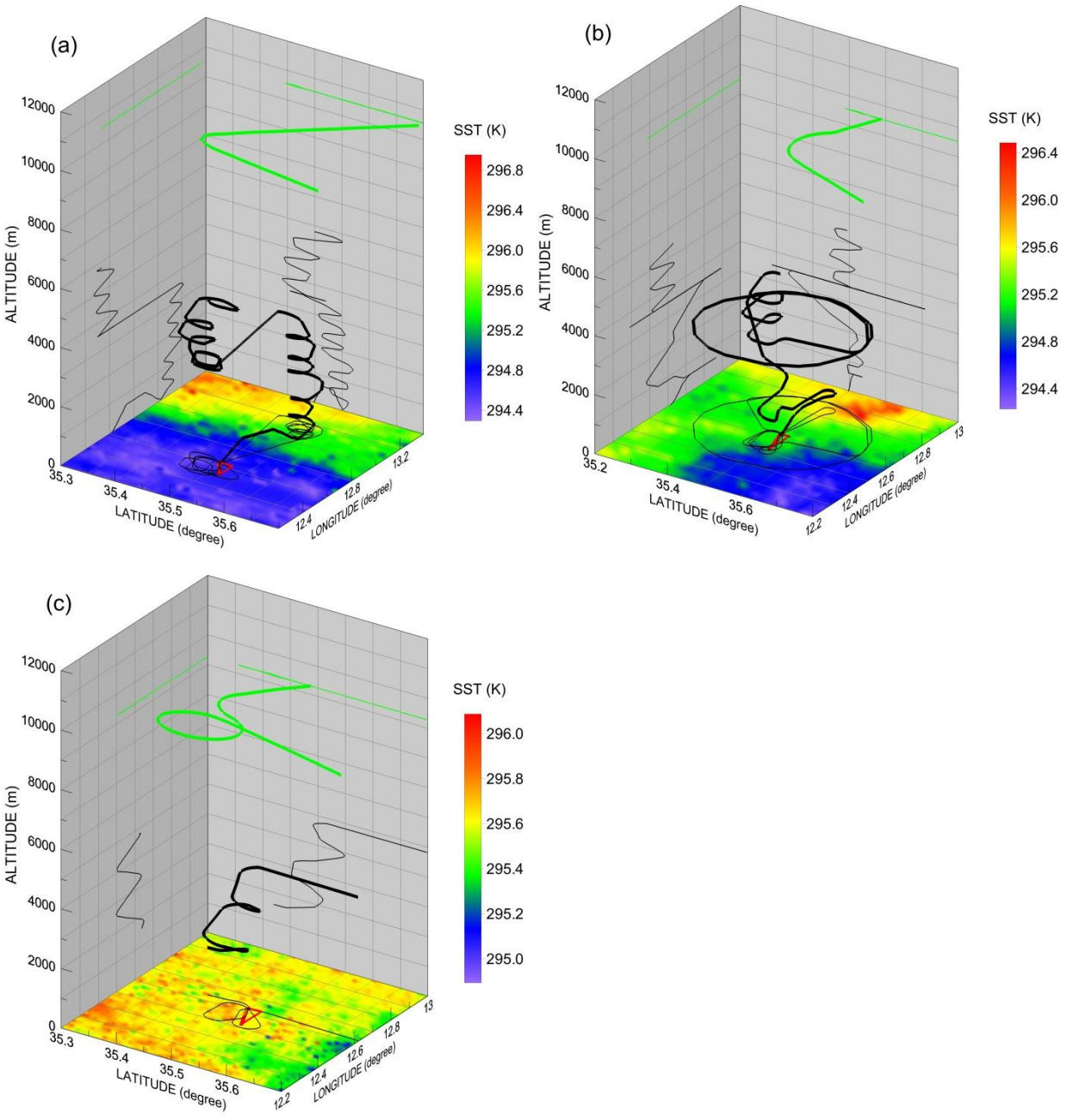

Figure 5: ATR-42 (black curve) and Falcon 20 (green curve) flight paths on (a) 22 June (F35), (b) 28 June (F38), and (c) 3 July (F42), and projections on horizontal and vertical planes. The surface map of the SST from MODIS is shown with the colour scale. A schematic map of Lampedusa contour is shown in red. Please, note that the latitude-longitude and the SST scales are different in each graph.

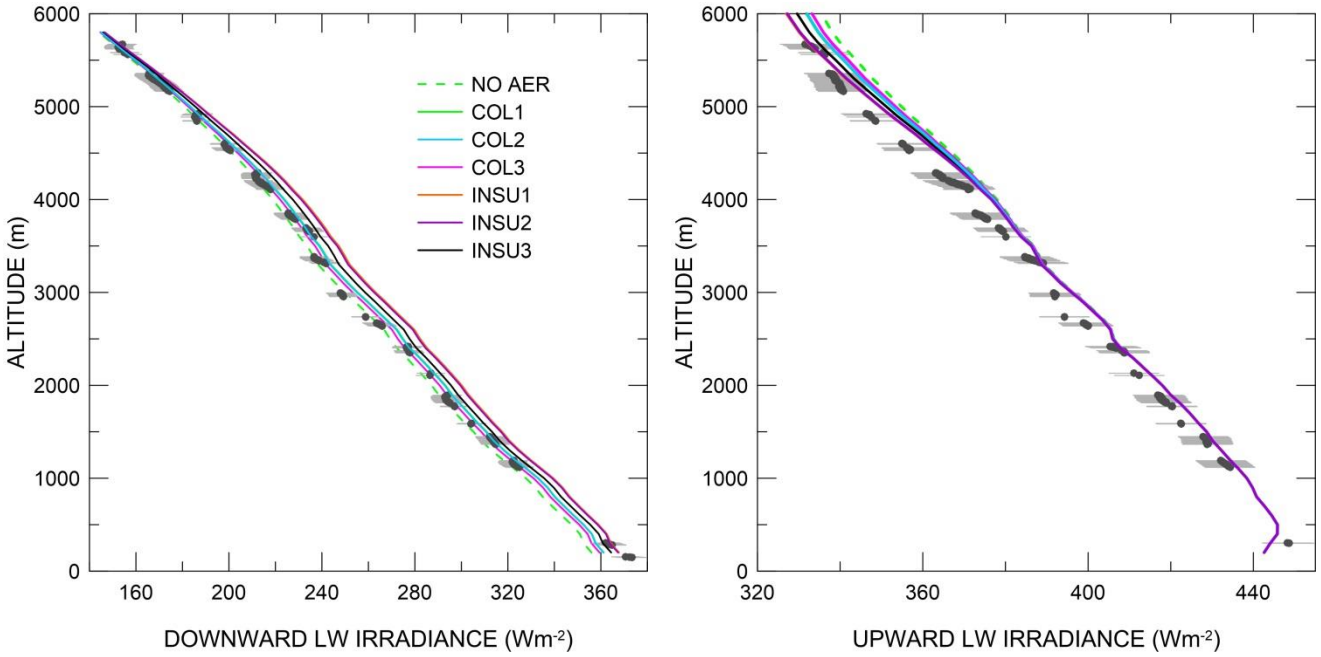

Figure 6: Downward (left) and upward (right) LW irradiance profiles for F35. Grey dots are the measurements selected for small pitch and roll angles, with the associated uncertainty (one sigma) in light grey. Simulated profiles with different SDs and RIs are shown in different colours. See text for details.

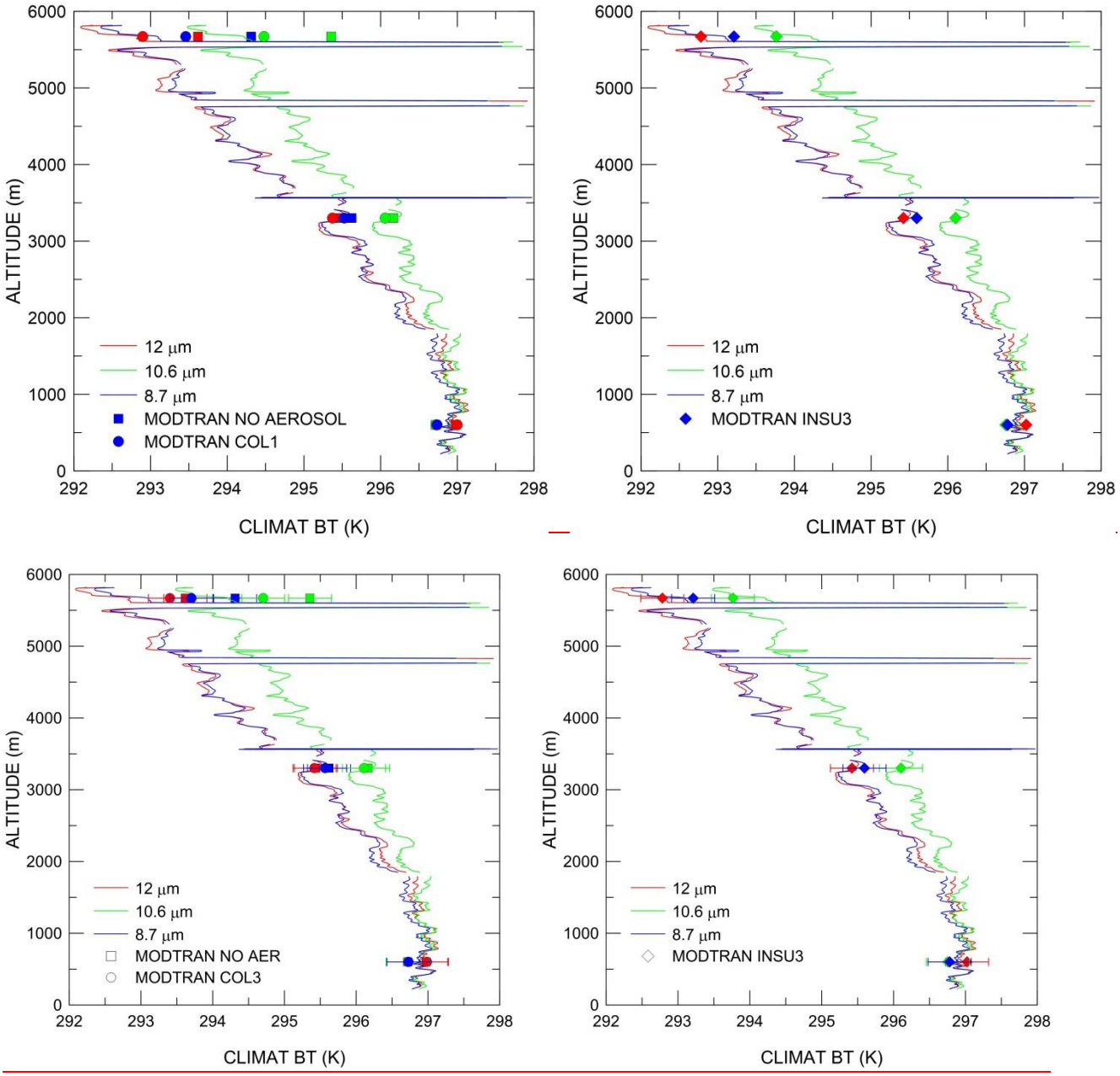

Figure 7: CLIMAT BTs vertical profiles and simulated BTs at selected altitudes during F35 for aerosol-free conditions and with different AOPs: Algerian and Moroccan dust RIs with AERONET ~~SD and OPAC RI (~~left) and *in situ* ~~SD and Algerian and Moroccan dust RIs~~ (right) SD.

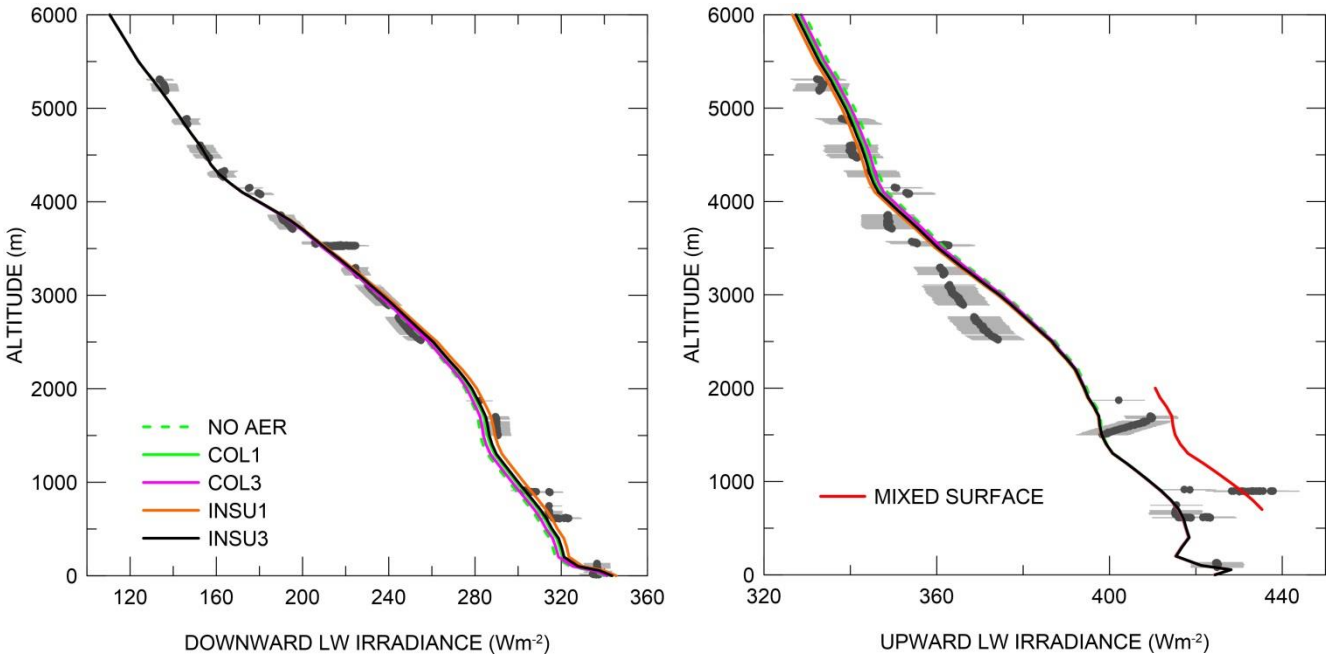

Figure 8: Same as Figure 6, but for profile F38. The red curve in the upward LW irradiance plot is obtained using Lampedusa surface temperature and emissivity. See text for details.

5

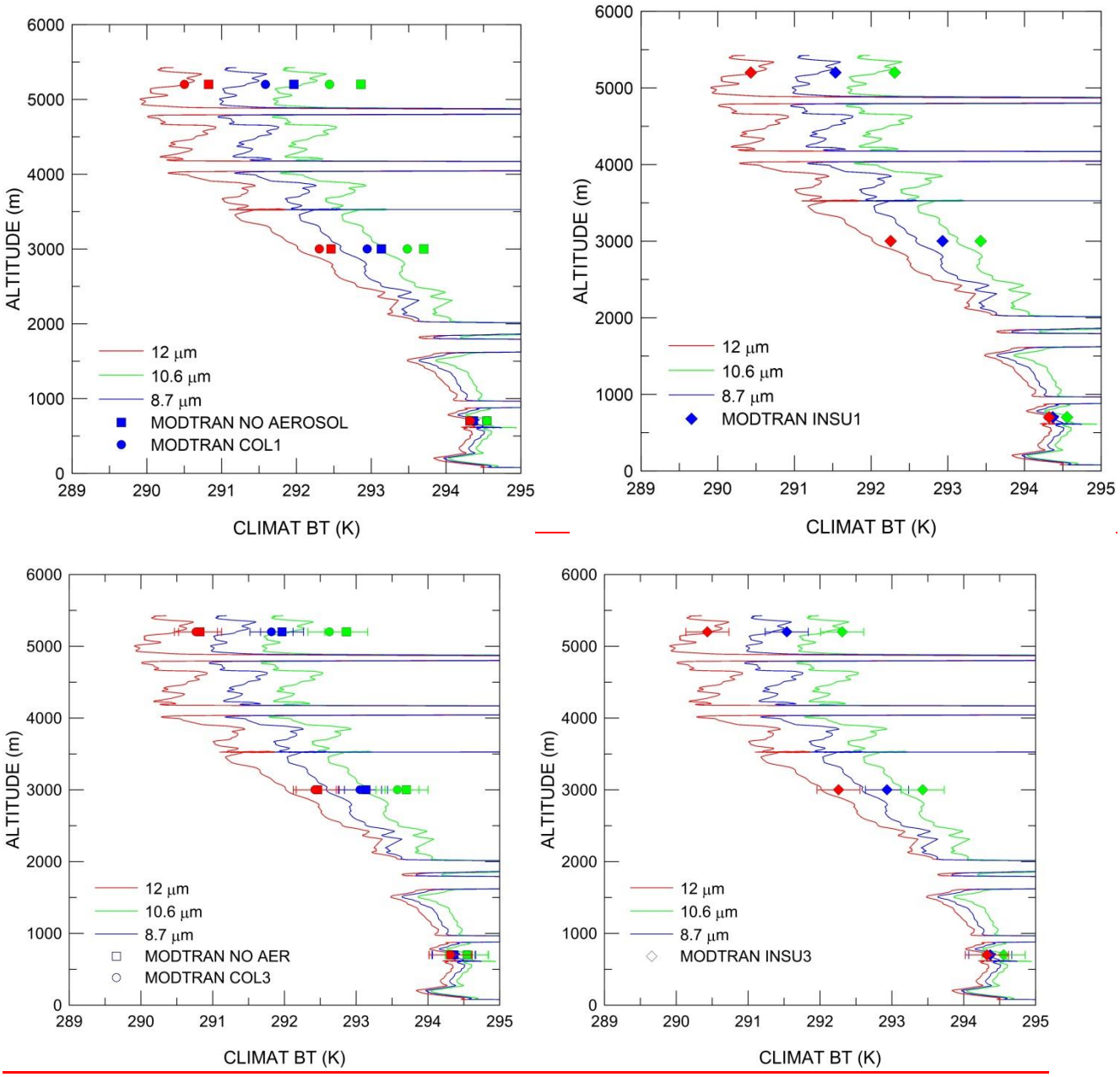

Figure 9: Same as Figure 7, but for profile F38. The simulations are made for *in situ* SD and Tunisian dust RI in the right plot.

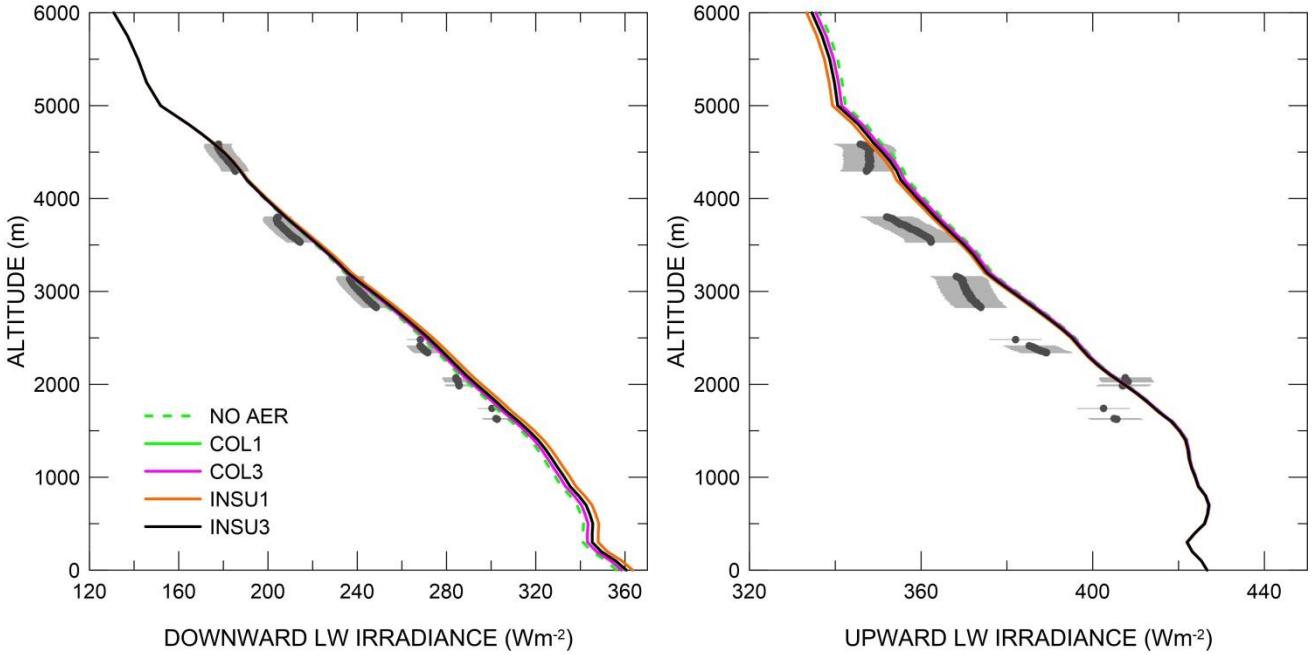

Figure 10: Same as Figure 6, but for profile F42.

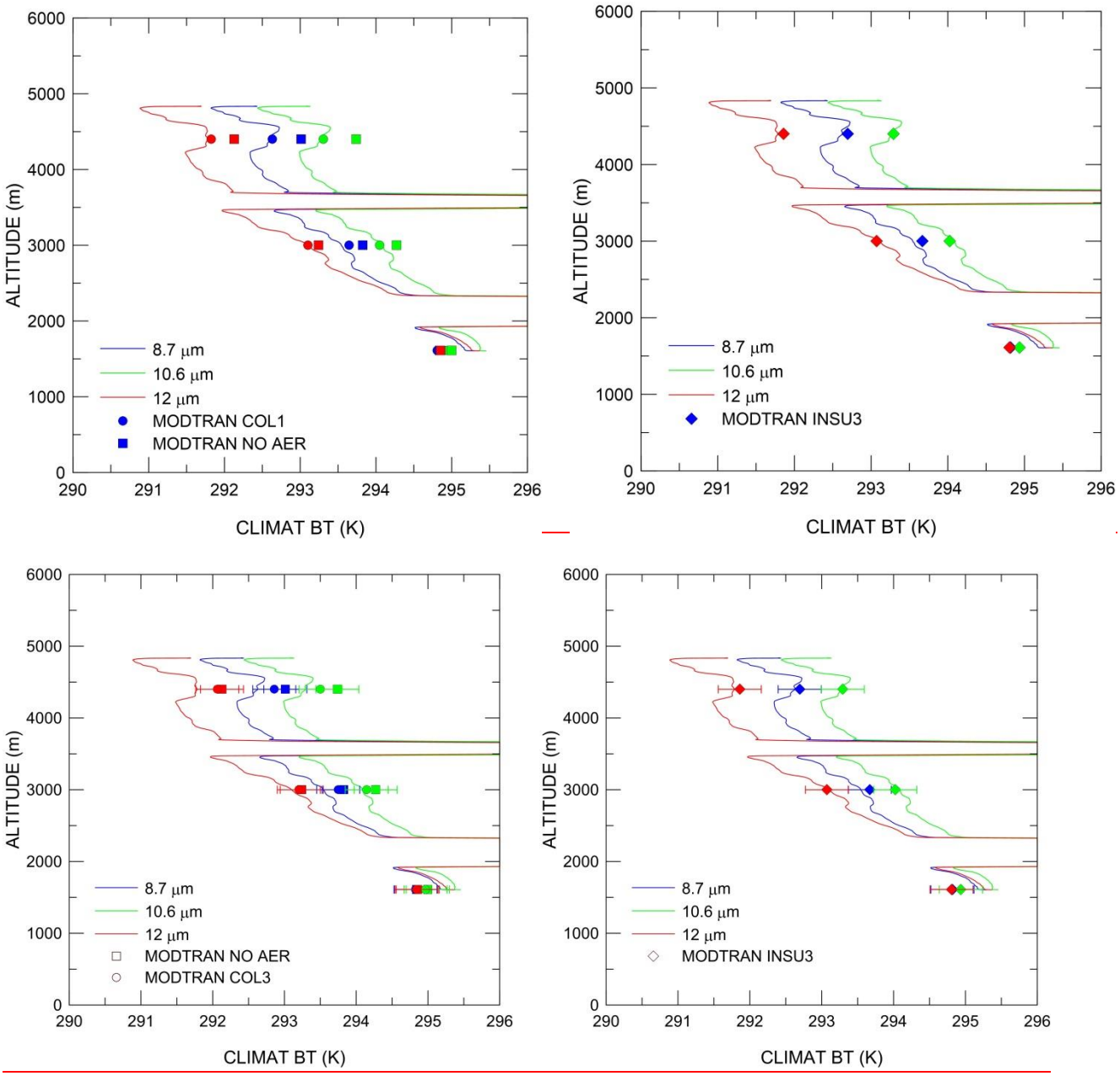

Figure 11: Same as Figure 9, but for profile F42. Simulated data are for the *in situ* SD and Tunisian and Moroccan dust RIs in the right panel.

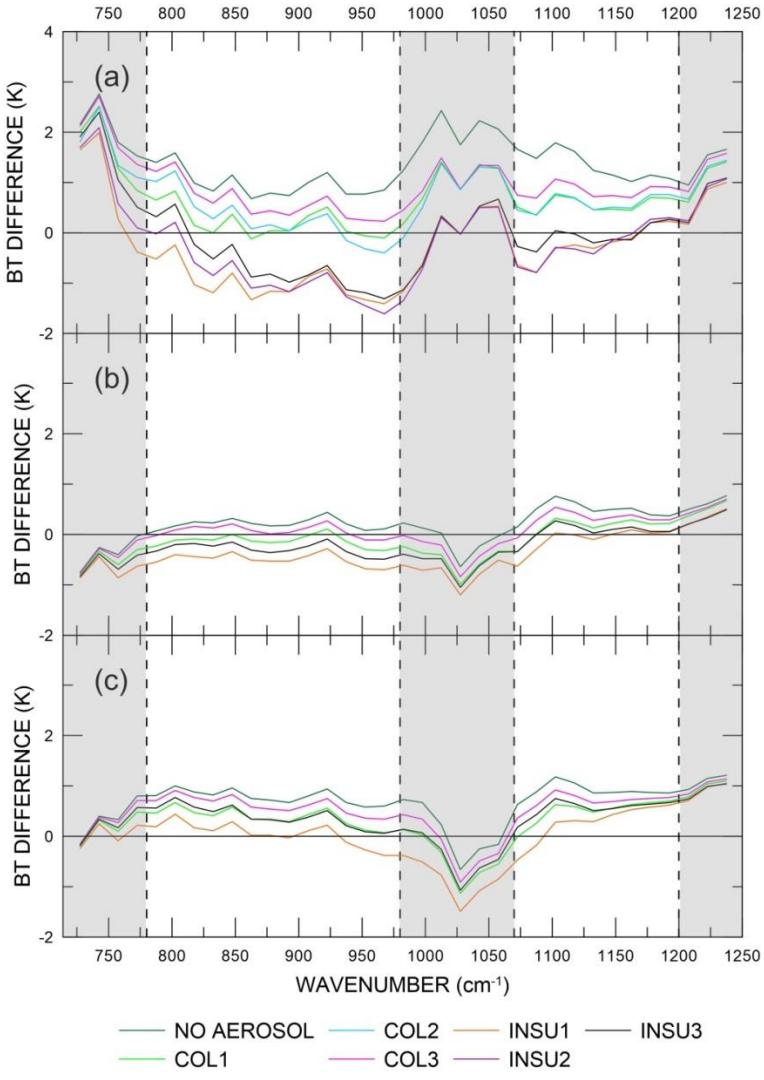
(a)
(b)
(c)
BT DIFFERENCE (K)
WAVENUMBER (cm-1)
NO AEROSOL
COL1
COL2
COL3
INSU1
INSU2
INSU3

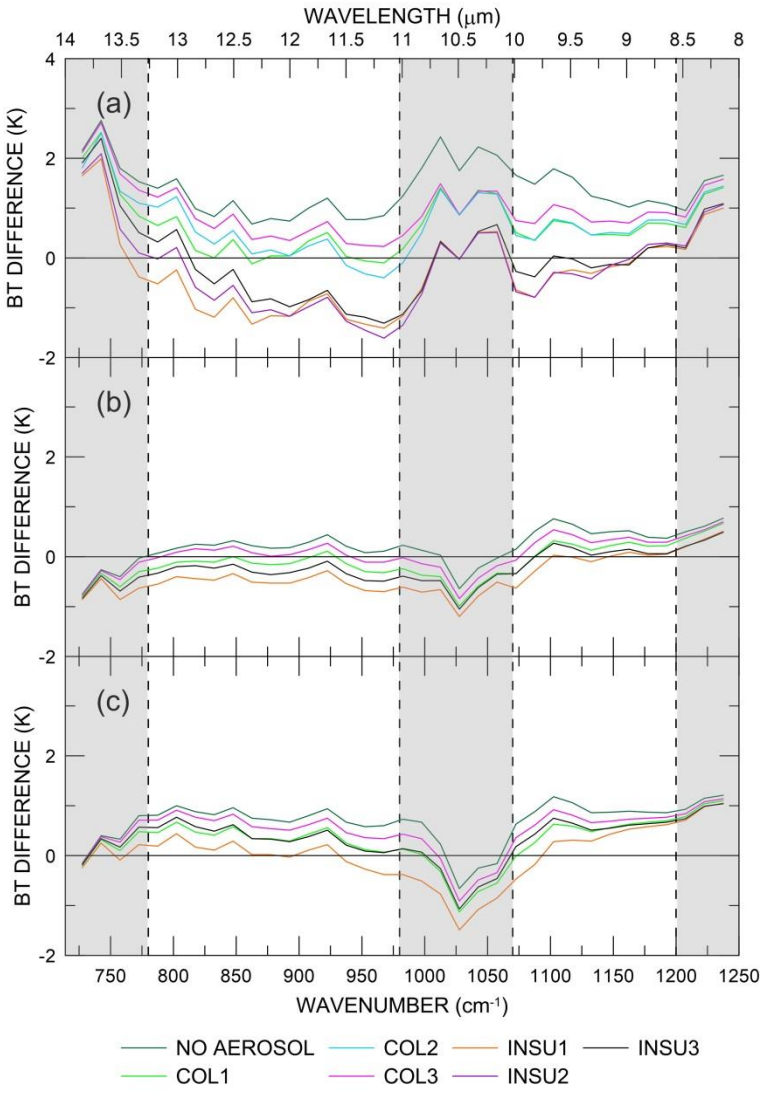

Figure 12: Differences between modelled and measured IASI BT spectra at TOA for (a) 22 June, (b) 28 June, and (c) 3 July. Simulations have been performed with different AOPs and sampled at 15 cm^{-1} intervals. The vertical black dashed lines delimit the two spectral intervals (780-980 cm^{-1} and 1070-1200 cm^{-1}) where the differences are discussed, while the shaded area are not considered in the analysis.

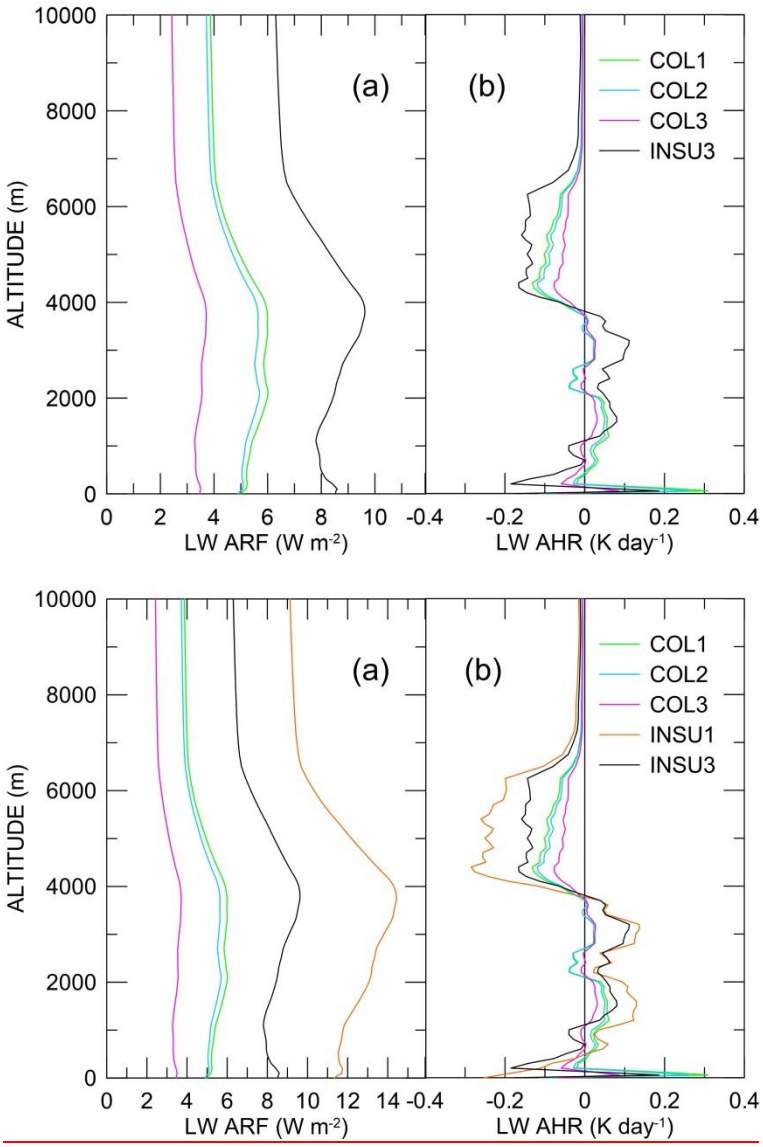

Figure 13: Dust LW radiative forcing (a) and heating rate (b) on 22 June calculated with different AOPs.